Emergent patterns of activity in disordered biological systems: Role of heterogeneities in organizing the collective dynamics of excitable cell-assemblies and tissues

By

Ria Ghosh

LIFE10201404001

The Institute of Mathematical Sciences, Chennai

A thesis submitted to the

Board of Studies in Life Sciences

In partial fulfillment of requirements

for the Degree of

DOCTOR OF PHILOSOPHY

of

HOMI BHABHA NATIONAL INSTITUTE

January, 2022

Homi Bhabha National Institute

Recommendations of the Viva Voce Committee

As members of the Viva Voce Committee, we certify that we have read the dissertation prepared by **Ria Ghosh** entitled "Emergent patterns of activity in disordered biological systems: Role of heterogeneities in organizing the collective dynamics of excitable cell-assemblies and tissues" and recommend that it may be accepted as fulfilling the thesis requirement for the award of Degree of Doctor of Philosophy.

Date: 21/09/2022

Chair - Gautam I. Menon

Date: 21.09.2022

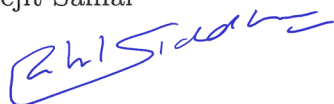Supervisor/Convener - Sitabhra Sinha

Date: 21/09/2022

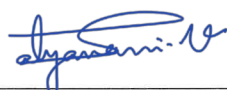External Examiner - Manish Dev Shrimali

Date: 21/09/2022

Member 1 - Areejit Samal

Date: 21/09/2022

Member 2 - Rahul Siddharthan

Date: 21/9/22

Member 3 - Satyavani Vemparala

Final approval and acceptance of this thesis is contingent upon the candidate's submission of the final copies of the thesis to HBNI.

I hereby certify that I have read this thesis prepared under my direction and recommend that it may be accepted as fulfilling the thesis requirement.

Date: 21.09.2022

Place: IMSc, Chennai

Supervisor

i

STATEMENT BY AUTHOR

This dissertation has been submitted in partial fulfillment of requirements for an advanced degree at Homi Bhabha National Institute (HBNI) and is deposited in the Library to be made available to borrowers under rules of the HBNI.

Brief quotations from this dissertation are allowable without special permission, provided that accurate acknowledgement of source is made. Requests for permission for extended quotation from or reproduction of this manuscript in whole or in part may be granted by the Competent Authority of HBNI when in his or her judgment the proposed use of the material is in the interests of scholarship. In all other instances, however, permission must be obtained from the author.

RIA GHOSH

Name & Signature
of the student

DECLARATION

I, hereby declare that the investigation presented in the thesis has been carried out by me. The work is original and has not been submitted earlier as a whole or in part for a degree / diploma at this or any other Institution / University.

Ria Ghosh

RIA GHOSH

Name & Signature

of the student

List of Publications arising from the thesis

Journal

- **Published**

  1. **Ghosh, R.** and Menon, S. N. *Spontaneous generation of persistent activity in diffusively coupled cellular assemblies.* Physical Review E 105(1):014311, 2022.

- **Communicated**

  1. **Ghosh, R.**, Seenivasan, P., Menon, S. N., Sridhar, S., Garnier, N. B., Pumir, A. and Sinha, S. *Frequency gradients in heterogeneous oscillatory media can spatially localize self-organized wave sources that coordinate system-wide activity.* Arxiv Preprint, 1912.07271

Conferences

1. Parallel session talk: "Biocircuits: Emergent complexity in motifs of electrically coupled excitable and passive cells" at NetSci 2019, The University of Vermont, USA, in May 2019.

2. Posters presented: "Role of gradients in the origin of synchronized activity in heterogeneous biological media" and "Emergent complexity of excitable-passive cell motifs" at 5th International Conference on Complex Dynamical Systems and Applications 2019, Indian Institute of Technology Guwahati, India in December 2017.

3. Poster presented: "Designing Bio-electrical Circuits: Emergent complexity of excitable -passive cell assemblies", at Complex Systems Approach to Self-Organization 2016, organized by the Indian Institute of Technology Madras, India in February 2016.

RIA GHOSH

Name & Signature
of the student

To my late grandparents,

who made my childhood wonderful,

and

to Ma and Baba,

who taught me to dream.

Acknowledgements

There are many individuals who have helped and supported me in my journey towards the successful completion of this thesis. The first person, to whom I am indebted, for his guidance, support and motivation, is my PhD supervisor Prof. Sitabhra Sinha. He is one of the best teachers I have ever had. He has always listened to my questions with patience and has helped solve them. The numerous discussions with him over the years have not only enriched me as a person but also taught me a lot about science and research.

I express my gratitude to my collaborators Pavithraa Seenivasan, Dr. Nicolas B. Garnier and Prof. Alain Pumir. This thesis would never have seen the light of the day without the guidance provided by Dr. S. Sridhar and Dr. Shakti N. Menon. They have been more than my co-authors and collaborators, they have helped me navigate my way around research problems. Dr. Sridhar has helped me a lot during my initial days of PhD, while Dr. Menon has been a huge support throughout, but more so towards the end. I would also like to sincerely thank the members of my doctoral committee, Prof. Gautam I. Menon, Prof. Areejit Samal, Prof. Rahul Siddharthan and Prof. Satyavani Vemparala for their valuable suggestions and encouragement throughout.

I want to thank the high performance computing facility at IMSc for providing me access to *Nandadevi* which was integral to my research. I would also like to thank the ever helpful and efficient administrative staff at IMSc. It has always been a pleasure to interact with them and with the technical, library and housekeeping staff. Special thanks to Mr. Vishnu Prasad, Ms. Indra R., Ms. Prema P., Ms. Geetha M., Mr. Siva Subbu Raj B. and Mr. Srinivasan G. for always resolving my issues. Furthermore, I am grateful to the

members of my group and to my office-mates for their help and co-operation.

Through the different schools and conferences that I attended, I have had the privilege of interacting with many researchers and scientists. I am thankful to all of them for enriching and motivating me. I had the opportunity of discussing my work with several people which has benefited me immensely. In particular, I would like to thank Dr. Purusattam Ray, Dr. Pinaki Chaudhuri, Dr. Sayantan Sharma, Dr. M. S. Santhanam, Dr. Pranay Goel, Dr. David Christini, Dr. Vijaykumar Krishnamurthy and Dr. Aditya Gilra.

Right from my school days, I have been fortunate to be taught by some great teachers and I owe my academic achievements to them. I would especially like to mention Kajal Sir, Ms. Samira Chakraborty, Dr. Arindam Rana, Dr. Tarun Banerjee, Dr. Swapan Kumar Chakraborty and Dr. Jugal K. Verma, who have inspired me to pursue research.

My friends at IMSc have helped break the monotony and loneliness that often sets in while pursuing a PhD. I would like to thank them all for making my hostel life so pleasant. A small wave of the hand or a little smile from them have made my days brighter. Ria, Devanand, Nabanita and Janaki have become close friends over the years and I hope our friendship continues to grow stronger with time. Thank you for creating so many wonderful memories with me. I would also like to thank my master and team-mates of the Kalaripayattu class, and my friends at the Kathak dance class. These classes, which I have thoroughly enjoyed attending, have helped me stay mentally and physically fit.

My family has been my greatest support in this journey. My parents have time and again helped me conquer my fears and find my strengths. Words will never be sufficient to express how grateful I am to have them as my parents. Thank you for believing in me. I thank my parents-in-law for loving me like their daughter and always encouraging me to strive forward, and my sister-in-law for her love. Birupaksha, my husband, and truly my better half, has kept me sane by motivating me during this arduous journey. None of this would have been possible without him by my side. Thank you for enriching my life.

Lastly, to the little sunshine in my life, my daughter Ritanya, thank you for coming into my life. Everytime I see your infectious smile and your unbounded energy, my heart gets filled with immense joy. You have made my life more fulfilling.

Contents

List of Figures

Summary

Many important physiological functions in living organisms are mediated by cells and tissue that are electrically excitable, such as neurons in the brain, cardiac myocytes, and uterine muscle cells. Excitable systems remain in a steady state in the absence of external perturbations. However, a supra-threshold stimulus results in the initiation of an excitation wave propagating through the medium. This allows a rich variety of collective dynamical patterns to be observed in such systems, including planar waves, spiral waves, spatio-temporal chaos and chimera states to name a few. Some of the observed dynamical regimes are especially important from the perspective of physiology for their functional implications. For example, spiral waves that can appear in cardiac tissue have been associated with potentially fatal arrhythmic phenomena such as tachycardia and fibrillation. In the gravid uterus, just prior to parturition, a transition to a coherent regime is observed where all cells exhibit phase synchrony. Thus, understanding the mechanisms underlying the emergence of these collective dynamical patterns observed in excitable media can have important benefits in terms of devising efficient therapies. While previous work has largely focused on homogeneous excitable media, biological systems are often quite heterogeneous. Biological tissue not only comprise different types of cells, but cellular processes can also have inherent randomness associated with them. The resulting disordered systems can yield collective phenomena unlike those observed in homogeneous systems and have possible relevance in understanding physiological anomalies.

Heterogeneities can manifest themselves in a system in a number of ways. For instance, the medium can exhibit variable excitability. This can either be for structural reasons,

such as the occurrence of cells with different properties, or because of transient changes in the medium arising from the non-linear nature of the wave propagation dynamics. It is observed that in organs and tissues, electrically passive cells are found alongside excitable cells, giving rise to structural heterogeneities in the medium. Unlike excitable cells, passive cells cannot generate action potentials. Such cells interact with neighboring excitable cells via diffusion-like local transport processes mediated by gap-junctions. A spatially extended system of coupled excitable and passive cells can show periodic activity and display a wide variety of complex spatio-temporal patterns. Thus, in recent years, there has been considerable effort in trying to understand the effect that passive cells have on the dynamics of excitable systems. In this thesis, we have investigated a spectrum of emergent complex patterns that can arise in cell-assemblies and tissues comprising excitable, oscillatory or passive cells.

Heterogeneity can be organized spatially, whereby the relative density of passive cells can vary in different regions of an organ. This can lead to a gradient in the frequency of periodic activity propagating through the medium that helps sustain directed waves of excitation in the tissue. We find that a sufficiently steep frequency gradient will result in the creation of one or few organizing centers in the domain that can drive system-wide activity. A possible consequence would be the appearance of coordinated unidirectional activation waves even in the absence of pacemaker cells, e.g., as seen in the gravid uterus. In this thesis we have also provided a generalisation of the mechanism of auto-rhythmicity in coupled heterogeneous quiescent units. Additionally, we have observed a reduction in the complexity of the collective dynamics - an emergent simplicity - when going from smaller units to a large, spatially extended system. Further, we have considered heterogeneous coupled biological oscillators, whose period varies depending on the cellular micro-environment, and have studied the topological transition to vortex unbinding in these systems - specifically to understand the creation and destruction of self-sustaining rotating waves and their potential role in generating Braxton-Hicks contraction of the uterus.

Chapter 1

Introduction

"Most of the organism, most of the time, is developing from one pattern into another, rather than from homogeneity into a pattern."

—Alan Turing

If we were to ask what is common between the stripes and spots in animals and the sand dunes in a desert, the answer would be patterns. Patterns in space and time are found in a multitude of forms in the natural world [1, 2, 3, 4, 5, 6, 7, 8, 9]. The segmentation of the embryo in insects [10], the aggregation of slime molds through chemotaxis [11], the flocking of birds [12] and spiral wave formation in the heart during abnormal cardiac activity [13] are some examples of pattern formation in biological systems. In physical systems, there are interference patterns in optical fibres [14] and vortex patterns in superconductors [15], while in chemical systems we can observe patterns in catalytic reactions [16] and domain patterns in alloys [17]. Most of these patterns have functional significance and the processes underlying their formation are sought to be explained using mathematical models.

Patterns in nature are often seen to manifest themselves in systems of interlinked components commonly referred to as a *Complex Systems*. Although there have been many

attempts at defining a complex system, the basic features that are common amongst them and therefore, which can be said to make a system "complex" are the presence of non-linearity, emergence, spontaneous order, feedback loops and adaptation. The interaction of the different parts of the system amongst themselves, and with their environment gives rise to new properties not originally present in the system, or as has been attributed to Aristotle: "The whole is more than the sum of the parts" [1]. This occurrence at the level of the system of properties that are absent in the components is what has been termed as *emergence.* While the basic components or ingredients of a system are studied at a particular scale, the emergent properties express themselves at a different scale. Complexity is found in a wide variety of systems, ranging from the macroscopic (for example, the study of the atmosphere, or that of the dynamics of a city) to the microscopic scale (the workings of a cell). A range of tools, drawing from diverse disciplines like nonlinear dynamics, statistical physics, information theory, computer science, sociology, economics and biology are employed to understand and comprehend complex systems.

Complex systems are usually open systems - that is, they dissipate energy and allow mass flows across the system boundary and are thermodynamically out of equilibrium. The emergent spatio-temporal patterns seen in biological complex systems arise due to a balance between the dissipated energy and the energy influx from internal sources. These patterns belong to self-organized processes that occur far from the thermodynamic equilibrium. Thus, self-organization and pattern formation are some of the non-linear processes by which spontaneous generation of order takes place in disordered biological systems.

In the following sections we discuss the relevant concepts that have been used in the subsequent chapters of the thesis.

---

[1]The actual quotation from Aristotle is "In the case of all things which have several parts and in which the totality is not, as it were, a mere heap, but the whole is something beside the parts, there is a cause" (Metaphysics, Book 8 Part 6, trans. W. D. Ross).

1.1 Excitable media

As was mentioned earlier, complex systems is a broad term encompassing many different subtopics. One such subtopic that we focus on in this thesis is of biological excitable media. An excitable medium is a spatially extended nonlinear dynamical system which can support propagating waves of activity, but does not allow the passage of successive waves until a certain amount of time has elapsed between them. This amount of time when the medium cannot be excited again is known as the refractory period [18]. One can understand excitable media by the example of a forest fire: if a wildfire burns through a forest, the burnt regions cannot catch fire again until vegetation has regrown after a refractory period. The Belousov-Zhabotinsky (BZ) reaction forms one of the earliest known examples of excitable media in chemistry [19, 3]. In biology, there are a wide class of systems that are excitable. Ocean plankton populations [20], Dictyostelium slime molds [11] and the electrically excitable tissues and organs of animal physiology are all examples of biological excitable systems.

While most cells of an organism can conduct electricity, in some tissues and organs, the ability of electrical conduction has a functional significance, like in the neurons, heart, uterus and gut. In fact, the naming of excitable media has its origin in the electrical activity of neurons. Originally the term excitability was used to refer to the property of cells (typically neurons) to respond strongly to a relatively weak external stimulus by the generation of a spike in the transmembrane potential. This is known as an action potential. Usually, the amplitude of the action potential is independent of the strength of stimulus, as long as it exceeds some threshold. After the generation of an action potential, the system returns to its resting state and a subsequent excitation can be generated only after the refractory period has passed. The rhythmic beating of the heart [21], the waves of contraction in the pregnant uterus [22], and the peristaltic movement of the gut [23]

- all owe their functionality to the electrical excitable cells found in these organs. It will not be out of place here to mention the passive cells which are found along with excitable cells in biological tissues. These cells cannot elicit an action potential-like response but in conjunction with excitable cells to which they can be coupled, display a wide range of dynamical patterns. We shall look into these patterns in detail in the subsequent chapters.

In an excitable media, excitation can pass between neighboring cells through diffusion-like local transport processes. As the excitation passes through local coupling and initiates excitation, it is capable of supporting re-generative, and hence, undamped excitation waves which can be solitary waves as well as wave trains. Diffferent types of waves are observed in excitable media. In one dimension, if the domain is a closed circuit like a ring, a travelling pulse can keep on rotating unless the origin is still refractory on the wave's return, in which case annihilation of the wave occurs [24, 25, 26]. In two dimensions, the waves commonly observed are planar travelling waves, concentric waves originating from a source and spreading outwards or, spiral waves originating from a source and spreading in a spiral fashion [27, 28, 29]. In three dimensions, the equivalent of spiral waves, known as scroll waves are observed [30]. Due to the non-linearity of excitable systems, upon collision, travelling waves in excitable media annihilate each other unlike in passive linear systems where superposition of the waves take place. All these dynamic characteristics are well-known examples of self-organization in complex systems which result in pattern formation [31].

1.2   Reaction-diffusion systems

The mathematical description of the dynamics of an excitable media are often represented by a reaction-diffusion equation. Reaction-diffusion systems typically comprise constituents that react locally and get transformed into each other with the constituents being trans-

ported in space by diffusion [7]. While they are naturally used to describe systems investigated in chemistry, they have also been used in biology, geology and physics [4, 32, 33]. The mathematical formulation of the reaction-diffusion system is given by the partial differential equation:

$$\frac{\partial \mathbf{q}(\mathbf{x}, t)}{\partial t} = \mathbf{D}\boldsymbol{\nabla}^2\mathbf{q}(\mathbf{x}, t) + \mathbf{R}(\mathbf{q})$$

where the vector $\mathbf{q}(\mathbf{x}, t)$ describes the state of a system (e.g., concentration of chemical species in case of chemical reactions). The first term corresponds to diffusion with D being the diagonal matrix of diffusion components, and the second term $\mathbf{R}(\mathbf{q})$ represents the different non-linear local reactions like growth, decay etc.

Reaction-diffusion systems in a closed environment eventually converge to an equilibrium state. However, in open reactors, with a steady supply of reagents from outside, they can be maintained in far-from-equilibrium states displaying a rich variety of spatial and spatio-temporal patterns. Pioneering contribution to this field was made by Alan Turing when he, while trying to understand the mechanism underlying morphogenesis, found that - contrary to intuition - diffusion could destabilize an otherwise stable steady state [34]. This important observation led to the discovery of a class of reaction-diffusion patterns which have been named after Turing. This mechanism has been successfully applied in modelling animal coat patterns [2, 7]. Some of the other types of patterns that are frequently observed in reaction-diffusion systems are dissipative solitons, pulse trains, spiral waves, and target patterns. In this thesis we do not consider Turing patterns but restrict our study mainly to the last three types of patterns which are generic features of reaction–diffusion systems in more than one dimension and where the local dynamics can settle to a stable limit cycle [35].

1.3 Coupled oscillators

Oscillations, or motion that repeats periodically in time, are seen in many different phenomena and objects in the natural world. Natural systems display limit-cycle oscillations, i.e., the oscillators have a standard waveform and amplitude to which they return after small perturbations [36]. These types of oscillators are essentially nonlinear. Much of the work on spatial patterns in two-dimensional biological media has relied on understanding the underlying oscillatory dynamics.

Spatially extended systems consist of oscillators which are coupled to each other through linear or non-linear terms. Perhaps the most widely observed collective phenomenon observed in systems of coupled oscillators is *synchronization* [37]. Christiaan Huygens, the inventor of pendulum clocks, was possibly the first to report this phenomenon in 1665 [38], when he observed two pendulum clocks mounted on a common wall to move together in tandem. Examples of synchronization observed in other systems include the synchrony of organ pipes [39], the synchronous flashing of fireflies [40], and the synchronization of triode electronic generators [41]. In 1926, Balthazar van der Pol apparently introduced the term *relaxation oscillations* to describe the nonlinear periodic trajectories characterizing the behavior of self-sustained oscillating systems [42]. Over time, relaxation oscillators were observed in diverse areas like electronics, geothermal geysers, thermostat controlled heating systems [43], the rhythmic beating of the heart, predator-prey populations of animals, and the oscillations of genes. Infact, almost all of the periodic phenomena in physiology are governed by relaxation oscillators [44]. Relaxation oscillations are characterized by two processes, one operating on a fast and the other on a slow time scale. There is a long relaxation period during which the system approaches an equilibrium point and a short impulsive period in which the system exhibits a sudden jump [45]. The period of oscillation is determined by the relaxation time constant.

The relaxation oscillator model of van der Pol is essentially identical to the model independently proposed by Fitzhugh [46] and Nagumo [47] to describe the action potentials of neurons, and which eventually served as a generic model of excitable elements in general. Fitzhugh had derived this *FitzHugh-Nagumo model* as a two-variable reduction of the Hodgkin-Huxley model [48], a detailed model of action potential initiation and propagation in the squid giant axon. The FitzHugh-Nagumo model is governed by the following equations:

$$\dot{V} = V - \frac{V^3}{3} - W + I_{ext},$$
$$\tau\dot{W} = V + a - bW,$$

where V is the membrane potential, W is a recovery variable, and I_{ext} is the magnitude of applied stimulus. The parameters a b and τ describe the kinetics. By changing these parameters the model can be made to show various regimes like excitability, oscillations or bi-stability. In a spatially extended system, the FitzHugh-Nagumo equations are essentially an example of a reaction-diffusion system, and are commonly used to model the propagation of waves in excitable media. In this thesis we use the FitzHugh-Nagumo equations to model electrically excitable cells.

Synchronization of coupled oscillators are normally studied in terms of the phase of the oscillators. The phase θ is the variable parametrizing the motion along the limit cycle of the oscillator. When two oscillators are coupled, they adjust their amplitudes and phases with respect to each other. But when the coupling between the oscillators is weak, the amplitudes are unchanged and their interaction can be described solely in terms of their phases. These kinds of models are commonly referred to as *phase oscillators* [49]. One of the popular models to describe synchronization in coupled oscillators in terms of their phases is the *Kuramoto model* [50]. This model has also found application in diverse fields

like neuroscience [51], oscillating flame dynamics, and Josephson junctions [38]. Even though Kuramoto had considered mean-field sinusoidal coupling in his model, subsequent studies have been carried out that have looked at variations of the original model. Different wave patterns have been observed in such systems [52]. In this thesis we have studied phase oscillators on a lattice with nearest neighbor coupling. Other than synchronization, there are various other regimes that are exhibited by coupled oscillator models, viz., oscillator death, inhomogeneous steady states, chimera, chaos, etc. We have described them later in the thesis.

1.4   Spiral waves

Spiral waves are self-regenerating rotating waves in excitable and oscillatory media [29] and are one of the most widely occurring dynamical patterns in chemical and biological systems. They have been known to occur in many organs and tissues that are excitable in nature, and have often been associated with physiological anomalies, like in the heart during abnormal heart rhythms or arrhythmias [13]. Perhaps the majority of studies done on spiral waves have been in the context of cardiac dynamics. In chemical systems, one of the earliest known observation of spiral waves in experiments have been in Belousov-Zhabotinsky (BZ) reactions [19].

One of the ways of creating spiral waves in a medium is by breaking a propagating wave-front with the help of "obstacles". These obstacles can be in the form of non-excitable heterogeneities in the medium. The free ends of the broken wave-front curls inwards to form spiral tips. These reentrant waves then evolve to form a spiral wave rotating with constant angular velocity about an organising center known as the spiral core [53, 54]. The size of the core depends on the excitability of the medium; highly excitable media give rise to cores whose size is of the order of the width of the interface whereas various core sizes

are found in less excitable media. In most cases, the dynamics of a spiral wave are often understood by the behavior of its core. The spiral tip and its immediate neighborhood are sometimes also referred to as a rotor or a vortex and these names are used interchangeably. We can also create a spiral wave by applying a spatially graded perturbation to the medium in the recovery phase after an excitation [55, 3]. Spiral waves do not always rotate rigidly about a spiral core, but can meander or drift about in the medium [56] depending on its underlying properties.

From a topological point of view, spiral waves have a phase defect at the spiral tip since the phase is not defined at that point [57]. Spiral waves also have a topological charge assigned to them depending on the number of arms and the direction of rotation of the wave. The principle of conservation of topological charges holds in infinite media supporting spiral waves. Due to the presence of a singularity in a spiral wave, once created, they cannot be easily destroyed and are seen to persist in the medium for a long time. In this thesis we look at the interactions of multiple spiral waves and describe them in terms of phase singularities.

1.5 Overview of the thesis

In this thesis, we have investigated the different collective patterns that can emerge in coupled cellular assemblies of excitable and passive cells. The main questions that we have asked are:

i How can wave sources that drive system-wide activity be spatially localized in heterogeneous oscillatory media ?

ii How can spontaneous activity be generated in coupled heterogeneous cellular assemblies that are quiescent in isolation ?

iii Can the interaction between vortices in coupled oscillators lead to a transition in the collective behavior ?

The uterus is an organ that exhibits organ-wide rhythmic contractile activity before childbirth despite mostly remaining quiescent at other times. In **Chapter 2**, we investigate the dynamics in the organ that lead to such a transition. Normally, in organs demonstrating coherent system-wide activity, specialized pacemaker cells are present that coordinate such behavior, similar to how the pacemaker cells of the sino-atrial node controls the beating of the heart. But in the uterus, despite there being observations of directed waves of excitation emanating from regions close to the upper end of the organ that drive the contractions [58], there has been little evidence of the existence of pacemaker cells. In this chapter, we use a spatially extended model to describe the collective dynamics of an excitable system such as uterine tissue. The uterine myometrium, which is heterogeneous in nature, comprises electrically excitable cells, viz., uterine muscle cells (myocytes) which are excitable and electrically passive cells such as the fibroblasts and Interstitial Cajal-Like Cells (ICLCs). We show that spatial heterogeneity in the density of passive cells coupled to excitable cells leads to an emergent gradient in the frequency of periodic activity across the medium. A sufficiently steep frequency gradient, along with cell-cell coupling (replicating the strengthening of gap-junctional connections over the course of pregnancy) results in the creation of one or more organizing centers of activity in the medium that remain confined to the region corresponding to the higher end of the gradient. These organizing centers send out waves that coordinate system-wide contractions. Thus, despite the absence of any specialized pacemaker cells, dynamical self-organization in the uterus can bring about propagating rhythmic activity being directed from a particular region. Our results could be of potential significance in understanding the genesis of labor dystocia, or abnormal labor, which is a major cause of maternal and foetal morbidity and is believed to result from breakdown in the coordination of uterine contractions.

In **Chapter 3**, we investigate in detail the emergence of spontaneous recurrent activity in cellular assemblies that we report in Chapter 2. Here we consider simple motifs comprising excitable cells coupled to a variable number of passive cells. We observe that such minimal systems, despite being relatively simple, can display a rich variety of dynamical behavior, including chaos. However, on embedding these motifs in a two-dimensional lattice, an emergent simplicity arises where many of the dynamical features present in the motifs are no longer observed. More intriguingly, we observe that the collective dynamics in a lattice, such as that used to model uterine tissue as described in Ref. [59] can be qualitatively reproduced in a system comprising excitable and oscillatory cells at each site. Furthermore, we find that coupling heterogeneous cellular units, each of which cannot oscillate in isolation, leads to spontaneous periodic activity in the coupled system, provided each of the cellular units have sufficiently distinct steady state values (corresponding to "low" and "high" states). This result suggests a generalization of the mechanism that was proposed in Ref. [60] where it was shown that spontaneous oscillations arise upon coupling excitable and passive cells under certain conditions.

Spiral waves, the main focus of **Chapter 4**, are an emerging pattern ubiquitous in electrically active media. Due to the self-sustaining nature of these re-entrant waves, they destroy the dynamics of the underlying tissue and have often been associated with life-threatening conditions. In this chapter we first study the emergence of heterogeneities in an excitable media due to the interaction of a single vortex with a target wave having the same frequency. We find that even though the creation of vortices due to spiral breakup is dependent on their initial position, it is independent of the direction of rotation of the spiral wave. Subsequently, we consider the interaction of multiple vortices with each other in a heterogeneous medium of coupled phase oscillators comprising excitable and passive cells, and in the presence of noise of varying intensity. We observe that on increasing the intensity of noise, a transition of the spatial correlation function of the vortices from a power-law

13

form to an exponential decaying form takes place that gets manifested in the unbinding and creation of numerous vortices. Our results can have potential relevance in understanding Braxton-Hicks contractions that sometimes occur in uterus prior to childbirth as they are characterized by incoherent activity and creation of multiple reentrant waves.

In **Chapter 5**, we conclude with a discussion of the implications of our results and summarize in brief the key findings of each of the chapters. We also outline in short the possible future scope of research that can be undertaken based on the studies presented in the thesis.

Chapter 2

Frequency gradients in heterogeneous oscillatory media can spatially localize self-organized wave sources that coordinate system-wide activity

2.1 Introduction

Rhythmic activity in many natural systems is centrally coordinated by specialized "pacemakers" [61, 62, 63, 64, 65, 66, 67, 68], examples ranging from the sino-atrial node of the heart [69, 70] to the interstitial cells of Cajal in the gastro-intestinal tract [23, 71, 72]. However, functionally critical rhythmic contractions can also appear in organs such as the uterus where no pacemaker cells have been identified [73]. In such cases, self-organized synchronization of activity can arise through cells communicating with their neighbors [74, 75, 59, 22]. However, this could lead to multiple oscillating clusters characterized by distinct frequencies and phases to co-exist in different locations in the medium.

The potential conflict between these competing coordination centers can prevent coherence [76]. In normal labor, regular contractions of the uterus progressively dilate the cervix, eventually resulting in natural delivery. This requires rhythmic wave-like activity that propagates along the myometrium to be directed from a source located near the fundus [Fig. 2.1 (a)] [77, 78, 79, 80, 58, 81]. Understanding how such apparent "fundal dominance" [82] comes about, despite the absence of any specialized group of pacemaker cells in the uterus, is important as labor dystocia, involving abnormally slow progress of labor or its complete arrest, is a significant cause of maternal as well as fetal morbidity [83]. Currently, the treatment of such birth disorders involve non-elective primary cesarean delivery (accounting for more than a third of such procedures in USA [84]), which increases the risk of adverse maternal and neonatal outcomes [85, 86]. Elucidating the mechanisms by which coordination over the entire organ is achieved prior to parturition can help in devising safer intervention methods.

From the perspective of dynamical systems, the problem is one of breaking the spatial symmetry so that certain regions impose their rhythmic pattern on the rest of the system by means of excitation wavefronts that initiate contraction as they propagate through the medium. Thus, although arising through self-organization, such a system may appear to possess a "pacemaker" region from which waves activating the rest of the medium originate. A feasible symmetry-breaking mechanism in biological oscillatory medium is to have a spatial gradient in the frequency of periodic activity. Indeed, we note that such a frequency gradient is known to exist for slow waves in the small intestine which provides polarity to peristaltic contractions [87, 88, 49]. In the case of the uterus, which has a highly heterogeneous cellular composition, the frequency of activity can be modulated by the coupling between excitable smooth muscle cells (myocytes) and electrically passive cells, such as fibroblasts and Interstitial Cajal-like cells (ICLC) [inset of Fig. 2.1 (a)]. Thus, a frequency gradient could arise from a variation in the density of passive cells

coupled to myocytes and/or the expression of connexin proteins forming gap junctions that regulate the inter-cellular coupling. This in turn could be the result of signaling molecules diffusing from a source, which, if located at the upper end of the uterus, e.g., near the fundus, will lead to a gradually decreasing concentration of coupled passive cells and/or gap junctions. In this chapter we investigate the consequences of the existence of such a spatial symmetry-breaking gradient on the dynamics of the system. Specifically, we show that a sufficiently steep gradient will result in the emergence of one (or few) organizing centers of activity that are spatially localized in the medium. Thus, even in the absence of pacemaker cells, contractions will appear to be coordinated by waves emanating from a source whose location, depending on the gradient, can be near the fundus.

2.2   The Model

To model dynamical activity in gravid uterine tissue, we note that the number of gap junctions increases significantly over the course of pregnancy [89, 90], eventually promoting co-ordination of periodic activity across the entire organ [91, 92, 93]. Following Refs. [60, 59], we consider rhythmogenesis in this system to be a self-organized outcome of interacting heterogeneous non-oscillating cells. Indeed, in the uterus, no experimental evidence for specialized pacemaker cells [94, 91] or for myocytes capable of auto-rhythmicity [95] has been found so far. We describe the activity of a uterine myocyte in terms of the cellular transmembrane potential V_e and effective conductance g using the FitzHugh-Nagumo model [18]. This is a generic representation of the dynamics of an excitable system [98], which qualitatively reproduces the behavior seen in more physiologically realistic models of uterine activity [22]. The pair of coupled equations specifying this model are: $\dot{V_e} = F_e(V_e, g) = AV_e(V_e - \alpha)(1 - V_e) - g, \dot{g} = G(V_e, g) = \epsilon(V_e - g)$, where the parameters $A(= 3), \alpha(= 0.2)$ and $\epsilon(= 0.08)$ govern the fast activation kinetics, excitation threshold

17

and recovery rate, respectively. The dynamical state of a passive cell is characterized by its membrane potential V_p which evolves as $\dot{V}_p = F_p(V_p) = K(V_p^R - V_p)$ where $V_p^R(= 1.5)$ is the resting state value of V_p and $K(= 0.25)$ is the corresponding timescale [99]. We investigate the propagation of electrical activity across the organ by considering a system comprising cells arranged in a 2-dimensional lattice of size $L \times L$. As the simulation domain is meant to represent electrical activity over the entire uterine myometrium, we implement periodic boundary condition along the vertical edges and no-flux along the horizontal edges of the lattice. Each lattice point i comprises an excitable cell coupled to n_p^i passive cells ($n_p^i = 0, 1, 2...$) with strength C_r, while neighboring excitable cells interact diffusively with strength D. Thus, the dynamics of the spatially extended system is described as:

$$
\begin{aligned}
\frac{dV_e^i}{dt} &= F_e(V_e^i, g^i) + n_p^i C_r(V_p^i - V_e^i) + D\sum_{\langle i,j \rangle}(V_e^j - V_e^i), \\
\frac{dg^i}{dt} &= G(V_e^i, g^i), \\
\frac{dV_p^i}{dt} &= K(V_p^R - V_p^i) - C_r(V_p^i - V_e^i).
\end{aligned}
\tag{2.1}
$$

where $\langle i, j \rangle$ represents the set of excitable cells that neighbor i ($i = 1, \ldots L^2$). For the simulations reported here we have chosen $L = 450$. We have verified that our results are qualitatively similar for smaller lattice sizes $L \geq 128$. We assume $D = C_r$ suggesting that gap-junctions are equally likely to couple excitable cells with other excitable cells and to passive cells. Note that, all the passive cells connected to a given excitable cell at i behave identically and hence are represented using the single variable V_p^i. The value of n_p at each lattice site (l, m) is randomly sampled from a Poisson distribution with parameter $\lambda(l, m)$, whose global average is the ratio f of the total number of passive cells to the number of excitable cells in the lattice.

Coupling excitable cells to passive ones can induce autonomous periodic activity which
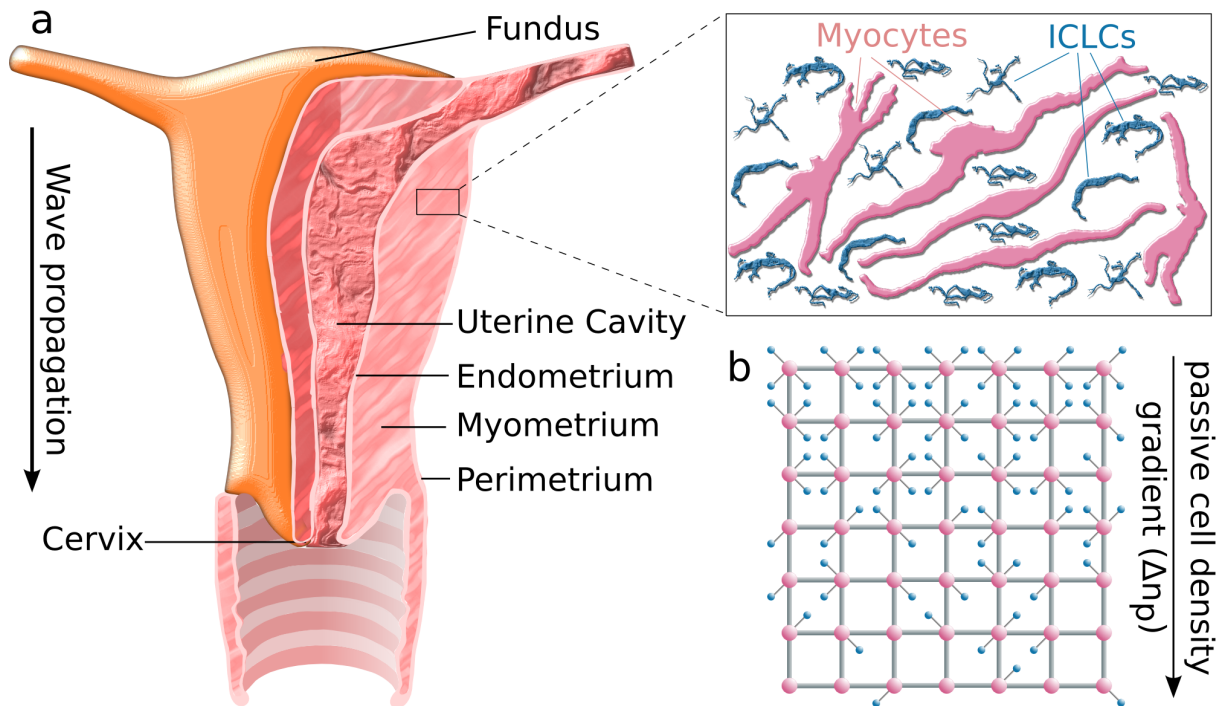
Figure 2.1: Schematic representations of a human uterus and the uterine myometrium. (a) Schematic diagram of a human uterus, which immediately before parturition exhibits coherent excitation activity appearing to propagate from the fundus to the cervix. A cross-section along the uterine wall is shown to indicate the myometrium, whose heterogeneous cellular composition, comprising excitable (myocytes) and passive (ICLCs) cells is shown in the inset [adapted from Refs. [96] and [97], respectively, and drawn to scale]. (b) The uterine myometrium is modeled as a two-dimensional square lattice with each site occupied by an excitable cell coupled to passive cells, whose density is proposed to decrease monotonically along the organ from the fundus to the cervix (i.e., along the vertical axis of the lattice).

is absent in isolation in either of the cell types [60, 59, 100]. The frequency of oscillations at each site (l, m) depends in a non-monotonic manner on n_p (see Fig. 1 b of Ref. [59]), and hence on $\lambda(l, m)$, as well as, the coupling constant $C_r(= D)$ (see Fig. 1 c of Ref. [59]). Thus, by introducing a linear gradient in the passive cell density along the longitudinal axis of the domain, viz., $\lambda(l, m) = [l - (L/2)]\Delta n_p + n_p^{mid}$ [Fig. 2.1 (b)], we can obtain a systematic variation in the frequency of oscillation across space. We have examined density gradients chosen from a range in which the frequency will, on average, change monotonically across the longitudinal axis, viz., $0 \leq \Delta n_p \leq 9 \times 10^{-4}$. For a system size L and slope Δn_p of the gradient, we choose n_p^{mid}, the value of n_p at the center of the domain, such that $f = 0.7$, which ensures oscillatory behavior. We have verified that the behavior reported here is robust over multiple realizations with random initial conditions and passive cell distributions. We note that similar frequency gradients can arise from variation in the gap-junction coupling strength (D, C_r) as a result of spatial heterogeneity in the expression of connexin proteins.

To model the increase in inter-cellular coupling in the gravid uterus over time [73], we have adiabatically increased $C_r(= D)$ over the entire simulation domain after starting from random initial conditions for a sufficiently low value of the coupling. For a dynamical system having multiple attractors, such an approach may yield strikingly different behavior for the evolving system compared to the states observed when the coupling strengths are temporally invariant (see Appendix A).

2.3   Results

In order to understand the effect of having a gradient in the density of passive cells, and by extension, the frequency of local spontaneous activation in the medium, we systematically vary the slope of the gradient Δn_p and the inter-cellular coupling strength $D(= C_r)$.
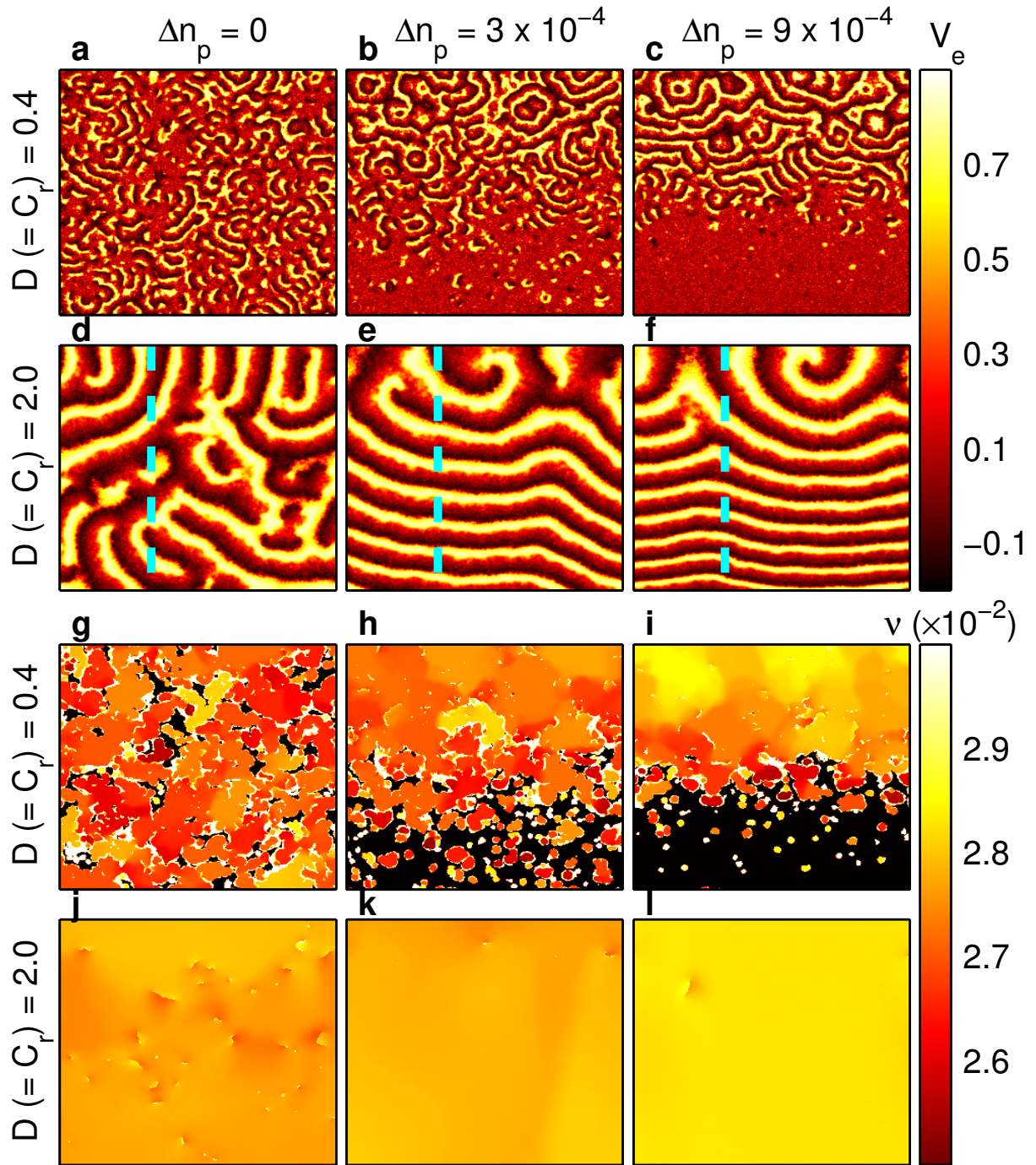
Figure 2.2: Propagation of excitation waves along the medium gets more organized with increasing slope Δn_p of the passive cell density gradient. (a-f) Snapshots of the activity V_e in a two-dimensional simulation domain ($L = 450$) for two different values of inter-cellular coupling strengths $D(= C_r)$ [first row: $D = 0.4$, second row: $D = 2$]. The homogeneous

Figure 2.2 *(previous page)*: system obtained in the absence of the density gradient [left column: $\Delta n_p = 0$] is compared with the situations seen for finite gradients [middle column: $\Delta n_p = 3 \times 10^{-4}$ and right column:$\Delta n_p = 9 \times 10^{-4}$]. (g-l) The corresponding pseudocolor plots indicating the oscillation frequencies of individual sites in the medium (black: absence of oscillation). For lower coupling strength [third row: $D = 0.4$], increasing passive cell density gradient results in distinct frequency clusters merging with each other. For sufficiently high gradient the medium is divided into a region exhibiting activity (corresponding to higher passive cell density) and an almost quiescent region (at lower density). However, for higher coupling strength, viz., $D = 2$ [fourth row: $\Delta n_p = 9 \times 10^{-4}$], the system exhibits global synchronization with effectively a single frequency dominating the activity in the entire medium. Localized phase defects correspond to tips of spiral waves (second row). With increasing density gradient, we observe fewer spiral waves. Furthermore, they are confined to the region having higher passive cell density, which appears as the source of excitation fronts propagating across the domain.

Fig. 2.2 shows snapshots of the collective dynamics, represented by the field corresponding to the excitable cell transmembrane potential (V_e, panels a-f) and that of the local frequencies (ν, panels g-l), for different choices of Δn_p and $D(= C_r)$. In the absence of a gradient ($\Delta n_p = 0$), the activity is not confined to any particular spatial domain even at low values of coupling (panel a). Through stochastic fluctuations certain lattice sites have higher values of n_p than their neighbors. As a result, the oscillating activity in such a site dominates the local region on account of having the highest frequency [98]. Thus, we observe a large number of autonomous sources of excitation, each generating waves that are confined to its local region of influence. Introducing a gradient with finite Δn_p (panels b and c) results in a spatial heterogeneity in the distribution of such excitation sources. At the upper end of the gradient, sites will typically have higher frequencies (arising from the larger values of n_p on average) compared to the rest of the medium (panel h). In contrast, n_p is small at the lower end of the gradient, resulting in either the absence of sources of oscillatory activity or ones having relatively much lower frequencies. On increasing the gradient, we observe the activity to become more localized (compare panels b and c) and the spatial ordering of frequencies to become more pronounced (see panels h and i).

When the inter-cellular coupling is increased (Fig. 2.2, d-f), we observe increased wave-

length for the propagating excitation fronts and in general, higher coordination in activity across regions. This is apparent on comparing between the corresponding spatial distributions of frequencies in panels g-i (low coupling) and panels j-l (high coupling). The clusters of distinct frequencies seen for low $D(=C_r)$ (panel g) become homogenized upon increasing the coupling (panel j), essentially resulting in synchronization of oscillatory activity across the domain. We also note in this case (i.e., for $\Delta n_p = 0$) the presence of rotating *spiral waves* which are characterized by the existence of a phase singularity at the spiral tip [98]. The propagating fronts have no preferred orientation as the passive cell density is homogeneous on average. There are also no constraints on where the spiral waves can occur, which is reflected in the coexistence of several competing organizing centers of wave activity. The introduction of a gradient in n_p (panel e) breaks this spatial symmetry, resulting in spiral waves at the upper end of the gradient activating the surrounding region at a frequency higher than that elsewhere. The activity of the entire domain is eventually enslaved to that of these organizing centers, which consequently are drastically reduced in number and spatially localized at the fundal end. This is consistent with empirical observations of multiple foci of activity in this region in different species [101]. This localization becomes more pronounced with increasing Δn_p (panel f), with activity appearing to emanate exclusively from a source at the upper end of the domain (the exact location of the source varies depending on the realization of the n_p distribution). These results demonstrate that unidirectional propagation of excitation waves can arise in a system with a gradient in the density of coupling between non-oscillatory cells.

This can be explicitly seen from Fig. 2.3 (a) which displays the space-time evolution of membrane potential along a longitudinal section of the simulation domain (indicated by the broken lines in Fig. 2.2, panels d-f). When $\Delta n_p = 0$, activity is seen to be initiated by multiple sources located at different parts of the domain (left panel). For finite Δn_p, a
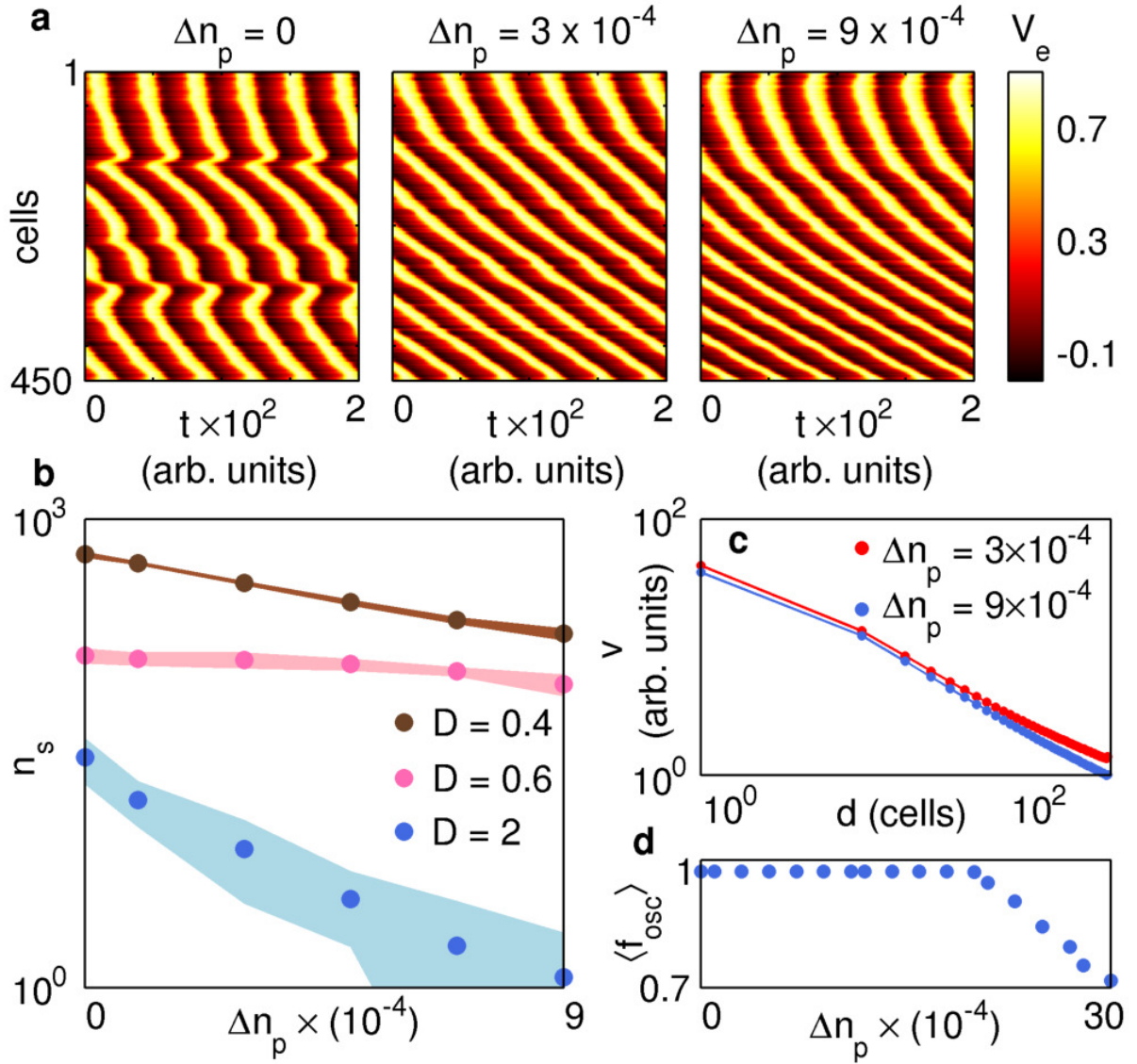
Figure 2.3: Increasing passive cell density gradient promotes unidirectional propagation of excitation waves through the medium. (a) Spatio-temporal evolution of the activity V_e for three different values of the gradient Δn_p in the medium along the broken line segments shown in Fig. 2.2 (d-f) respectively. In the absence of a gradient, the system exhibits multiple coordination centers, characterized by excitation fronts propagating away from them. Introducing a gradient in n_p results in a sharp reduction in their number, with the waves emanating from centers that are localized at the higher end of the gradient. (b) Decrease in the number of phase singularities with increasing Δn_p shown for different values of inter-cellular coupling $D(=C_r)$. The mean (filled circles) and standard deviation (shaded regions) of the temporal average of the number of phase singularities n_s, calculated over an ensemble, are displayed. (c) The phase

Figure 2.3 *(previous page)*: velocity v of the excitation front is measured along a one-dimensional chain with linear gradients in n_p, and decreases with distance d from the higher end of the gradient. (d) The mean fraction of oscillating cells f_{osc} in the medium obtained by averaging over an ensemble shown as a function of the slope Δn_p of the passive cell density gradient.

single source located at the upper end drives activity across the domain, with waves originating from this site propagating through the entire medium (center and right panels). As already mentioned above, the number of organizing centers decreases with increasing slope Δn_p of the passive cell density gradient and/or the inter-cellular coupling strength $D(= C_r)$. We quantitatively establish this in terms of the variation in the number of phase singularities n_s corresponding to the spiral tips as a function of these parameters (Fig. 2.3, b). [1] Taken together, these results demonstrate that the existence of a centralized pacemaker region near the fundus is not necessary to explain the coordination of uterine activity.

The phase velocity v of the propagating excitation front is seen to be a decreasing function of the distance d from the organizing center (Fig. 2.3, c). [2] It reflects the decrease in the intrinsic frequencies of the oscillators arising from the reduction in n_p along the longitudinal axis. As can be seen from the figure, v drops with d more sharply as Δn_p is increased. We note that this observation suggests a testable prediction of the mechanism proposed here for the coordination of uterine activity. Specifically, a spatial gradient of cellular coupling being responsible for the observed phenomena cannot be ruled out unless the phase velocity for propagating activity on the uterus is shown to be independent of the distance from a putative pacemaker region. Moreover, by measuring the dependence of the phase velocity on this distance, it may be possible to infer the steepness of this gradient

---

[1]Phase singularities are identified as the points of intersection of the isoclines of the V_e field at two different times separated by a small interval.

[2]To prevent the stochastic fluctuations in the passive cell density gradient from obscuring the relation between phase velocity and the distance of the wave from the organizing center, we have obtained it along a one-dimensional section parallel to the gradient with the n_p at site l equal to $\lambda(l)(= [l-(L/2)]\Delta n_p + n_p^{mid})$.

empirically.

Further increase of Δn_p beyond the range considered so far eventually results in partial cessation of activity in the medium. Fig. 2.3 (d) shows that when the slope $\Delta n_p \geq 2 \times 10^{-3}$, the fraction of oscillating cells in the lattice begins to reduce from 1 as the number of passive cells at the lower end of the density gradient become insufficient for supporting spontaneous activity. We note that in the limit of extremely high Δn_p (corresponding to the passive cell density varying as a step function), the system reduces to one having all oscillating cells confined in the upper segment, with no activity propagating to the lower segment of the domain. While the oscillating region at the top has the potential to effectively function as a pacemaker, its inability to activate the rest of the medium rules this out as a plausible mechanism operating in the uterus. [3]

2.4   Discussion and Conclusion

Recent studies have suggested that for smaller mammals, such as guinea pigs, activity can arise from anywhere within the myometrium [101]. However, it has been pointed out that successful vaginal delivery in humans is usually associated with fundal dominance [82, 58, 81]. Our results suggest that coherence can be achieved even in the absence of a spatially localized coordinating center in animals whose uteri have linear dimensions smaller than the wavelength of the propagating activity. Thus, a spatial symmetry-breaking gradient may be crucial only for animals with extended uteri, where co-existing wave sources need to be coordinated in order to achieve coherent contraction. Indeed, arrested labor may result if the source of activity is located far below the fundus in the human uterus [81], and in some cases, the presence of multiple sources may also cause uterine fibrillation [82].

---

[3]Reducing the excitation threshold results in an abrupt transition from no activity to high-frequency synchronized oscillations on increasing coupling, inconsistent with the gradual increase in frequency observed in the gravid uterus.

Furthermore, we note that the location of the coordination centers in different realizations can vary because of the stochastic nature of the n_p distribution along the gradient. This suggests a possible explanation for the continuing uncertainty regarding the position of the foci of uterine activity in experimental studies [102, 93].

Chapter 3

Spontaneous generation of persistent activity in diffusively coupled cellular assemblies

3.1 Introduction

Spontaneously recurring electrical activity is of crucial significance in a number of physiological contexts [103, 67, 98]. This is typically driven by pacemaker cells [23, 71, 72], such as the sinoatrial node in the heart which comprises specialized cells that periodically generate signals initiating excitatory activity, leading to mechanical contraction [104]. However, such cells have not been observed in other contractile tissue, such as the myometrium of the gravid uterus [73]. It has been hypothesized that spontaneous activity in the latter contexts arise through interactions between electrically active and passive cells, local assemblies of which are capable of generating periodic waves of activation in the tissue through diffusive coupling [74, 75]. These waves traveling through an organ are capable of sustaining spatio-temporally coherent contractions [59, 105]. Indeed it has been demonstrated that one of

the simplest ways to achieve this is by having an excitable cell coupled by gap-junctions to one (or more) electrically passive cells characterized by a resting state membrane potential that is much higher than that of the excitable cell [60]. The coupling between these heterogeneous cell types causes the membrane potential of the excitable cell to be driven beyond its threshold, resulting in the generation of an action potential. Subsequently, the excitable cell attempts to return to its resting state, but after a period of recovery is again driven to exceed its threshold by the passive cells coupled to it, thereby resulting in a periodically recurring series of action potentials. Thus, although neither excitable nor passive cells are individually capable of spontaneous sustained activation, an assembly of these two cell types can generate periodic oscillations [106].

The emergence of periodic activity in a heterogeneous assembly of excitable and passive cells makes such a mechanism a viable candidate for self-organized system-wide coherent oscillations in physiological contexts where no pacemakers have been reported [94, 107]. Indeed, it has been demonstrated that a lattice of excitable cells that are each coupled to a variable number of passive cells, can exhibit a range of spatio-temporal phenomena consistent with those observed in the uterus during the transition to coherent activity seen prior to parturition [59, 100, 22, 105]. However, noting that each local cellular assembly are either in an excitable or an oscillatory dynamical regime in isolation, raises an important question: can the observed collective behavior be reproduced in an even simpler setting, viz., where each lattice site is occupied by either an oscillatory or an excitable element, a situation reminiscent of percolation [108]. In this chapter, we consider the dynamics of two classes of systems, each capable of exhibiting spontaneous collective dynamics, one comprising electrically active and passive cells (EP) and the other comprising oscillatory and excitable cells (OE). We observe that simple motifs of cells described using the EP model are capable of exhibiting a wide range of complex collective dynamical patterns. However, several of these are no longer observed when such cells are embedded in a spatially

extended system, suggesting an emergent simplicity of the collective dynamics. More importantly, we observe that when cells described by the OE model are placed on a lattice, the resulting dynamics are qualitatively very similar to that obtained using the EP model. This points towards a more fundamental mechanism that could explain the emergence of spontaneous recurrent activity in physiologically relevant contexts.

3.2   The Model

To investigate in detail the range of complex behavior that emerges upon diffusively coupling excitable cells, each of which are in turn coupled to one or more passive cells, we consider the simplest possible assemblies of these cells capable of exhibiting spontaneous oscillatory activity. Following Ref. [59], we simulate the electrical activity of an excitable cell using the FitzHugh-Nagumo (FHN) model [18], which is capable of both excitable and oscillatory dynamics. The model describes the temporal evolution of an activation variable V_e (the membrane potential), and an inactivation variable g (an effective trans-membrane conductance) as $\dot{V}_e = \mathcal{F}(V_e, g)$, $\dot{g} = \mathcal{G}(V_e, g)$. Here, $\mathcal{F}(V_e, g) = A\,V_e\,(V_e - \alpha)(1 - V_e) - g$ and $\mathcal{G}(V_e, g) = \epsilon(k_e V_e - g - b)$, where $A(=3)$ and $k_e(=1)$ govern the kinetics, $\alpha(=0.2)$ is the excitation threshold and $\epsilon(=0.08)$ is the recovery rate, while b provides a measure of the asymmetry of the limit cycle.

We observe that the real part of the eigenvalues (λ_R) of a single FHN unit, obtained from a linear stability analysis, is negative below a lower critical value $b_{c1} \simeq 0.136$ and above a higher critical value $b_{c2} \simeq 0.376$, indicating that the system does not oscillate for these ranges of b [Fig. 3.1 (a)]. As seen in Fig. 3.1 (b), the value of V_e in the resting state is close to 0 for $b < b_{c1}$ and is relatively large for $b > b_{c2}$. These regimes are hence referred to as "low" and "high" stable states, respectively. Furthermore, the system is capable of oscillatory behavior for $b_{c1} < b < b_{c2}$, as λ_R is positive in this range. The frequency of
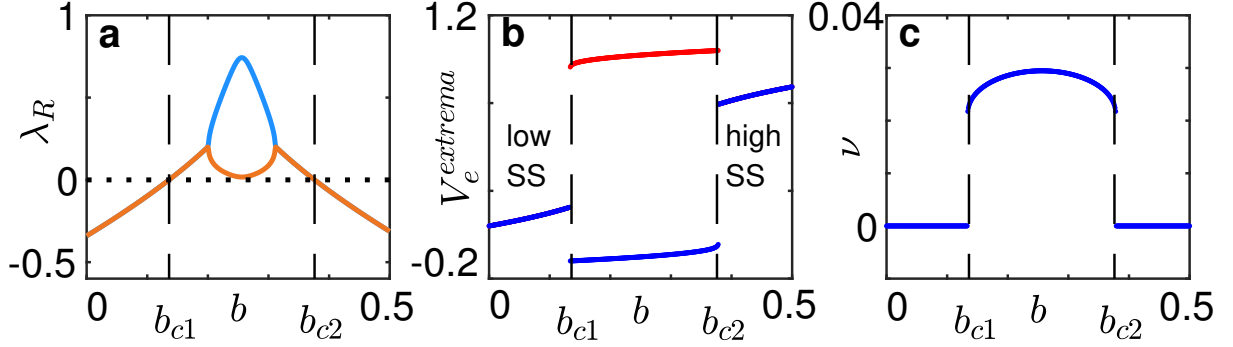
Figure 3.1: Dependence of the dynamics of a single uncoupled FHN oscillator on the parameter b. (a) Real part of the eigenvalues (λ_R), obtained through a linear stability analysis, for a range of values of b. We find that λ_R crosses zero (horizontal broken line) at $b = b_{c1} (\simeq 0.136)$ and $b = b_{c2} (\simeq 0.376)$. (b) The system exhibits a low steady state ("low SS") for $b < b_{c1}$ and a high steady state ("high SS") for $b > b_{c2}$, as can be seen from the fact that the extrema of V_e (red and blue markers) coincide over these values of b. (c) In the range $b_{c1} < b < b_{c2}$, we observe oscillatory behavior, with the frequency ν exhibiting a maximum value at the center of this range. For reference, we display vertical dashed lines at $b = b_{c1}$ and $b = b_{c2}$ in each of the panels.

oscillations ν exhibits a maximum value at the midpoint $(b_{c1} + b_{c2})/2$ [Fig. 3.1 (c)].

The temporal evolution of the passive cell is described in terms of its membrane potential V_p as $\dot{V}_p = K\,(V_p^R - V_p)$, where $V_p^R(= 1.5)$ is the resting state and $K(= 0.25)$ is the relaxation rate [99]. Each excitable cell is electrically coupled to $n_p \,(= 0, 1, 2 \dots)$ passive cells, where the conductance of the gap junctions between the two cell types is C_r. The set of equations used to describe the dynamics of an excitable cell i coupled to n_p^i passive cells, as well as to other excitable cells j, is:

$$
\begin{aligned}
\frac{dV_e^i}{dt} &= \mathcal{F}(V_e^i, g^i) + n_p^i C_r(V_p^i - V_e^i) + D \sum_{j \neq i}(V_e^j - V_e^i)\,, \\
\frac{dg^i}{dt} &= \mathcal{G}(V_e^i, g^i)\,, \\
\frac{dV_p^i}{dt} &= K(V_p^R - V_p^i) - C_r(V_p^i - V_e^i)\,.
\end{aligned}
\tag{3.1}
$$

The dynamics of an isolated excitable cell coupled to one or more passive cells depends

on n_p and C_r. As V_p^R is much higher than the excitation threshold α, for a range of n_p and C_r the coupled excitable-passive system can exhibit oscillations. To demonstrate that such emergent oscillations result exclusively from the coupling we have chosen $b = 0$, so that in isolation the FHN dynamics converges to the low stable state. It is important to note in the context of the results reported here that when $C_r > 0.5$, oscillations are seen only for $n_p = 1$ while those excitable cells coupled to $n_p > 1$ passive cells converge to high stable states.

3.3   Results

We first consider the simplest non-trivial assembly of dissimilar excitable-passive units, viz., a pair of excitable cells diffusively coupled with strength D, each interacting with a different number n_p of passive cells with strength C_r. The heterogeneity in n_p implies that the intrinsic behavior of the two units are dissimilar, and this can lead to a range of distinct collective dynamical patterns. The dynamical regimes obtained can be classified on the basis of the V_e time-series of the excitable cells, using a set of order parameters with specified threshold values (see Fig. 3.2 and Appendix B for details): (i) oscillation death (OD), where both cells are in the same temporally invariant non-zero steady state; (ii) inhomogeneous steady state (ISS), where both cells are in different temporally invariant steady states; (iii) chimera (Ch), where only one of the two cells oscillate; (iv) inhomogeneous in-phase synchronization (IIS), where both cells oscillate in-phase; (v) inhomogeneous out-of-phase synchronization (IOS), where both cells have the same frequency but are out-of-phase with each other, and, (vi) cluster synchronization (CS), where the two cells have different oscillation frequencies. The dynamical patterns obtained upon varying D and C_r are shown in Fig. 3.3 (a-d) for four distinct connection topologies of the assemblies [illustrated in the top right corners of the corresponding panels]. The regions are identified according to
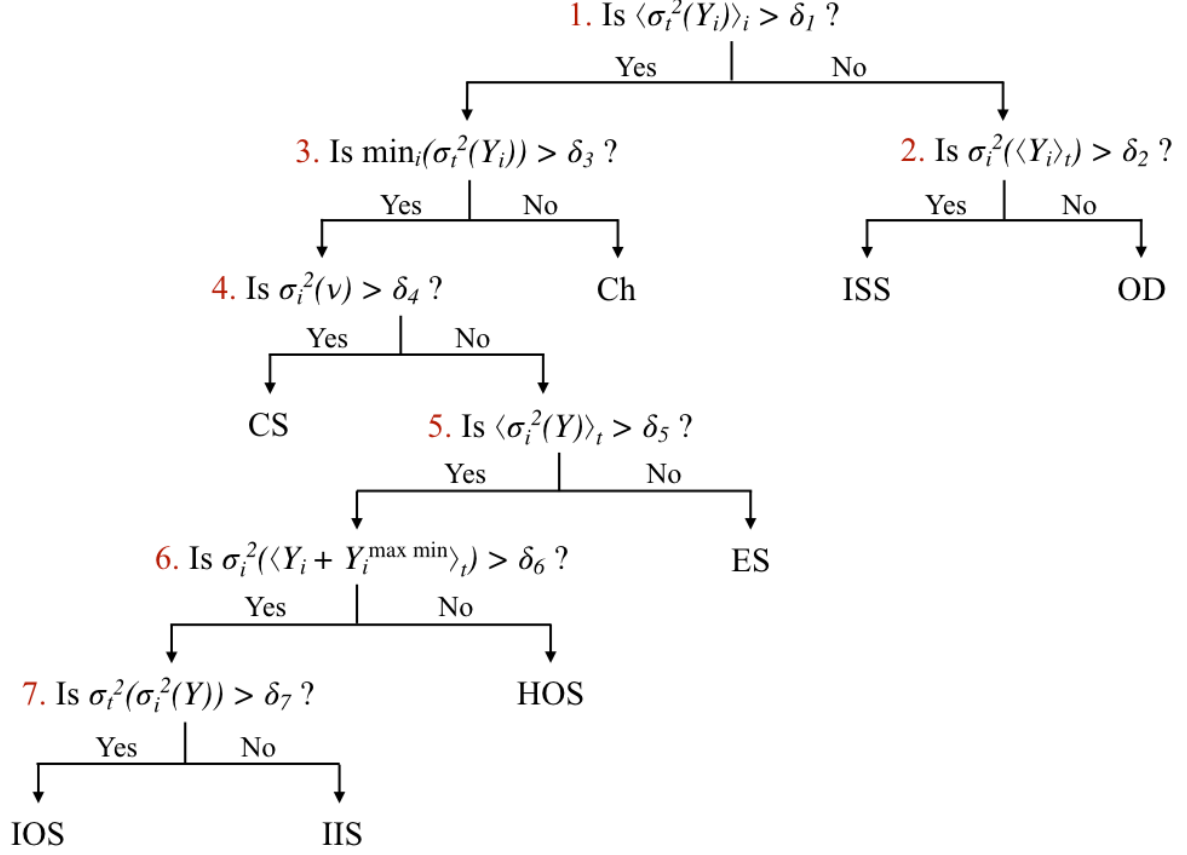
Figure 3.2: Decision tree for identifying the dynamical state of a system of coupled excitable cells, each of which are connected to a variable number of passive cells (EP model). The order parameters used for determining the nature of the spatio-temporal pattern observed include the dispersions calculated across space $[\sigma_i^2(\ )]$, or across time $[\sigma_t^2(\ )]$, for the state variables Y_i $(i = 1, \ldots, N)$ or the oscillation frequencies ν. Averages calculated over space and over time are denoted by $\langle\ \rangle_i$ and $\langle\ \rangle_t$ respectively, while the deviation of the lowest value of the state variable for any node from its maximum calculated across space is denoted by $Y_i^{\max\min} = \max_i(\min_t(Y_i)) - \min_t(Y_i)$ (see Appendix B). The threshold values used to distinguish between the different states, viz., Oscillation Death (OD), Inhomogeneous Steady State (ISS), Chimera (Ch), Cluster Synchronization (CS), Exact Synchronization (ES), Homogeneous Out-of-phase Synchronization (HOS), Inhomogeneous In-phase Synchronization (IIS), and Inhomogeneous Out-of-phase Synchronization (IOS), are: $\delta_1 = 10^{-3}$, $\delta_2 = 10^{-5}$, $\delta_3 = 10^{-3}$, $\delta_4 = 10^{-7}$, $\delta_5 = 10^{-5}$, $\delta_6 = 10^{-7}$, and $\delta_7 = 10^{-4}$.
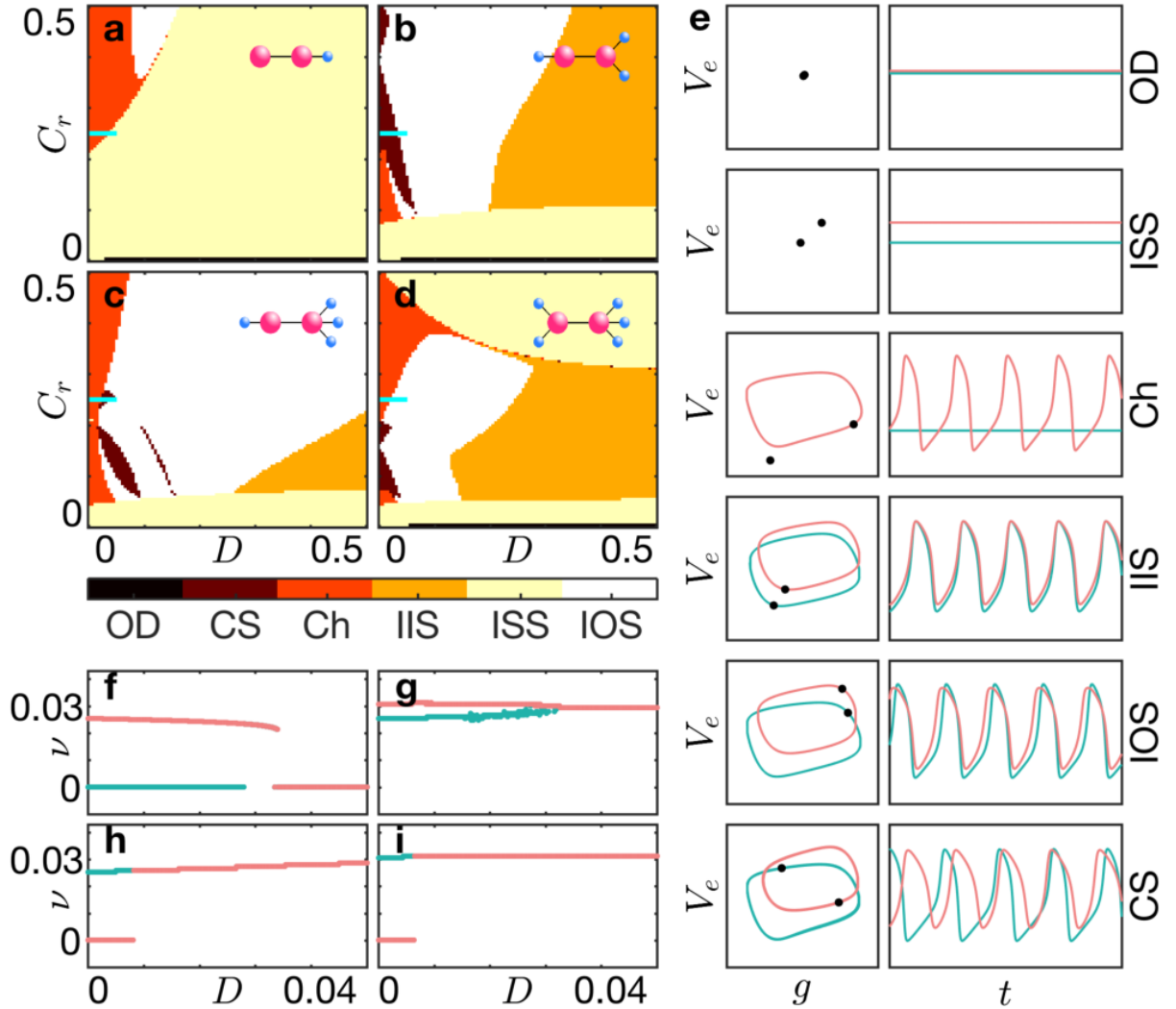
Figure 3.3: Emergent dynamics obtained with different motifs of diffusively coupled excitable and passive cells. (a-d) Collective dynamical patterns observed over a range of values of coupling strengths D and C_r, obtained using different motifs (shown as insets in the corresponding panels, where the larger and smaller circles represent excitable and passive cells, respectively). The regimes are classified according to the dominant attractor obtained for the given parameter set [see Fig. 3.2]. (e) Qualitative nature of the patterns in (a-d), in terms of the phase plane trajectories and time series of the excitable cells (see Appendix B). The black dots represent the instantaneous position of the two cells on the corresponding limit cycle. (f-i) Variation of the frequency ν of the excitable cells on the left (green) and right (maroon) in each of the four motifs in (a-d) for $C_r = 0.25$, over the range of D indicated by horizontal cyan bars in (a-d). As D increases, the frequencies of the two cells merge, and for sufficiently strong coupling the system can either stop oscillating (f), or display a frequency that is between (g), greater than (h) or equal to (i) the maximum of the intrinsic frequencies.

the collective dynamics observed for the majority ($> 50\%$) of initial conditions. At low values of D, the two units can behave very differently, and we observe collective states such as Ch or CS. As D increases, the cells either become frequency locked or cease oscillating altogether. Note that the intrinsic heterogeneity of the two units prevents exact synchronization between them even for large D. For a given value of D, as C_r is decreased, eventually the cells stop oscillating (in isolation, neither an excitable nor a passive cell is capable of spontaneous activity). The qualitative nature of the collective dynamical patterns, in terms of (V_e,g) phase plane trajectories and individual time series, is displayed in Fig. 3.3 (e).

In Fig. 3.3 (f-i), we display the variation of the frequency ν of the periodic activity exhibited by the excitable cells in the low D regime in each of the different assemblies (C_r is fixed at 0.25 in each case). We observe that an increase in D either gives rise to the cessation of oscillations [Fig. 3.3(f)] or a synchronized state in which the two units oscillate at a common frequency that is either lower [Fig. 3.3(g)], higher [Fig. 3.3(h)] or equal to [Fig. 3.3(i)] the higher of the pair of intrinsic frequencies (i.e., the frequencies of each unit at $D = 0$). We note that these results are qualitatively robust with respect to changes in V_p^R (see Appendix B).

Just as coupling an excitable cell to one or more passive cells can, under appropriate conditions, give rise to oscillatory dynamics, we observe that spontaneous activity can arise upon coupling a pair of dissimilar units that do not oscillate in isolation. Fig. 3.4 (a) shows a pair of excitable cells, having $n_p = 0$ and $n_p = 2$ respectively, such that neither can independently oscillate for $C_r = 0.6$. However, upon increasing D sufficiently, we eventually observe a transition to a frequency synchronized state of the two units. We characterize this transition in terms of the eigenvalues obtained from a linear stability analysis. As seen in Fig. 3.4(b), we find that the real part of the eigenvalues λ_R are negative for small values of D, and that two of them change sign at $D \simeq 0.072$ [see inset of Fig. 3.4(b)]. This

35
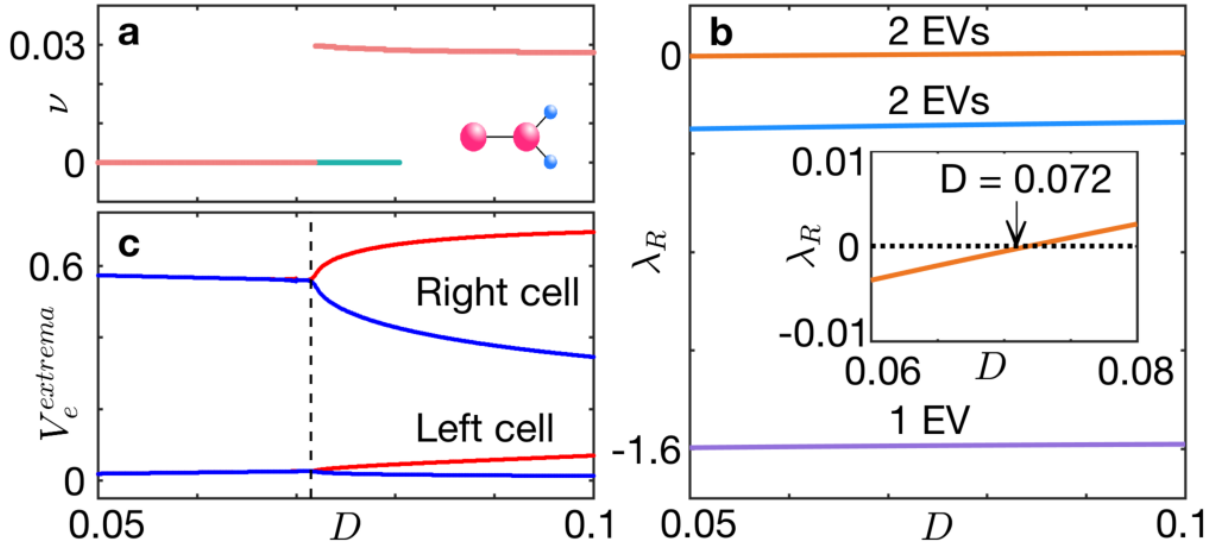
Figure 3.4: Spontaneous emergence of oscillatory activity upon coupling a pair of quiescent units. (a) Variation of ν with D for $C_r = 0.6$, obtained using the motif shown as an inset, i.e. a pair of coupled excitable cells that are attached to zero and two passive cells, respectively. Although both cells are quiescent for low D, they exhibit oscillations for sufficiently large D. (b) Dependence of λ_R, corresponding to the real parts of the five eigenvalues of the system, on D. We note that two pairs of eigenvalues (EV) are complex conjugates and hence their real parts overlap, as indicated above the corresponding branches. The inset displays a zoomed-in segment of the panel, indicating the value of D at which two of the eigenvalues changes sign. (c) Bifurcation diagram of the extrema values of V_e for this system, showing the transition from a stable steady state to oscillations, where the maximum and minimum values for each of the two excitable cells are indicated by red and blue markers, respectively.

corresponds to the onset of oscillations, as can be seen in Fig. 3.4(c).

Upon increasing the number of units in an assembly, we observe that the system becomes capable of exhibiting more complex collective behavior including chaotic activity. However, a particularly intriguing collective state of coexisting chaotic and non-chaotic activity is observed in an assembly of three excitable cells, having $n_p = 1, 2, 3$ respectively, that are coupled in a chain [see top right corner of Fig. 3.5 (a)]. For a large range of values of C_r and D, the system exhibits IOS [Fig. 3.5 (a)]. However, in the CS regime, we observe a collective dynamical state that is characterized by chaotic behavior in the excitable cell with $n_p = 1$ with non-chaotic, periodic oscillations in the other two cells [Fig. 3.5 (b-d)] The qualitative difference in the dynamics of the three excitable cells is evident upon comparing their time series [Fig. 3.5(b)], phase plane portraits [Fig. 3.5(c)] and power spectral densities [Fig. 3.5(d)]. A more rigorous comparison, considering the response of each cell to small perturbations, shows rapid divergence of the resulting trajectory from the unperturbed one for the chaotic unit, with no such deviation observed for the other two units (see Appendix B). We note that permutations of the connection topology of this assembly, i.e. changing the order in which the cells with different values of n_p are placed in the chain, yields similar qualitative behavior, with chaotic dynamics consistently observed in the unit with the lowest n_p.

It may appear that increasing the size of the assemblies further, by adding more coupled excitable-passive units, can only lead to a further increase in the complexity of the collective dynamics. However, surprisingly, we observe an *emergent simplicity* in the behavior of large lattices of such units, with neighboring elements coupled diffusively to each other. Indeed, such an example is provided by a spatially extended model of uterine tissue, which is heterogeneous by nature, comprising electrically active myocytes that are excitable (thereby facilitating muscle contractions), as well as electrically passive cells such as interstitial Cajal-like cells (ICLC) [97] and fibroblasts [see top panel of Fig. 3.6 (a)]. The
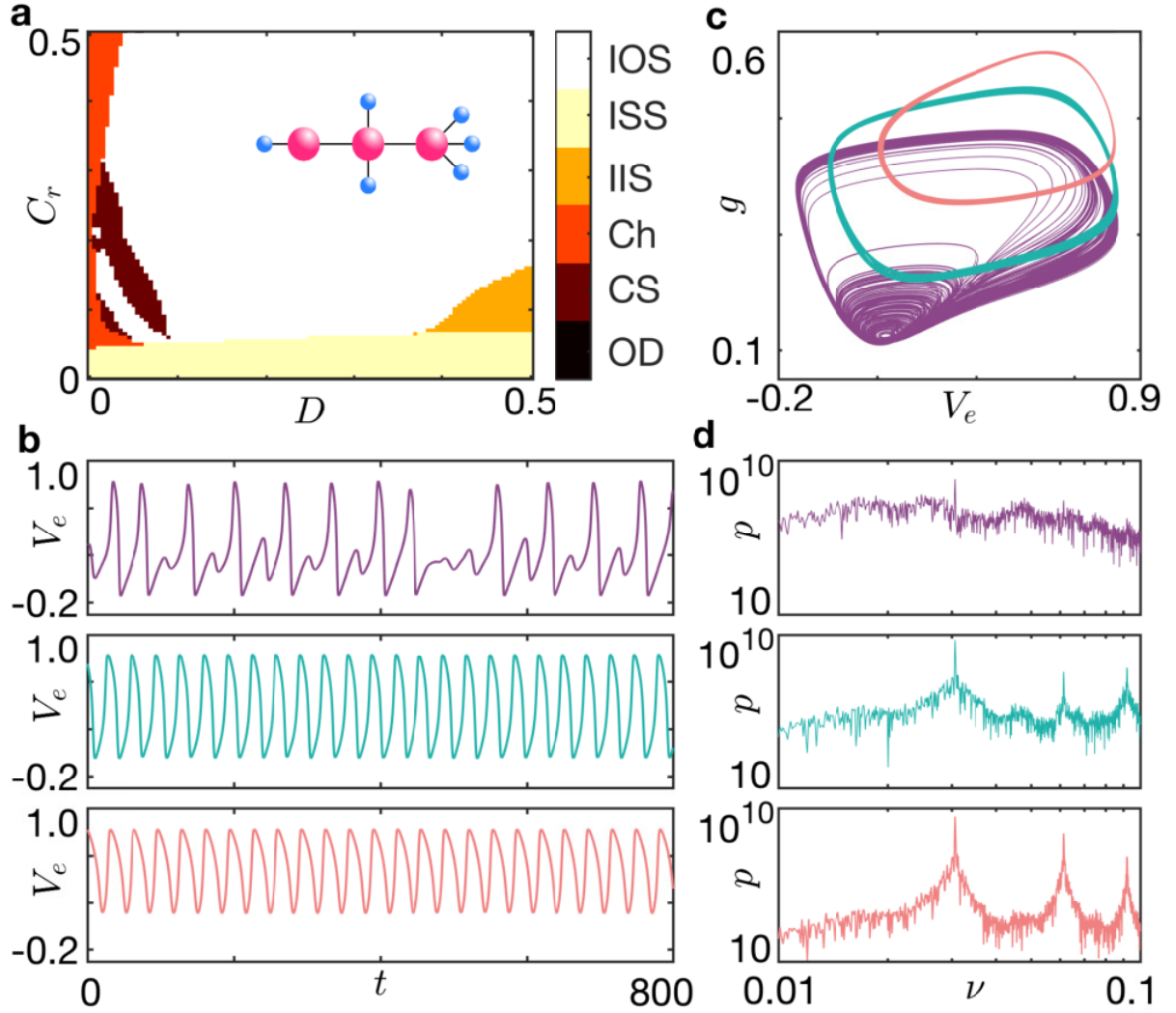
Figure 3.5: Coexistence of chaotic and non-chaotic dynamical activity in a system comprising three diffusively coupled excitable cells, each connected to a different number (n_p) of passive cells. (a) Collective dynamical patterns observed over a range of values of diffusive coupling strengths D between excitable cells and the coupling C_r between excitable and passive cells for the system shown as an inset. The dynamical regimes are classified according to the dominant attractor obtained for the given parameter set, and are the same as those detailed in Fig. 3.3 (a-d). (b) Time series of membrane potential V_e of the excitable cells coupled to (top) $n_p = 1$, (middle) $n_p = 2$ and (bottom) $n_p = 3$ passive cells, for $D = 0.02$ and $C_r = 0.19$. (c-d) Phase plane trajectories and power spectral densities of the three excitable cells, colored as in the corresponding panels of (b).

system exhibits spontaneous oscillations for a range of values of C_r even though, in isolation, none of the individual cells are capable of autonomous periodic activity, as has been experimentally observed in uterine tissue [94, 107]. More important from the perspective of the dynamical transition to periodic coordinated contraction of the myometrium, it is seen that increasing D results in the self-organized emergence of global synchronization, and eventually coherence [59, 22]. It is striking that such coordination is achieved exclusively through local interactions between cells and does not require a centralized pacemaker such as that present in the heart (viz., the sino-atrial node).

The relative simplicity of the collective behavior of such a lattice of heterogeneous coupled cells can be shown by demonstrating that it can be captured by a reduced description of the system in terms of interacting dynamical elements, each of which are either in an oscillating or a steady state. In particular, we can replace excitable-passive cell assemblies that are capable of spontaneous periodic activation by a single FHN unit with $b_{c1} < b < b_{c2}$ (for concreteness, we choose $b_{osc} = 0.192$ for the simulations whose results are shown here), and FHN units with $b < b_{c1}$ ($> b_{c2}$) for cell assemblies exhibiting a low (high) stable state (we choose $b_{exc}^{low} = 0$ and $b_{exc}^{high} = 0.394$ for the simulations shown here). The resulting equivalent lattice now comprises only FHN units, a fraction f of which are in an oscillatory regime with the remaining being excitable by virtue of having different values of b [see Fig. 3.6 (a), bottom panel]. Nevertheless, the system exhibits qualitatively identical behavior to that seen in models of uterine tissue simulated by coupling assemblies of excitable and passive elements, e.g., the occurrence of cluster synchronization at relatively low inter-cellular coupling that gives way to global synchronization of periodic activity (coordinated by propagating waves of excitation that traverse the lattice) for stronger coupling [Fig. 3.6 (b)].

The similarity of the emergent properties of the simpler model can be established further by comparing the different dynamical regimes of the $f - D$ parameter space with that
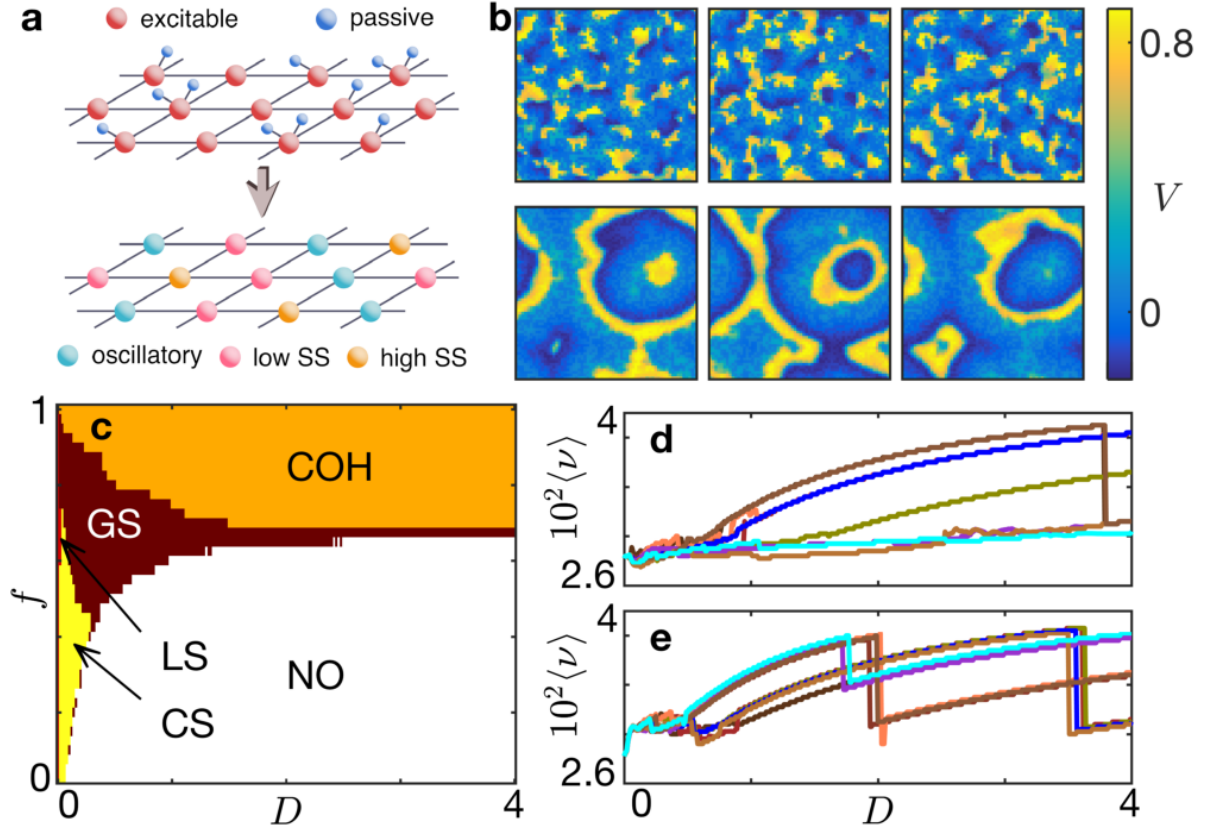
Figure 3.6: Collective dynamics of a lattice of diffusively coupled elements that can be either excitable or oscillatory. (a) Schematic diagram of uterine tissue, modeled as a two-dimensional lattice where each site comprises an excitable cell coupled to n_p passive cells (top, the "EP" model), where the value of n_p at each site is drawn from a Poisson distribution. The dynamics at each site can equivalently be described through cells that are either oscillatory or excitable (bottom, the "OE" model). The latter cell type could be in one of two possible steady states (SS), characterized by low and high values of the state variable V. Note that the state of a cell in the lower panel (high SS, low SS or oscillatory) is chosen such that the uncoupled dynamics at that site is qualitatively the same as that of the corresponding site in the upper panel. (b) Snapshots of the activity V in a planar simulation domain comprising an equal mixture of excitable and oscillatory elements ($f = 0.5$) diffusively coupled with strength D to nearest neighbors, showing (top row, $D = 0.1$) cluster synchronization (CS) and (bottom row, $D = 0.3$) global synchronization (GS). (c) Varying the diffusion coefficient D and the fraction of oscillatory cells f in the lattice for the case of the OE model, several distinct dynamical regimes are observed [see Fig. 3.7 for details]. (d-e) Variation of the mean oscillatory frequency $\langle \nu \rangle$ with D. Each curve is obtained by starting from different random initial states at low D and then gradually increasing D over time. In panel (d), the cell at each site can be either oscillatory (with probability $f = 0.7$) or excitable (with probability $1 - f$). In panel (e), we associate each lattice site with either an excitable or an oscillatory cell, following the procedure outlined in the main text. All simulations are performed on square lattices comprising 64×64 cells, with periodic boundary conditions.

40
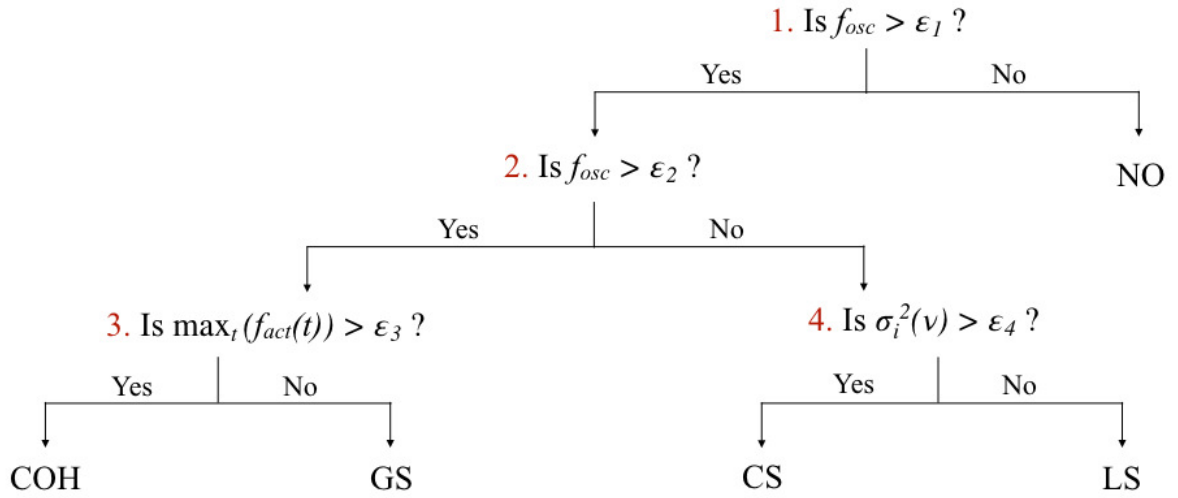
Figure 3.7: Decision tree for identifying the dynamical state of a heterogeneous system of coupled cells, each of which can either be in the oscillatory or the excitable regime (OE model). The order parameters used for determining the nature of the spatio-temporal pattern observed include (i) f_{osc}: the number of oscillating nodes in the lattice, (ii) $\max_t(f_{act}(t))$: the maximum number of nodes that were active (i.e., above the excitation threshold α) together over the period of observation, and (iii) $\sigma_i^2(\nu)$ is the dispersion of frequencies of all oscillating nodes calculated across space (see Appendix B). The threshold values used to distinguish between the states, viz., No Oscillations (NO), Cluster Synchronization (CS), Local Synchronization (LS), Global Synchronization (GS), and Coherence (COH), are: $\epsilon_1 = 10^{-3}$, $\epsilon_2 = 0.999$, $\epsilon_3 = 0.995$ and $\epsilon_4 = 10^{-10}$.

observed in the uterine model having heterogeneous cell types [59]. Indeed all the qualitatively distinct types of behavior reported in the latter can be seen in Fig. 3.6 (c), including No Oscillation (NO, with all cells in steady states), Cluster Synchronization (CS, marked by coexistence of multiple groups of cells, each characterized by a different frequency), Local Synchronization (LS, coexistence of quiescent cells with cells oscillating at a common frequency), Global Synchronization (GS, all cells have the same oscillation frequency) and Coherence (COH, all cells exhibit phase synchrony). The decision tree used to classify these dynamical patterns is displayed in Fig. 3.7 (see Appendix B for details). As in the EP model, the regions are identified according to the collective dynamics observed for the majority ($> 50\%$) of initial conditions.

In the limit of large D, the lattice dynamics can be further simplified and an implicit analytical equation can be obtained for f_c, the fraction of FHN units that should be oscillatory for the system to exhibit persistent periodic excitations. It marks the boundary between the NO and COH regimes and is given as $b_{c1} = (1 - f_c) \, b_{exc} + f_c \, b_{osc}$. For the situation shown in Fig. 3.6 (c), $b_{exc} = b_{exc}^{low}$, which yields $f_c \sim 0.7$ upon inserting the corresponding numerical values.

We can investigate the collective dynamics around this asymptotic boundary between persistent oscillatory activity and a quiescent steady state by considering the case $f = 0.7$. In particular, we focus on the variation of the overall activation rate, measured by the mean frequency of periodic activation $\langle \nu \rangle$ (averaged over all oscillating elements in the lattice), as D is increased. In order to be consistent with the physiological setting, where the coupling between cells increases over the gestation period (as a result of hormone induced increased expression of gap junctions that electrically couple the cells [109]), D is increased adiabatically over the course of a single realization, from a random initial condition at a low value of D. For the situation when $b_{exc} = b_{exc}^{low}$, shown in Fig. 3.6 (d), $\langle \nu \rangle$ increases with D until it reaches a maximum value related to the reciprocal of the refractory period
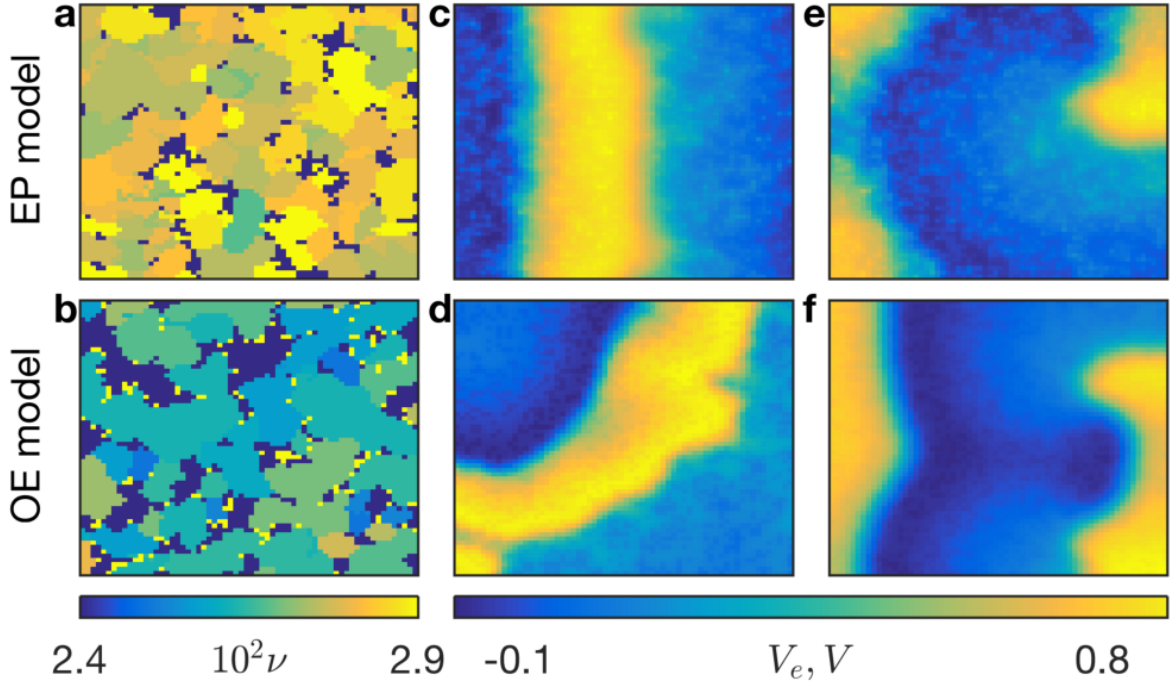
Figure 3.8: Comparison of the spatio-temporal activity in two-dimensional lattices of cells described by the EP and OE models. We find that similar behavior can be seen for systems characterized by a large number of coupled units arranged in two-dimensional lattices, where each cell is described by the EP model (top row) or the OE model (bottom row). The two models can yield (a,b) cluster synchronization, as evident from the spatial distribution of frequencies ν. In addition, both systems exhibit (c,d) travelling wavefronts, and (e,f) spiral waves, as can be seen from the instantaneous spatial distribution of V_e (top row) and V (bottom row), respectively.

(set by the parameters of the FHN model). Increasing D further results in an abrupt drop in $\langle \nu \rangle$ as the number of propagating wavefronts in the system changes. A subsequent increase in D results in an increase in $\langle \nu \rangle$ generated by the new spatio-temporal pattern. This is qualitatively the same as the phenomenon observed for the model of uterine tissue involving assemblies of excitable and passive cells.

An even closer match between the two classes of models can be obtained if we replace each of the excitable elements with FHN elements having either $b_{exc} = b_{exc}^{low}$ or $= b_{exc}^{high}$ according to the following procedure: first, each lattice site is assigned a value n chosen

from a Poisson distribution with mean $\lambda = f$. Note that this is identical to the process by which the number of passive cells (given by n) coupled to an excitable cell are determined in modeling uterine tissue with excitable-passive cell assemblies [59]. Next, FHN units in the oscillatory regime ($b = b_{osc}$) are placed at sites having $n = 1$, while FHN units with $b = b_{exc}^{low}$ (i.e., excitable element with a low stable state) are placed at sites with $n = 0$. At sites having $n > 1$, corresponding to excitable-passive cell assemblies whose activity is arrested at a high stable state, FHN units with $b = b_{exc}^{high}$ are placed. Fig. 3.6 (e) shows the evolution of the mean frequency with D for $f = 0.7$ when the cellular coupling is increased adiabatically starting from a random initial condition over the course of a single realization. The resulting oscillatory-excitable (OE) model can accurately reproduce dynamical behaviors reported for the model comprising excitable-passive (EP) cell assemblies [59]. These include the emergence of clusters characterized by a common oscillation frequency [Fig. 3.8 (a,b)], propagating wavefronts [Fig. 3.8 (c,d)], as well as self-sustained spiral waves in the GS regime [Fig. 3.8 (e,f)]. In addition, we observe that persistent periodic activity can arise upon coupling two FHN units that cannot independently oscillate, provided one of them is in the low and the other in the high stable state - a phenomenon analogous to the appearance of oscillations in assemblies of excitable and passive cells which cannot sustain autonomous activity (see Appendix B).

The qualitative equivalence of the collective behavior in large lattices for the two classes of models is all the more surprising as the dynamics of network motifs comprising excitable-passive cell assemblies [as seen in Figs. 3.3 and 3.5] is much more complex than that observed upon replacing each assembly by a FHN unit in the oscillatory or excitable regime. For instance, coupling a pair of EP cell assemblies, each of which oscillate at different frequencies, cannot give rise to exact synchronization even at large D. However, two FHN oscillators characterized by distinct b values (and hence, frequencies) can exhibit exact synchronization when coupled with sufficient strength. Furthermore, while we have

reported motifs of connected EP cell assemblies that exhibit chimera (Ch) regimes over a range of coupling strengths, such behavior cannot be seen in two coupled FHN oscillators with distinct intrinsic frequencies. We would also like to point out that nothing equivalent to the chaotic behavior observed in a motif comprising coupled EP cell assemblies [see Fig. 3.5] is seen in systems of coupled FHN oscillators arranged in a similar topology (viz., a chain comprising two oscillators having different intrinsic frequencies and an excitable element). Thus, even though the OE model reproduces the collective behavior of a large system of coupled EP cell assemblies, the dynamics at the microscopic level (i.e., motifs comprising only a few elements) can be extremely different for the two classes of models (see Appendix B).

3.4   Discussion and Conclusion

To conclude, in this chapter we have shown that while coupled excitable-passive cell assemblies are capable of exhibiting a wide range of dynamical behaviors including chaos, a macroscopic system comprising a large number of such elements diffusively coupled to their nearest neighbors on a lattice shows relatively simpler spatio-temporal phenomena. In particular, this resulting collective dynamics can be reproduced by a model comprising many elements, each described by a generic model for an excitable cell that is either in a steady state or in an oscillatory regime. Indeed, it suggests that the behavior associated with physiologically detailed models of uterine tissue activity [110, 100, 22] can be understood in terms of a reduced model involving a heterogeneous assembly of coupled oscillatory and excitable elements. More importantly, our results point towards a generalization of the mechanism proposed in Ref. [60] for the emergence of periodic activity in systems where none of the individual elements are intrinsically capable of oscillating. While it was shown there that persistent oscillations arise upon coupling excitable and electrically passive cells

under certain circumstances, here we have shown that an oscillating system may emerge upon coupling elements, each of which are in isolation at time-invariant steady states - provided these states are dissimilar (i.e., the state variables associated with them have sufficiently distinct numerical values, corresponding to "low" and "high"). Furthermore, our demonstration of a large variety of dynamical attractors in small assemblies of excitable and passive elements can provide an understanding of the complex dynamics seen in electrically coupled heterogeneous sub-cellular compartments in neurons [111, 112] and small networks of neurons interacting via gap-junctions [113].

Chapter 4

Interaction between spiral waves and the topological transition to vortex unbinding in systems of coupled biological oscillators

4.1 Introduction

Spiral waves, modelled by reaction-diffusion equations [29, 114], are a common phenomenon observed in a broad class of physical, biological and chemical excitable media [18]. In the biological context, they can be seen in a wide range of systems like egg fertilization in the *Xenopus* oocyte [115], cell aggregation patterns in *Dictyostelium* [116], spreading depression in the chick retina [117] and cardiac arrhythmias [56]. In the heart, spiral waves act as high-frequency sources of wave activity [98]. The resulting disruptions of the regular rhythmic activity of the heart are termed as arrhythmia [118]. Due to the robust nature of spiral wave dynamics, they have also been known to contribute to not just cardiac

47

arrhythmia, but to other pathological anomalies such as the patterns of activity found in epilepsy [119] and possibly, premature organ-wide excitation in the gravid uterus [120, 22]. Thus, understanding the dynamics of spiral waves may potentially lead to improved methods for controlling such phenomena.

Spiral waves, also referred to as a reentrant wave or a self-regenerative rotating wave, circles about an organizing center which is known as the spiral core and is a point of phase singularity [121, 122, 123]. A single-armed spiral is associated with a topological charge +1 or −1 according to the sense of its rotation (clockwise or counter-clockwise) [124, 125]. Depending on the underlying properties of the medium, a spiral can either rotate in a fixed position or meander in the medium or degenerate into multiple rotating wave fragments [126]. Other than spiral waves, planar travelling waves are also observed to coexist in excitable media [28]. Planar waves do not have any singularity attached to them making them dynamically distinct from the spiral waves and can be seen to propagate as a linear front or as concentric circles arising from a source. However, away from the source of a spiral or a target wave, it is not possible to distinguish one from the other as both send out circular wavefronts. In Ref. [127], it has been shown that in a homogeneous excitable medium, on giving a perturbation to one of the two arms of a double armed spiral, a stable asymmetric master-slave pair is formed. The perturbed arm of the spiral wave slows down and gets enslaved to the unperturbed arm which goes around the former tracing an involute. Here we investigate the difference in the dynamics observed in the medium due to the presence of a single topological defect. More specifically, we try to see if a stable master-slave combination can be formed if one of the spiral waves is replaced by a target wave which has zero topological charge.

In reality, excitable or oscillatory systems of biological relevance have more than one spiral wave present in the medium. We conduct initial studies regarding the association of the sign of the topological charge to the chirality of a spiral wave using one of the most

representative models of coupled phase oscillators, the Kuramoto model. Subsequently, we consider a relatively more detailed model of coupled biological oscillators, the EP model - comprising excitable Fitzhugh Nagumo (FHN) elements connected to passive cells - which was previously considered in Chapter 3 and in our earlier work [128]. Here we consider the EP model with additive noise which is introduced in the system via the fast variable of the FHN unit. The addition of noise to the FHN equations has a biological motivation. The presence of membrane noise due to stochasticity has long been established experimentally [129, 130]. This membrane noise can give rise to threshold fluctuations in the firing of excitable cells. One of the simplest ways to model this membrane noise is by considering an additive channel noise meant to represent the effect of stochastic activity of ion channels on the dynamics of the cell. On gradually increasing the intensity of noise in the system, we see a transition to vortex unbinding, reminiscent of what is observed in the 2-dimensional XY spin model investigate in statistical physics [131]. Our results can be relevant in understanding the genesis of Braxton-Hicks contractions or false labor [132], which are common organ-wide muscle activity experienced by some women in the third trimester of their pregnancy and are said to have a significant impact on foetal well-being. These contractions happen as a result of spontaneous but sporadic uterine activity that occurs much before true labor begins. Although the cause of these contractions is unknown, they have been suggested to happen in the absence of sufficient gap-junctional connectivity in the uterus [133]. We suggest that the formation of multiple vortices in the uterine myometrium can act as sources of wave activity that can give rise to these incoherent contractions.

4.2   The Model

To study the interaction of a single spiral wave with a target wave source we consider the Barkley model [134], a commonly used model of excitable and oscillatory media which is most often used to perform fast and efficient simulations of spiral and scroll waves. It is described by a set of reaction-diffusion equations involving a fast activation or excitation variable u and a slow inactivation or recovery variable v. The behavior of a single cell is described by:

$$\frac{\partial u}{\partial t} = f(u,v) + D\nabla^2 u$$

$$\frac{\partial v}{\partial t} = g(u,v)$$

(4.1)

where the reaction terms are $f(u,v)$ and $g(u,v)$ are $f(u,v) = \frac{1}{\epsilon}u(1-u)(u - \frac{v+b}{a})$ and $g(u,v) = u - v$. Diffusive coupling (having strength D) is via the fast variable, while ϵ sets the separation of the timescale between the two variables. The parameter a helps tune the duration of excitation while b/a is the excitability threshold. For our simulations, we choose $a = 0.9, b = 0.08, \epsilon = 0.02$ and $D = 1$, unless otherwise mentioned. We consider a two-dimensional lattice of size 320×320 with diffusive coupling between nearest neighbors and no-flux boundary conditions.

The phase of a spiral wave is undefined at the spiral tip, thereby making the spiral tip a point of singularity, i.e., a topological defect. A spiral is assigned a topological charge depending on the direction of the rotation of the spiral wave. For a 2-dimensional domain, the topological charge n is defined as the winding number

$$n = \frac{1}{2\pi} \oint_\Gamma \nabla \theta \, dl \qquad (4.2)$$

where θ is the phase and Γ is a closed curve such that θ is defined everywhere on Γ. The winding number of the curve Γ, n, is also known as the index of the curve [135]. It

measures the number of anti-clockwise windings of the vector field on Γ as a point on Γ moves anti-clockwise [see Appendix C].

We next study the behaviour of spiral waves in a lattice of coupled phase oscillators. One of the most widely used models for coupled phase oscillators is the Kuramoto model [50]. It is well known for its applications in various fields and for being able to show sufficiently complex dynamics and yet having an analytic solution. For a two-dimensional square lattice with nearest neighbor coupling, the evolution of the phase θ_i of the ith oscillator is given by:

$$\frac{d\theta_i}{dt} = \omega_i + \frac{K}{N} + \sum_{\langle i,j \rangle} sin(\theta_j - \theta_i), \tag{4.3}$$

where ω_i is the intrinsic frequency of the ith oscillator, $K(= 0.8)$ is the strength of coupling and $\langle i, j \rangle$ denotes the summation over the nearest neighbors of the ith oscillator. For our simulations, we consider the four nearest neighbors of the lattice and consider no-flux boundary conditions. The intrinsic frequencies ω_i are randomly sampled from a normal distribution having mean 0.5 and standard deviation 0.02.

We perform our initial study using the Kuramoto oscillators, and subsequently, to better capture the underlying biological structure of the uterine tissue, we use a system comprising excitable cells coupled to passive cells. As mentioned in earlier chapters, the thick muscular layer of the human uterus, viz., the myometrium, mainly consists of two types of cells, the uterine myocytes, which are excitable in nature, and electrically passive cells [99], such as fibroblasts and Interstitial Cajal-like cells (ICLC). We stimulate the electrical activity of uterine myocytes using the two-component FitzHugh-Nagumo model [18]. This describes the temporal evolution of the excitable cell membrane potential V_e and the effective conductance g of a single excitable unit. The general form of this model is: $\dot{V_e} = AV_e(V_e - \alpha)(1 - V_e) - g$, $\dot{g} = \epsilon(V_e - g)$ where $A(= 3), \alpha(= 0.15)$ and $\epsilon(= 0.08)$ are the fast activation kinetics, excitation threshold and the recovery rate of the medium,

respectively. We describe the temporal evolution of the membrane potential V_p of a uterine passive cell using $\dot{V}_p = K(V_p^R - V_p)$ where $V_p^R(= 1.5)$ is the resting potential of the electrically passive cell and $K(= 0.25)$ sets the timescale over which perturbations from V_p^R decay back to it. We consider electrical coupling between myocytes and passive cells as in uterine tissue and denote the conductance of the gap junctions that connect myocytes and passive cells as C_r. In order to describe the propagation of electrical activity over space, we consider a spatially extended system of myocytes arranged in a two-dimensional lattice, where each myocyte cell is, on average, coupled to n_p ($n_p = 0, 1, 2...$) passive cells [105, 128]. In addition, we assume that each myocyte is electrically coupled to neighboring myocytes on the lattice with a diffusion constant D. The effect of the stochasticity on the opening and closing of the gated ion channels of the uterine myocyte is captured by adding noise to the fast variable V_e. Thus, the complete set of equations that we use to describe the dynamics of the system are:

$$
\begin{aligned}
\frac{dV_e^i}{dt} &= F_e(V_e^i, g^i) + n_p^i C_r(V_p^i - V_e^i) + D\sum_{\langle i,j \rangle}(V_e^j - V_e^i) + \xi_E \xi^i(t)\,, \\
\frac{dg^i}{dt} &= G(V_e^i, g^i)\,, \\
\frac{dV_p^i}{dt} &= K(V_p^R - V_p^i) - C_r(V_p^i - V_e^i)\,.
\end{aligned}
\tag{4.4}
$$

where $\xi^i(t)$ is a Gaussian white noise, i.e, $\langle \xi^i(t) \rangle = 0$ and $\langle \xi^i(t), \xi^i(t') \rangle = \delta(t - t')$ with ξ_E being the noise intensity. For the purpose of our simulations, we assume that the myocytes lie on a regular square lattice of size $L \times L$, where $L = 200$. We assume that the density of passive cells is spatially heterogeneous and the number of passive cell at a particular lattice site is selected from a Poisson distribution with mean 0.7. We note that an isolated myocyte is incapable of exhibiting spontaneous oscillations, but on coupling to a passive cell, the combined unit can spontaneously excite itself periodically and thus behaves as an

oscillator [60, 128].

4.3   Results

4.3.1   Interaction between spiral waves and target waves

A spiral wave has a topological charge associated with it. The magnitude of the topological charge is equal to the number of arms of a spiral wave, while the sign of the charge depends on the chirality of the spiral wave. Depending on whether a single armed spiral moves in the clockwise or anti-clockwise direction, it is assigned a topological charge of $+1$ or -1. A target wave, on the other hand, is a wave which emanates from a source. It does not have a topological defect, and hence no topological charge can be associated with it. When multiple spiral waves are present in a medium, they can influence each other and cause the spiral waves to drift in a complicated manner. Depending on the properties of the underlying medium, there exists a threshold in the distance of separation of two spiral waves beyond which they do not influence each other. If two spiral waves rotating in the same direction, i.e., having like charges, are sufficiently close to each other, they will be mutual repulsion between them. In contrast, two spiral waves having unlike charges (i.e., which rotate in opposite directions) attract each other when they are adjacent. Thus, two oppositely rotating spirals form a bound pair which behaves as a unit rotating about an axially symmetric line and move with a constant velocity along that line. However, two spiral waves having the same chirality form a bound pair which has a centre of symmetry and move with a velocity which is not constant. The oscillations at a particular point near the spiral tips are also not periodic. The formation of bound pairs depend on the geometry and dynamics of the system but after formation, the pairs are independent of their initial state [136]. In Fig. 4.1(a), we show that when the two oppositely rotating spiral tips are sufficiently separated (lattice distance of 120), the two arms do not influence each other

and each arm traces out a perfect circle (the locus of the spiral tip movement over time is shown in white). When the lattice distance between the two arms is reduced to 20 [Fig. 4.1(b)], one arm influences the other and the spiral core does not remain a circle but drifts over time.

The interaction between a spiral wave and a target wave is shown in Figs. 4.1(c-f). We consider the Barkley model with the parameters as in Ref. [127], i.e., $a = 1.1, b = 0.2135$ and $\epsilon = 0.02$. For these parameter values, the system is in a regime where the spiral wave traces out a circle at the core. We consider a particular point in the domain and find the time-period of the spiral wave to be 7.35. We next select the center of the spiral core and initiate a periodic pulse having the same frequency from there [Fig. 4.1(c)]. Concentric waves propagate through the medium from the pulse source and they interact with the arm of the spiral wave. Due to the interaction between the arm of the spiral and the concentric wave, the core of the spiral shifts and it starts to go around the original core tracing an involute [Figs. 4.1(d-e)], similar to the formation of a master-slave pair. But this behaviour is not stable and we observe two types of dynamics: (i) either the spiral breaks up away from the tip, or (ii) the spiral wave does not break up and instead annihilates the target wave source. In Figs. 4.1(d and e), we plot the trajectory traced by the spiral tip for cases (i) and (ii), respectively. When spiral breakup is observed, new spiral waves are created in the medium. Subsequent breakups happen due to interaction between the target wave that is still present and the broken spiral arms. The original spiral continues moving while making involutes till it gets absorbed into the boundary or gets broken up after hitting another spiral arm. After evolving the system for a sufficiently long duration, we observe that the broken waves form bound pairs and the number of tips present in the domain ranges from 2 to 4. In the case where spiral breakup does not happen, the arm of the spiral wave sweeps over the target wave source thereby annihilating it. With the target source extinguished, the spiral wave does not have any competing wave in the
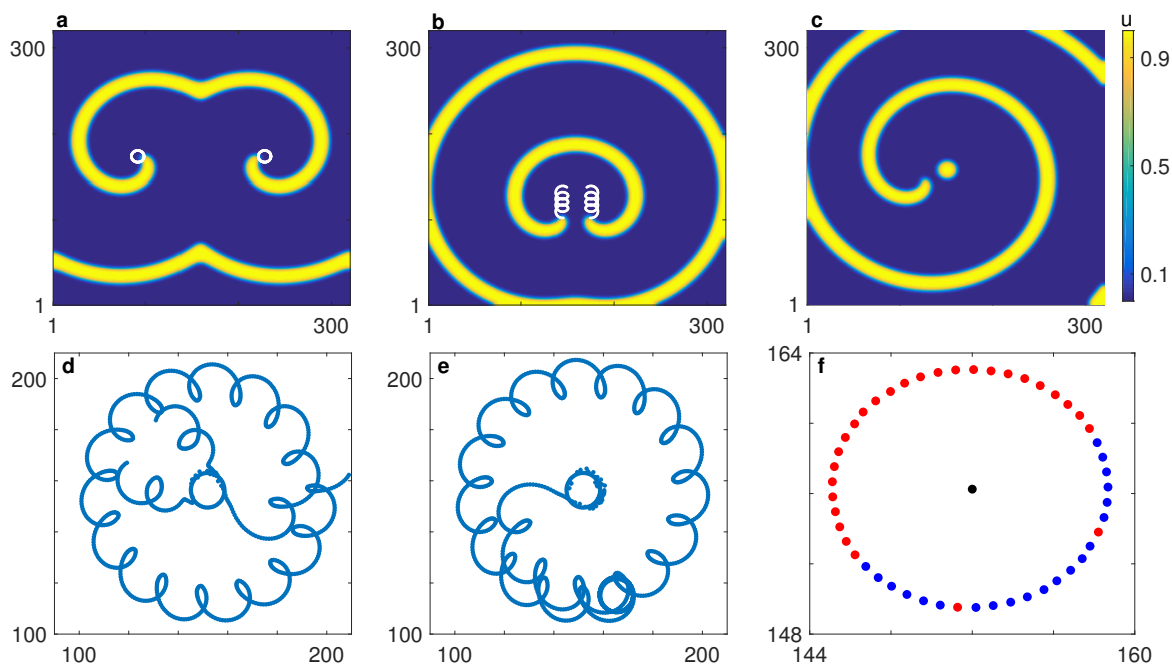
Figure 4.1: Interaction between a spiral wave and a wave source having the same frequency. (a,b) Snapshots of the activity u showing a double armed spiral wave with the arms having opposite chirality. The simulation domain is of size 320×320 lattice units. Due to the large separation (~ 120) between the two arms in (a), they do not influence each other and each arm moves unperturbed tracing out a circular core (shown in white). In (b), the separation between the two arms has reduced to 20 and each of the arms drift due to the influence of the other. (c) Snapshot of the activity of u in a simulation domain of the same size as in (a) showing a single armed spiral in the medium interacting with target wave having the same frequency originating from the center of the circular core traced out by the spiral wave. (d,e) The path traced out by the spiral tip over time. Depending on the initial position of the spiral wave, the final outcome can be either (d) spiral breakup, or (e) no breakup. (f) Regions of starting tip position along the initial spiral core that correspond to spiral breakup and annihilation of target wave. The red and blue dots form the spiral core. Blue dots: starting tip positions where the spiral sweeps over the target source thereby annihilating it. Red dots: starting tip positions where the spiral has a far from the tip breakup. The black dot at the center is the target wave source.

medium and it starts rotating about its core in a new position. Whether spiral breakup occurs or not depends on the initial position of the spiral wave along its core. We try to systematically classify the final outcome based on the initial position of the spiral. For this, we record the tip position at equally spaced time intervals and obtain 49 distinct positions along the original spiral core. We run the simulation considering each of these positions as the starting position of the spiral wave and record the final outcome of the tip trajectory. We observe that the starting tip positions separate into regions corresponding to spiral breakup and no breakup. In Fig. 4.1(f), the spiral core is represented by red and blue dots while the black dot in the center is the source of the target wave. Red dots represent the initial position of the spiral wave for which spiral breakup occurs (more than one spiral tip present in the medium) while blue dots represent those initial positions for which spiral breakup does not occur and annihilation of the target wave source takes place (only one spiral tip present in the medium). We find that the separation of the tip positions on the basis of the outcome of spiral breakup is independent of the chirality of the spiral. We thus observe that the interaction between two spiral waves differ from that between a spiral and a target wave. Unlike the former, we do not see the spiral going around the target wave to form a stable pattern. Thus we do not see a stable master-slave pair forming when a spiral wave interacts with a source of wave having the same frequency and emanating from the center of the erstwhile spiral core position.

4.3.2 Topological transition to vortex unbinding in systems of coupled biological oscillators

In this subsection, we have investigated the interaction between multiple topological charges or vortices in an oscillatory medium. First, we consider a system of coupled Kuramoto oscillators in a two-dimensional lattice. We observe multiple re-entrant activity (each hav-

ing a topological defect at its core) in the medium having both clockwise and counter clockwise rotation. In Figs. 4.2(a and c), we show the time evolution of the domain at times $t = 50$ and $t = 300$ arbitrary units respectively. It is evident from the snapshots that the number of spirals in the medium decreases as time progresses. This happens through spirals having opposite chirality drifting towards each other and mutually annihilating. As mentioned earlier, spirals are characterized by their topological charge. One of the simplest ways of finding the spiral cores, which are topological defects, is by computing the determinant of the Jacobian matrix of the phase vectors $(cos\theta, sin\theta)$ for phase θ at each lattice site. The determinant is strictly positive at lattice sites which correspond to phase singularities at the center of clockwise rotating spirals while it is strictly negative at lattice sites which correspond to centers of counter-clockwise rotating spirals. The determinant is ~ 0 elsewhere in the domain. The topological defects in the snapshots of panels (a) and (c), identified by the above method, are shown in Figs. 4.2(b and d) respectively. We can see that compared to panel (b), the defects have drifted and a number of them have disappeared, thereby reducing down the total number of defects in panel (d). In Fig. 4.2(e) we plot the phase vectors of the flow field at each lattice site. We see a slight variation in the direction of the vectors for nearby sites of the lattice except at sites corresponding to the phase defects where we see the phase vectors arrange themselves such that the winding number about the site of defect is ∓ 1.

We note that the phase vectors form a saddle whenever the corresponding spiral rotates anti-clockwise. When the spiral rotates clockwise, we can see that the phase vectors form a node or a center about the phase defect (see appendix C). From nonlinear dynamics theory, we know that a node or a center has a winding number of $+1$ while for a saddle it is -1 [135]. Thus, for any spiral wave rotating in an anti-clockwise direction, the topological charge is -1 and it is $+1$ for spiral waves rotating in the clockwise direction. In panel (e), the saddle, corresponding to an anti-clockwise rotating spiral and a node corresponding to
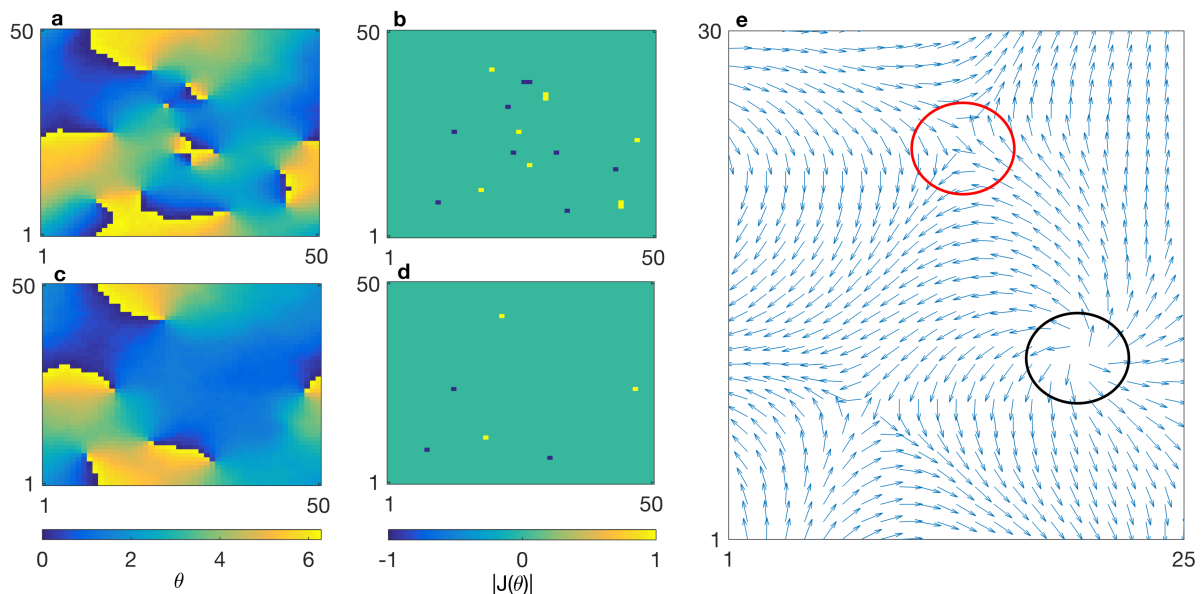
Figure 4.2: Interaction of multiple spiral waves in an array of locally coupled phase oscillators. (a,c) Snapshots showing the time evolution of a two-dimensional lattice of phase oscillators of size 50×50. (a) Initially, at $t = 50$, both clockwise and anti-clockwise spirals can be observed in the system. (b) Spiral tips marked yellow denote the clockwise rotating spirals having topological charge $+1$ and blue denotes the anti-clockwise rotating spirals having topological charge -1. The spiral tips are located by calculating the determinant of the Jacobian matrix of the field formed by the phase vectors $(cos\theta, sin\theta)$. The determinant is strictly positive at locations corresponding to the tips of clockwise rotating spirals, while it is strictly negative at locations corresponding to the tips of counter-clockwise rotating spirals. The determinant is ~ 0 everywhere else in the domain. (c) At time $t = 300$, the spirals having opposite chirality attract and then annihilate each other, leaving behind fewer defects as shown in (d). (e) The phase vectors are plotted at each lattice site. Near a topological defect, the vectors form a saddle when the defect corresponds to a counter clockwise rotating spiral (marked by a red circle in the figure) while the vectors form a node when the topological defect corresponds to a clockwise rotating spiral (black circle).

a clockwise rotating spiral, are marked with red and black circles respectively. The phase vector field representation of the interacting self-rotating waves in the two-dimensional lattice of coupled oscillators is reminiscent of the classical XY model [137] with the phase of the oscillator corresponding to the direction of the spins. The tips of the self-rotating waves are equivalent to the vortices and anti-vortices seen in the XY model. Given that the Hamiltonian of the XY model is similar to the governing equation of the two-dimensional Kuramoto model on a lattice, there have been attempts to find the equivalence between them [52, 138, 139]. A particularly intriguing phenomenon observed in the XY model is the Kosterlitz–Thouless transition (KT transition) [140], a topological phase transition that occurs beyond a critical temperature. It is characterized by a transition from bound vortex-antivortex pairs to unpaired vortices and anti-vortices, which takes place despite the absence of symmetry-breaking. The high-temperature disordered phase has an exponential decay of the spatial correlation function, while at low temperatures, the spin-spin correlation shows a power law dependence on distance. As temperature rises, more and more vortex-antivortex pairs (which are similar to nodes/centers and saddles, and hence to clockwise and anti-clockwise spirals, respectively) are created, and the distance between them increases until there is an unbinding transition where all the vortices and antivortices are free to move. This destroys the correlations between two distant spins. If any such transition analogous to KT transition is found to take place in the oscillator system, it would provide us a simple description of the spiral wave dynamics in terms of the interaction of the vortices. As is evident from Fig. 4.2, vortex annihilation takes place as time progresses without the creation of any new defects. One of the ways in which new defects can be created is by introducing noise of varying intensity in the system. This noise can be considered to be analogous to temperature in the XY model. However, despite adding noise to the system comprising phase oscillators, we are not able to observe creation of any new defects. Instead, the system settles into a synchronized state after a long time.
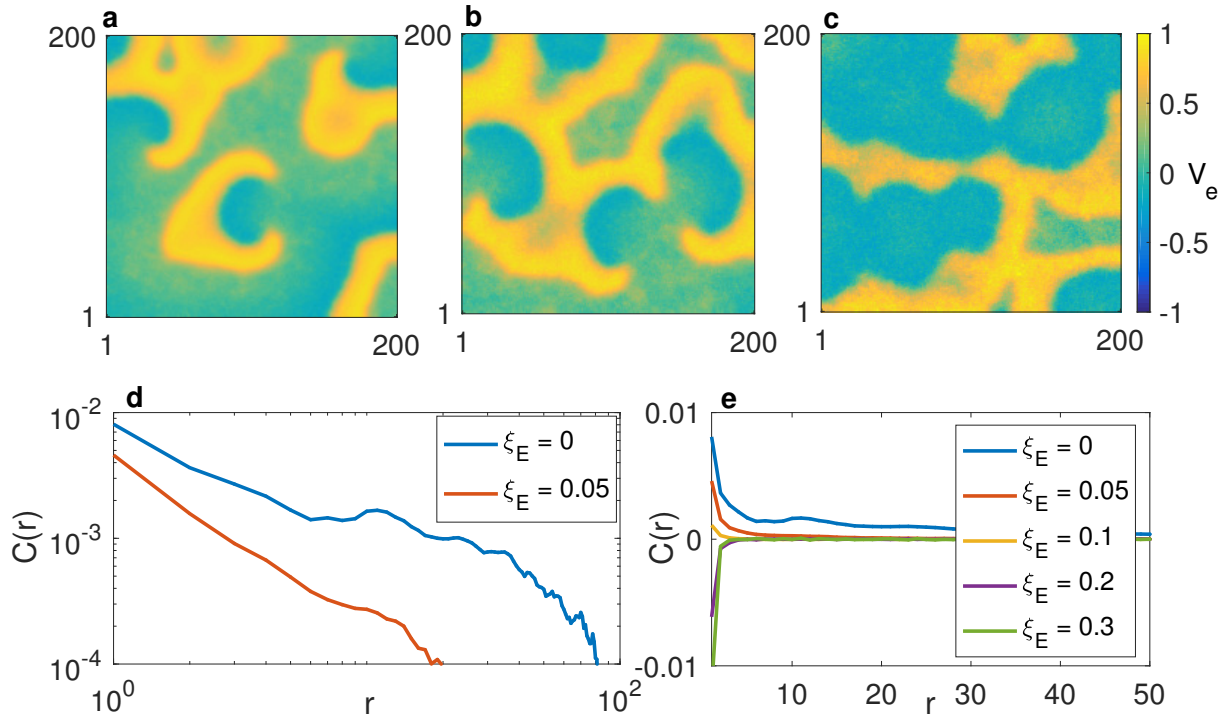
Figure 4.3: The creation and annihilation of spirals in the EP model for different values of noise intensity ξ_E. (a-c) Snapshots of the activity of V_e in a square lattice of size 200×200 with noise intensity (a) $\xi_E = 0$, (b) $\xi_E = 0.1$, and (c) $\xi_E = 0.2$, respectively. As the noise level increases, we see more heterogeneity in the medium and the creation of more defects which destroy the spirals. (d) Long tailed behaviour of the spatial correlation function $C(r)$ observed for low values of ξ_E. (e) An abrupt drop in the spatial correlation function $C(r)$ is observed around the noise intensity level $\xi_E = 0.12$.

A more biologically realistic system of oscillators is an array of excitable cells coupled to passive cells (EP model), as was considered in the previous chapters. As mentioned earlier, a unit of this system, comprising an excitable cell coupled to one or more passive cells, is capable of spontaneous oscillation. To account for the stochasticity in the opening and closing of the ion channels present in the biological tissues, we introduce an additive white noise into the system. Fig. 4.3(a-c) shows the activity in the system for different values of noise intensity, viz., $\xi_E = 0, \xi_E = 0.1$, and $\xi_E = 0.2$ respectively. We observe that as the intensity of noise increases, defects are created in the medium giving rise to new regions of activity and more heterogeneity in the medium till, at high noise levels, the spiral nature of the waves are no longer properly discernible. The presence of noise results in heterogeneities in the frequencies of the oscillating units. The high frequency regions can give rise to new organizing centers in the medium and thereby, a self-rotating wave can form anchored at these organizing centers. We quantify the presence of these multiple defects in the medium and their interaction by computing the spatial correlation function of the determinant of the Jacobian matrix obtained from the phase angles. This is shown in Fig. 4.3 (d and e). As we vary the noise amplitude ξ_E, we observe a long tailed behaviour in the correlation function for small ξ_E [shown in loglog scale in Fig. 4.3(d)] which then drops for larger values of ξ_E [Fig. 4.3(e)], resulting in the absence of any correlation. This abrupt drop occurs at $\xi_E \sim 0.12$. Thus, a transition from the long tailed behaviour of the correlation function to an exponential decay is observed in this system.

4.4   Discussion and Conclusion

The presence of a topological defect at the tip of a spiral wave implies that it creates a discontinuity in the system which cannot be removed unless the spiral wave drifts and gets absorbed into the boundary of the domain, or it gets annihilated by a rotating wave of

opposite chirality. Due to the persistent nature of these waves, they have been often associated with clinical abnormalities. Hence understanding the dynamics of the interaction of the phase singularities is of considerable practical interest. In this chapter we have shown that, unlike in the case of an interacting pair of spirals where one spiral may enslave the other, when a spiral wave interacts with a wave source giving rise to concentric circular wavefronts, it either leads to the annihilation of the wave source or spiral breakup. In the case where there are multiple vortices in the medium, the interaction between them can lead to a topological transition where vortex unbinding takes place. This result can have potential significance in understanding Braxton-Hicks contractions (false labor) in the uterus.

Chapter 5

Conclusions

"...from so simple a beginning endless forms most beautiful and most wonderful ..."

— Charles Darwin, *On the Origin of Species*, 1859

The work described in this thesis is aimed at understanding the role of different types of heterogeneity in influencing and organizing the emergent collective behavior that can arise in cell-assemblies and tissues comprising excitable and passive cells. The principal model that we consider in this thesis, of a system capable of exhibiting spontaneous activity, is used for describing the dynamics of self-organized persistent activity in the pregnant uterus, especially in understanding the dynamical causes behind variations from normal human labor, like abnormal labor and false labor. In the following subsections, we summarize the key results that have been presented in the thesis, and conclude with a short discussion on the possible extensions of the work that is reported here.

5.1 Summary of main results

Frequency gradients in heterogeneous oscillatory media can spatially localize self-organized wave sources that coordinate system-wide activity

Rhythmogenesis, which is critical for many biological functions, involves a transition to coherent activity through cell-cell communication. The first stage of labor during childbirth involves the contraction of uterine smooth muscle tissue, which is achieved through organ-wide coordination of electrical activity. Irregularities in these contractions lead to dysfunctional labor - a significant cause of maternal and foetal morbidity. Successful parturition is contingent on regular contractions that are associated with directed propagation of electrical activity from the fundal to the cervical end of the uterus. However no specialized pacemaker cells that might initiate activity are known to exist in the pregnant uterus. In absence of centralized coordination, it is possible that competing oscillating clusters can impede global synchrony. A possible solution is that directed waves of excitation in the tissue may be sustained through a gradient in the frequency of electrical activity, as is indeed the case in several biological systems. We show that increasing the steepness of this gradient, along with strength of cell-cell coupling, results in the spontaneous creation of localized wave sources. These are confined to the region corresponding to the higher end of the gradient and are capable of driving system-wide activity. Such gradients, arising through heterogeneous inter-cellular coupling, may explain directed rhythmic activity during labor in the uterus despite the absence of pacemakers.

Spontaneous generation of persistent activity in diffusively coupled cellular assemblies

The spontaneous generation of electrical activity underpins a number of essential physiological processes, and is observed even in tissues where specialized pacemaker cells have not been identified. The emergence of periodic oscillations in diffusively coupled assemblies of excitable and electrically passive cells (which are individually incapable of sustaining autonomous activity) has been suggested as a possible mechanism underlying such phenomena. In this chapter we investigated the dynamics of such assemblies in more detail by considering simple motifs of coupled electrically active and passive cells. The resulting behavior encompasses a wide range of dynamical phenomena, including chaos. However, embedding such assemblies in a lattice yields spatio-temporal patterns that either correspond to a quiescent state or to partial or globally synchronized oscillations. The resulting reduction in dynamical complexity suggests an emergent simplicity in the collective dynamics of such large, spatially extended systems. Furthermore, we show that such patterns can be reproduced by a reduced model comprising only excitatory and oscillatory elements. Our results suggest a generalization of the mechanism by which periodic activity can emerge in a heterogeneous system comprising non-oscillatory elements by coupling them diffusively, provided their steady states in isolation are sufficiently dissimilar.

Interaction between spiral waves and the topological transition to vortex unbinding in systems of coupled biological oscillators

Rotating spiral waves represent an important example of emergent dynamical patterns observed in many physical, chemical and biological excitable systems. In this chapter we investigated the emergence of vortices under specific conditions in a homogeneous medium due to the interaction of a single vortex with target waves having the same frequency

emanating from a localized source. We found that even though the creation of vortices due to spiral breakup is dependent on the initial position of the reentrant wave, it is independent of its chirality. We also considered the interaction of multiple vortices in a medium comprising coupled excitable and passive cells with additive noise representing the random opening and closing of cellular ion channels. The presence of multiple reentrant waves in such a system of coupled phase oscillators can lead to competing sources of high frequency excitation and can be the cause of several physiological anomalies. We observed that a transition of the spatial correlation function of the vortices from a power-law form to an exponential decaying form takes place upon increasing the intensity of noise. Our results can be potentially relevant in understanding Braxton-Hicks contractions (false labor) that are occasionally observed in the human uterus prior to childbirth.

5.2   Outlook

In this thesis we have looked at the collective dynamics that can arise in excitable tissues and organs on coupling heterogeneous cell types. The main model of excitabilty that we use in this thesis, the FitzHugh-Nagumo model, is phenomenological in nature. Owing to the apparent universality of the complex spatiotemporal patterns that it displays, it can be applied to a host of other areas not restricted to electrically excitable systems in physiology. For example, it has been applied to model earthquake faults where the coupling is elastic rather than diffusive [141]. In biology, relaxation oscillators, of which FitzHugh-Nagumo model is a particular example, has been applied to model ecological systems [142, 143] and gene circuits [144] to name a few. Thus, we can use the insights and findings of this thesis and investigate their applicability in excitable systems arising in other contexts.

In Chapter 2, we have modelled the dynamics of the excitable muscular layer of the uterine tissue. While for simplicity we have considered a square geometry with periodic

condition on the sides and no-flux conditions at the top and bottom, this can be modified to account for more realistic geometries. At present, with the above-mentioned boundary conditions, our domain represents a cylinder. But the human uterus is not cylindrical and resembles more a pear-shaped organ. A conical frustum can act as a better representation of the shape and it would be interesting to see the changes in dynamics, if any, due to a change in the geometry of the domain. In our work, we have restricted our analysis to the condition that the coupling strengths between two excitable cells is equal to that between an excitable and a passive cell. However, one can investigate the robustness of the patterns obtained, especially that of spiral waves, when the two coupling strengths are unequal.

To capture the uterine activity more realistically, there are a few ways in which the model of the uterus considered by us can be extended. Hormones, alongwith other metabolites, have been known to play an important part in regulating uterine contractions during childbirth [145]. There have been studies in the past that have looked at the role hormones play in pregnancy [146, 147]. The uterine model that we have considered can be modified easily to include the effect of hormones. Intra-uterine pressure is another component that is tracked by clinicians to check the progression of labor [148] and the rate of change of this pressure can be an added component of the model. The uterine myometrium is a thick, muscular layer. Hence it might be worthwhile to consider the model in three-dimensions instead of two, taking into account the thickness of the myometrial domain. Since the uterine myocytes are similar in shape and property to their cardiac counterparts, one of the ways to model the electrical propagation in the myometrial tissue would be by using the bidomain model [149]. The bidomain model is a continuum model of the electrical activity of the heart which accounts for the anisotropic properties of the intracellular and extracellular spaces. The uterine myocytes in a term-pregnant human uterus are organized into bundles that make action potential propagation anisotropic [150]. Thus, it might be appropriate to use the bidomain model provided the anisotropy ratios are known. Based on

67

our work, we also suggest some testable observations that can be verified experimentally. It might be useful to find the phase velocity of the propagating excitation front of uterine activity. If the velocity is seen to depend on the distance from a supposed pacemaker region, our hypothesis regarding the existence of the frequency gradient will be further strengthened. By calculating the wave velocity, the actual slope of the gradient can also be found out.

We have shown in Chapter 3 that a spatially extended model comprising oscillatory and excitable cells (OE model) can reproduce the macroscopic properties observed in a model comprising electrically active and passive cells (EP model). The model considered in Chapter 2 is similar to the EP model with the difference being in how the passive cells are connected to the excitable cells. Instead of having a gradient in the passive cell density, the EP model has passive cells taken from a Poisson distribution randomly coupled to the excitable cells. Thus, it might be possible to use the OE model to reproduce the main properties that we observe in the uterine model considered in Chapter 2, like the unidirectional propagation of waves with the organizing centers (reentrant waves) localized at the top of the domain.

Another possible extension of our work would be to explicitly formulate the interaction between topological charges. This in turn will provide a precise expression for the interaction of spiral waves since the characteristic property of a spiral wave depends on its tip (the phase singularity which is a topological defect). The topological charges behave in an analogous manner to point electrical charges, e.g., like charges repel each other while unlike charges attract. Hence, as in electrostatics, it might be possible to calculate physical quantities such as energy, or the force of attraction or repulsion in these systems. As has been mentioned in Chapter 4, spiral waves unexpectedly appearing in biological tissues may result in life-threatening disorders. Thus, having a concise mathematical characterization is not only of great theoretical importance but may have practical applications.

Appendix A

The following comprise the supporting information related to the frequency gradients in heterogeneous oscillatory media, as described in Chapter 2.

Simulation details

We use the forward Euler scheme to integrate the system numerically, using the time-step $dt = 0.01$. We have explicitly verified that the results are qualitatively similar for smaller values of dt. The lattice spacing dx and dy are both taken to be 1 and we use the standard 5-point stencil for the Laplacian describing the spatial coupling between the neighbouring elements of the lattice. Periodic boundary conditions are imposed on the two vertical sides of the domain while the top and bottom edges have no-flux boundary conditions. Thus, the domain in effect resembles an open cylinder in three dimensions. In order to remove transient activity, the system is allowed to evolve for 10^5 time steps before recording the data.

As the observed collective dynamics of such complex systems are typically initial condition dependent, we employ two different simulation approaches. In chapter 2 we have used the biologically realistic "annealed" approach, where we gradually vary the cellular coupling parameters($C_r = D$) such that the state of the system for a given choice of parameter values is used as the initial condition for the next set of parameters. We start our

simulations with $D = C_r = 0.2$ and increase the value of the parameters in steps of 0.2, every 3×10^5 iterations. In the other approach, viz., the "quenched" approach, every realization for each choice of the cellular coupling parameters is obtained using random initial conditions for each variable of the system. In the annealed simulations, we determine the spiral tips at a particular time t, by determining the point of intersection of the isocontours of the fast-variable V_e and V_e^τ, which is the time delay embedding of V_e, (delay $\tau = 1$) at the level $V_e = 0.6$.

Dynamics of the system for "quenched" simulation approach

We observe that for small coupling values ($D = C_r = 0.4$), there is no qualitative difference between the annealed ([Fig. 2.2(a-c)(g-i)]) and quenched ([Fig. A1(a-c)(g-i)]) membrane potentials V_e for different values of Δn_p. However as the coupling strength is gradually increased, we observe that the dynamics for the case of "quenched" ([Fig. A1(d-f)]) becomes markedly different from that of the "annealed" ([Fig. 2.2(d-f)]). On increasing the coupling D, for the case of $\Delta n_p = 0$, these sources emit "blob-like" activity that traverses the entire medium, as seen in Fig. A1(d). But as the strength of the gradient increases, the "blob-like" activity get transformed into directed plane waves, that travel from regions of higher n_p density to that of lower n_p density [figure A1(e-f)]. We note that spiral waves, which were observed in case of annealed simulations are not seen here. We next determine the spatial distribution of frequencies in the medium, both in the presence and absence of n_p gradient ([Fig. A1(g-l)]). For the no gradient case (Fig. A1(g)), the different oscillators form clusters characterized by different frequencies, while some cells do not oscillate at all. As Δn_p increases, proximal regions of similar frequencies start to synchronize and form bigger clusters [Fig. A1(h, i)].

70
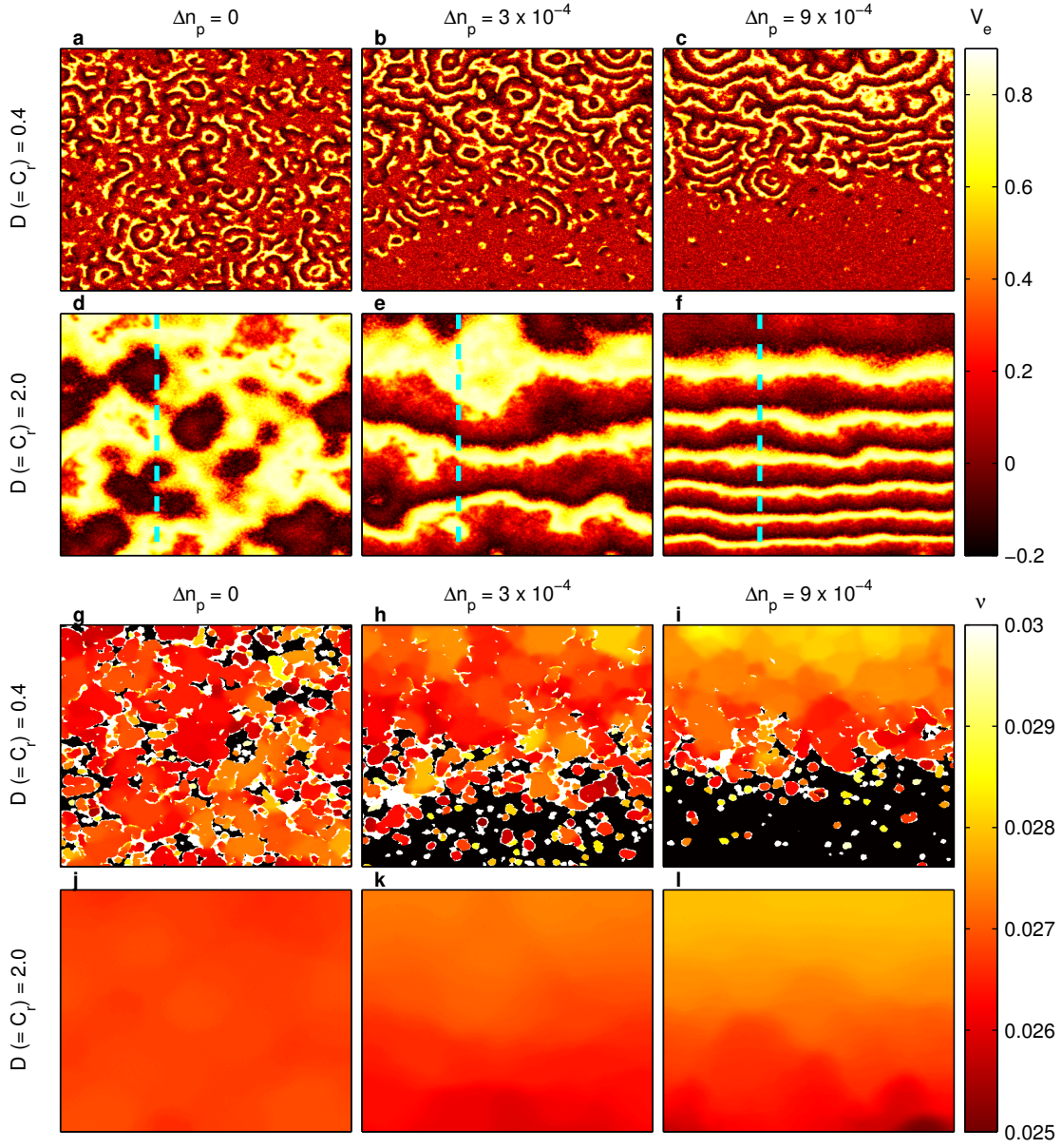
Figure A1: Propagation of excitation waves along a medium having a gradient in the passive cell density for quenched simulations. (a-f) Snapshots of the activity V_e in a two-dimensional simulation domain ($L = 450$) for two different values of inter-cellular coupling strengths $D(= C_r)$ [first row: $D = 0.4$, second row: $D = 2$]. The homogeneous system obtained in the absence of the density gradient [left column: $\Delta n_p = 0$] is compared with the situations seen for finite gradients [middle column: $\Delta n_p = 3 \times 10^{-4}$ and right column: $\Delta n_p = 9 \times 10^{-4}$], for a specific realization of the passive cell distribution. Space-time plots of the activity along the broken line segments are shown in Fig. A2. (g-l) The corresponding pseudocolor plots indicating the oscillation frequencies

Figure A1 *(previous page)*: of individual sites in the medium (black corresponding to absence of oscillation). For lower coupling strength [third row: $D = 0.4$], increasing passive cell density gradient results in local coordination of activity leading to spatial organization of the frequency clusters along a direction transverse to that of the gradient. For sufficiently high gradient the medium is divided into a region exhibiting activity (corresponding to higher passive cell density) and an almost quiescent region (at lower density). For higher coupling strength, viz., $D = 2$ [fourth row: $\Delta n_p = 9 \times 10^{-4}$], the entire medium is active with the emergence of a spatial gradient in the oscillation frequencies which reflects the underlying passive cell density gradient. Seen in conjunction with the activity snapshots (second row), it suggests an organization of disordered phase wave-like spatial patterns into ordered wavefronts propagating from higher to lower passive cell density regions as Δn_p increases.

A spatial ordering of frequencies is introduced into the medium, with the higher frequencies occurring in the regions of higher passive cell densities. At the region of lower passive cell density, the frequencies decrease and for the case of a large gradient, we find that most cells in the low n_p region do not oscillate if D is insufficiently large Fig. A1(i), but get entrained to oscillations for larger values of D. For small Δn_p, the system synchronises to the same frequency throughout the domain [Fig. A1(j)]. On the other hand for steeper gradients larger frequencies are observed at higher passive cell densities and regions with smaller n_p support smaller frequencies [Fig. A1(k, l)].

To pinpoint the source of these waves, we consider the temporal evolution of V_e along the dashed lines of Fig. A1(d-f). This is shown in the spacetime plots of Fig. A2, where the passive cell density increases from the 1st to the 450th cell. It is clear from these plots that in the absence of a gradient all the cells get activated almost simultaneously. In the presence of a gradient, a distinct wave of activity is seen to originate from the region of higher n_p density that acts as a "source", with the slope of the wavefront (inversely related to its speed) increasing with strength of the gradient.
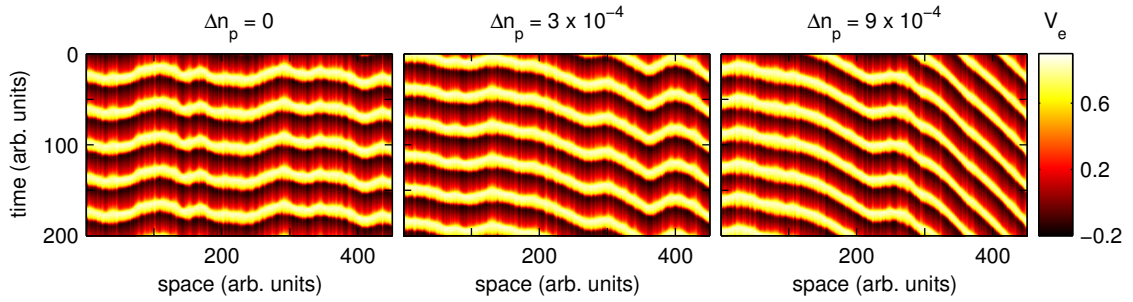
Figure A2: Unidirectional propagation of excitation waves through the medium in quenched simulations. The three panels show spatio-temporal evolution of the activity V_e for individual sites located along the broken line segments in Fig. A1 (d-f) respectively. The passive cell density n_p is spatially homogeneous in the left panel, while it decreases proceeding from the left to the right boundaries in the central and right panels, in accordance with the slope Δn_p of the linear density gradient [centre: $\Delta n_p = 3 \times 10^{-4}$, right: $\Delta n_p = 9 \times 10^{-4}$]. We see that the system exhibits multiple wave sources that are characterized by excitation fronts propagating away from them. As Δn_p increases, the number of such sources reduces eventually resulting in unidirectional propagation of a wavefront starting from the end having the highest passive cell density and continuing to the other end. This suggests that in the presence of a passive cell density gradient, the region of higher density can appear as a "pacemaker" initiating wave propagation in the system.

Appendix B

The following comprise the supporting information for the spontaneous generation of persistent activity in diffusively coupled cellular assemblies, as described in Chapter 3.

Simulation details

For all simulations reported in Chapter 3, we consider the FitzHugh Nagumo (FHN) model [18], which is capable of exhibiting both excitable and oscillatory dynamics. As detailed in Chapter 3, an FHN unit in the excitable regime can display oscillatory behaviour upon being coupled to one or more passive cells [60]. This forms the basis of the two distinct paradigms that we consider, viz. (i) the EP model (earlier considered in [59]), which describes a system of excitable cells (modeled by an FHN unit) and passive cells, and (ii) the OE model, wherein we consider a spatial array of coupled FHN units that are either oscillatory or excitable.

All simulations for the case of the EP model were performed by integrating the differential equations using the inbuilt ODE solvers of MATLAB (specifically, ode45 and odes15s), which implement adaptive time-stepping algorithms, where the relative and absolute tolerances are both set to 10^{-6}. The initial conditions for both excitable and passive cells (i.e. V_e^i and V_p^i) are chosen from a uniform random distribution in the range $(0, 1)$.

74

For each simulation, we discard the data obtained over an initial duration of 5×10^3 system time units, which corresponds to ~ 100 oscillations, to eliminate any transient activity.

The simulations for the OE model were performed on a lattice of size 64×64 with periodic boundary conditions, and where each site is coupled to its four nearest neighbours with strength D. The differential equations were integrated using GSL's inbuilt ODE solver in C, where the absolute tolerance was set to 10^{-6} and the relative tolerance was set to 10^{-8}. In the OE model, each lattice site can contain one of either two distinct cell types, viz. oscillatory or excitable. Hence, we use a common notation V for the state variable of each lattice site in the system described by this model. For these simulations, the initial conditions for V in each cell is chosen from a uniform random distribution in the range $[0, 1]$. The system is first allowed to evolve for a duration of 50 system time units upon setting $D = 0$. We then set D to the required value and allowed the system to evolve for 5×10^3 time units to eliminate any transient activity, and then recorded the data for the subsequent time interval of duration 5×10^3.

Identifying the collective dynamical states in the two models

To characterize the various spatiotemporal patterns of collective dynamics that are observed in the models investigated in Chapter 3, we measure several order parameters to aid in distinguishing the states. This is done with the help of the decision trees shown in Fig. 3.2 (for the EP model) and Fig. 3.7 (for the OE model) of Chapter 3, respectively. At each numbered decision point, threshold values $\delta_{1,\dots,7}$ [Fig. 3.2] or $\epsilon_{1,\dots,4}$ [Fig. 3.7], whose numerical values are indicated in the respective captions, are used to determine the answer to the corresponding question.

For the EP model comprising N coupled nodes [Fig. 3.2], where the order parameters are calculated using the time-series $Y_i(t)$ representing the activation variable V_e of i-th node ($i = 1, \ldots, N$), the questions asked at the different decision points are:

1. Is there temporal variation in Y ? In practice, we measure the dispersion of each time-series Y_i and check if the average of this quantity over the nodes is greater than a threshold $\delta_1 \ll 1$. If true, at least one of the nodes is oscillating; else, the nodes are in time-invariant states.

2. If the nodes are in a time-invariant state, are the values of Y_i identical for all i ? In practice, we calculate the dispersion of the mean of the time-series across the nodes and check if it exceeds a threshold $\delta_2 \sim 0$. If true, it indicates that at least some of the Y_i are different, which characterizes an Inhomogeneous Steady State (ISS); else, all Y_i are the same indicating that it is an Oscillator Death (OD) state.

3. If there is temporal variation in Y, are all nodes oscillating ? In practice, we check if the smallest dispersion of Y calculated for all nodes is greater than a threshold $\delta_3 \ll 1$. If not satisfied, it implies that at least one of the nodes is not oscillating and hence the state corresponds to a Chimera (Ch).

4. If all nodes are oscillating, do they all the same frequency ? In practice, we check if the dispersion of the oscillation frequencies is greater than a threshold $\delta_4 \sim 0$. If true, then it corresponds to nodes having distinct frequencies which characterizes the Cluster Synchronization (CS) state.

5. If all nodes are oscillating at the same frequency, are they oscillating in phase ? In practice, we measure the instantaneous dispersion between the amplitudes of the different nodes and check if its temporal average exceeds the threshold $\delta_5 \sim 0$. If it does not, the state corresponds to Exact Synchronization (ES) (belonging to the

76

broader category of coherent states).

6. If the oscillators are not in phase, are their amplitudes the same ? For this, we vertically displace each time series Y_i such that their minima $min(Y_i)$ are the same. We then calculate the dispersion in the amplitude and check if the difference is greater than the threshold $\delta_6 \sim 0$. If not, it corresponds to Homogeneous Out of phase Synchronization (HOS), where the oscillations have the same amplitude but are not phase synchronized (one of the two states that belong to the broader class of Global Synchronization).

7. If the oscillators have different amplitudes, are they phase synchronized ? This can be determined by asking if the dispersion of Y calculated over the different nodes is invariant in time. In practice we calculate the dispersion of this quantity over time and check if it is greater than the threshold $\delta_7 \ll 1$. If not satisfied, then the nodes are synchronized in phase although oscillating with different amplitudes, corresponding to the state of Inhomogeneous In-phase Synchronization (IIS) (belonging to the broader category of coherent states); else, the state is Inhomogeneous Out of phase Synchronization (IOS) (the other state that belongs to the broader class of Global Synchronization).

Note that we do not observe ES or HOS for the range of parameters used for the results reported here.

For the OE model [Fig. 3.7], the questions asked in the different decision points are:

1. Is there a finite number of oscillating nodes in the system ? In practice, we ask if the fraction of oscillating nodes f_{osc} is above a threshold $\epsilon_1 \ll 1$. If this is not satisfied, we classify the state as No Oscillations (NO).

2. Are all nodes oscillating ? Again, in practice, we determine if f_{osc} is greater than a threshold $\epsilon_2 \sim 1$. If the answer is yes, we go on to ask if the oscillations are synchronized, while if the answer is no, we ask if the frequencies of the oscillating nodes are identical.

3. Are all the oscillating nodes synchronized in their phase ? This is true if almost the entire set of nodes were simultaneously active (a node is considered to be active if its activation variable V_e is above the excitation threshold) and determined in practice by checking if the fraction of active nodes is larger than a threshold $\epsilon_3 \sim 1$. If true, then the states corresponds to Coherence (COH), else it is labeled as Global Synchronization (GS).

4. Are the frequencies of the oscillating nodes identical ? We measure the dispersion of the frequencies and check if this is greater than a threshold $\epsilon_4 \sim 0$. If true, then the state is labeled as Cluster Synchronization (CS) characterized by the existence of many groups of oscillators having distinct frequencies; otherwise, the state is referred to as Local Synchronization (LS) in which all oscillating nodes have the same frequency.

Dynamics of an excitable cell coupled to a passive cell

The simplest possible system that can be described by the EP model comprises an excitable cell coupled to a passive cell with strength C_r. Such a system can oscillate over a range of values of C_r and the resting state of the passive cell V_p^R, as seen in Fig. B1 (a). For a fixed value of C_r, the system exhibits a bifurcation at a critical value of V_p^R, and transitions from a steady state to oscillatory dynamics [Fig. B1 (b)], as has been previously reported in [60]. We note that qualitatively similar behavior can be obtained by plotting $V_e^{extrema}$

as a function of C_r for a fixed value of V_p^R. In Fig. B1 (c) we display the dependence of the frequency ν on C_r for a certain value of V_p^R. We note that ν has a qualitatively similar dependence on V_p^R for a fixed value of C_r.
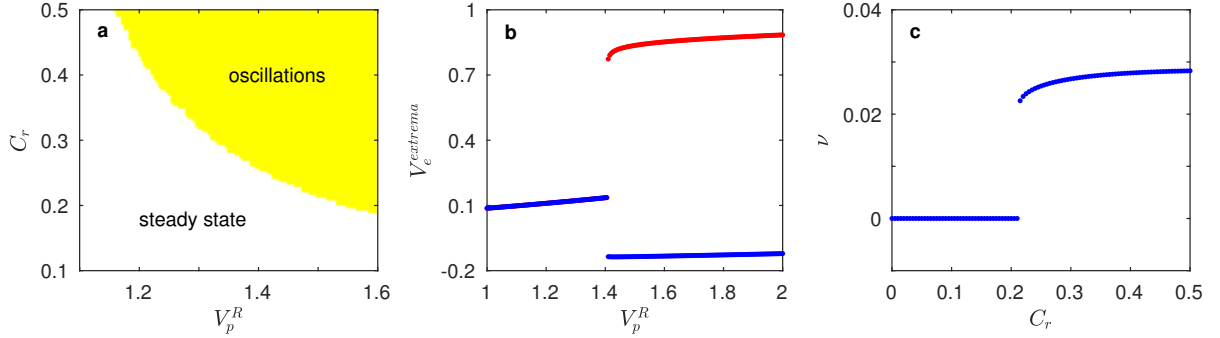

Figure B1: Conditions for the emergence of oscillations in the simplest system that can be described by the EP model, viz. an excitable cell coupled to a passive cell with strength C_r. (a) The system exhibits oscillatory activity (region displayed in yellow) for a suitable range of values of C_r and the resting state potential V_p^R of the passive cell. In the remainder of the parameter space, the system exhibits steady state behavior. (b) For a given value of C_r, oscillations are observed beyond a critical value of V_p^R, as can be seen from the extrema of V_e (red and blue markers), shown here for $C_r = 0.25$. (c) Dependence of the oscillatory frequency ν on the coupling strength C_r for a fixed value of V_p^R (shown here for $V_p^R = 1.5$). For all simulations in (a)-(c), we set $b = 0$, so that the excitable cell converges to a low stable state in the case $C_r = 0$.

Characterizing the collective dynamics of motifs described by the EP model and quantifying the robustness

In Fig. B2, we display an enlarged version of the parameter space diagram shown in Fig. 3.3(b) of the Chapter 3. This figure displays the collective dynamical patterns obtained over a range of values of strengths of coupling between a pair of excitable cells, D, as well as between an excitable and passive cell, C_r, for the case of a motif comprising
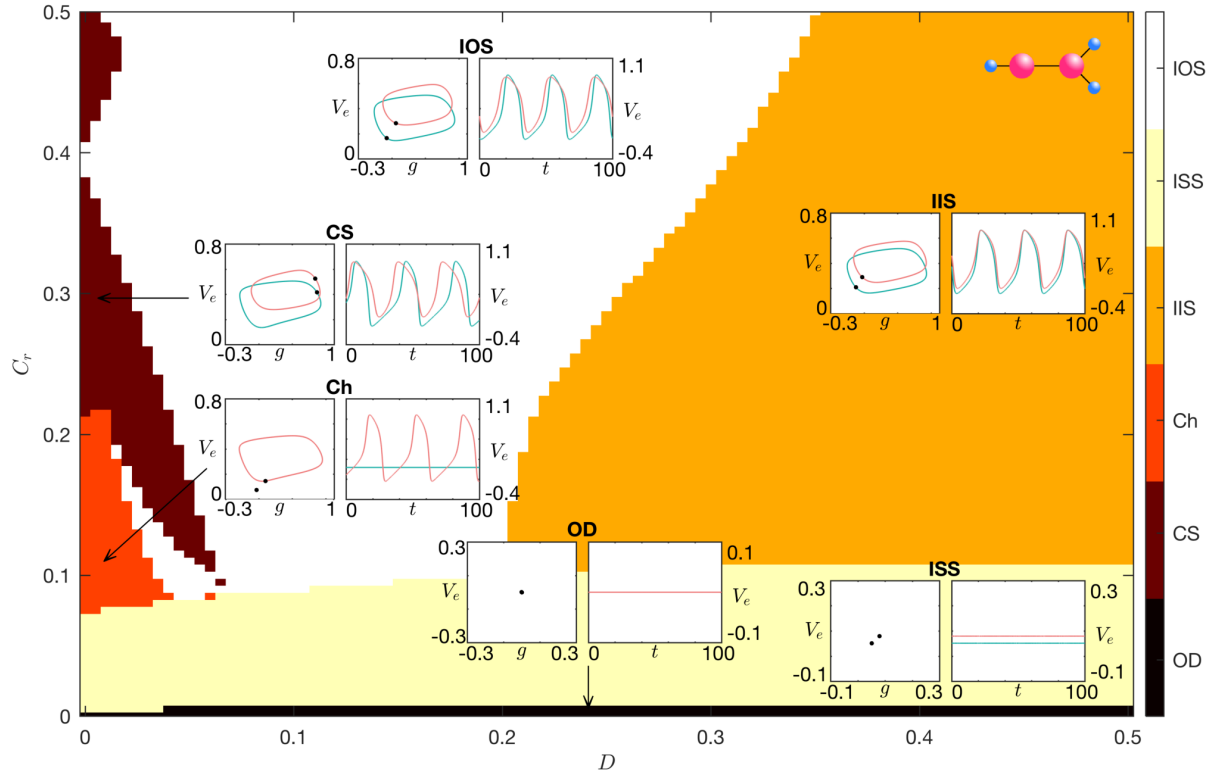
Figure B2: Enlarged version of Fig 3.3. (b) of Chapter 3, displaying the collective dynamical patterns observed over a range of values of coupling strengths between a pair of excitable cells (D) and between an excitable and a passive cell (C_r), obtained using the motif shown as an inset. For each of the dynamical regimes, we display characteristic time series of V_e for the two excitable cells, as well as the corresponding trajectories in the (V_e, g) phase plane. The time series and the phase plane portraits of the left and right excitable cell in the motif are colored green and maroon, respectively.

a pair of coupled excitable cells connected to one and two passive cells, respectively (as shown in the inset of the figure). Characteristic timeseries of V_e as well as (V_e, g) phase plane portraits are shown for each of the six observed dynamical regimes.

To show that the qualitative behaviour of the system is robust with respect to changes in the resting state of the passive cell, V_p^R, we consider the dependence of the frequencies ν of the excitable cells on the coupling strength D. In Fig. B3, we display ν as function of D for each of the four motifs considered in Fig. 3.3(a)-(d). Whereas in Fig. 3.3, we chose
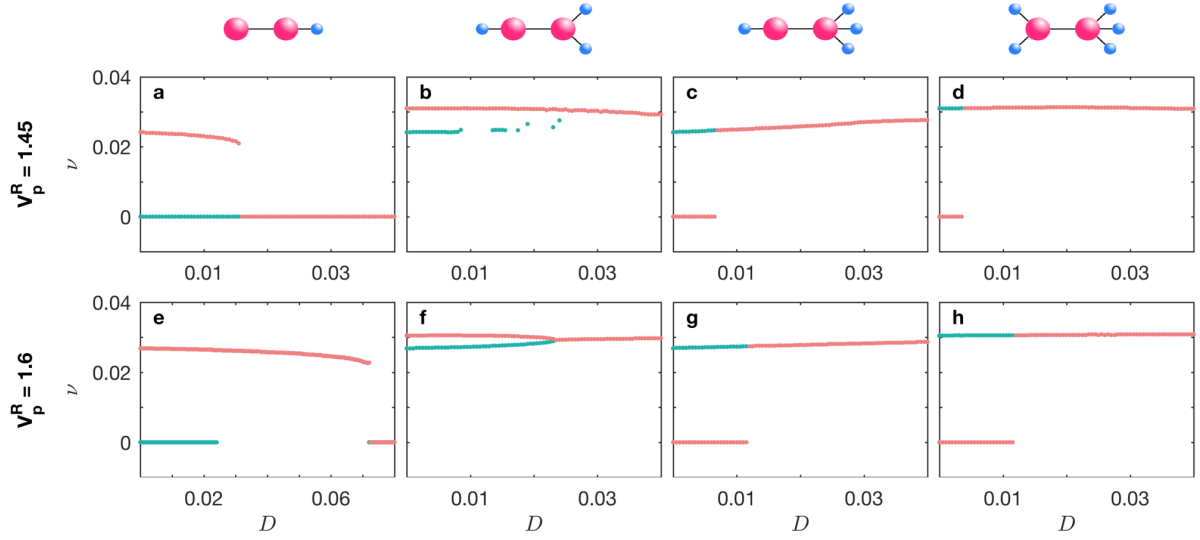
Figure B3: Variation of the frequency ν of the excitable cells on the left (green) and right (maroon) for each of the four motifs considered in Fig. 3.3(a)-(d) for $C_r = 0.25$ over a range of values of coupling strengths D for two different choices of V_p^R. The motif considered in each case is displayed above the corresponding column, whereas the value of the resting state potential is displayed to the left of each row, viz. $V_p^R = 1.45$ (top row) and $V_p^R = 1.6$ (bottom row). As can be seen by comparing these panels with those obtained for the case $V_p^R = 1.5$, displayed in Fig. 3.3(f)-(i) of Chapter 3, the qualitative behaviour is robust with respect to changes in V_p^R.

$V_p^R = 1.5$, here we consider $V_p^R = 1.45$ and $V_p^R = 1.6$. We observe that the qualitative nature of the dynamics does not change upon perturbing the value of V_p^R. For the case of the motif considered in panels (a) and (e), we see that there exists a region, characterized by both cells oscillating, that shrinks upon reducing V_p^R. Comparing the behaviour seen in these panels with that seen in Fig. 3.3(f), we see that the region appears to vanish at a value between $V_p^R = 1.45$ and $V_p^R = 1.5$.

Characterizing the coexistence of chaotic and non-chaotic dynamics in a 3-node motif of the EP model

In Chapter 3, we report the coexistence of chaotic and non-chaotic activity in a motif comprising 3 FHN nodes coupled to $n_p = 1, 2$ and 3 passive cells respectively [see Fig. 3.5 of Chapter 3]. We note that the usual method of demonstrating chaotic activity in a system is to show that its dynamics is sensitively dependent on initial conditions. In other words, two trajectories that begin from points that lie very close to each other in phase space will exponentially diverge with time.
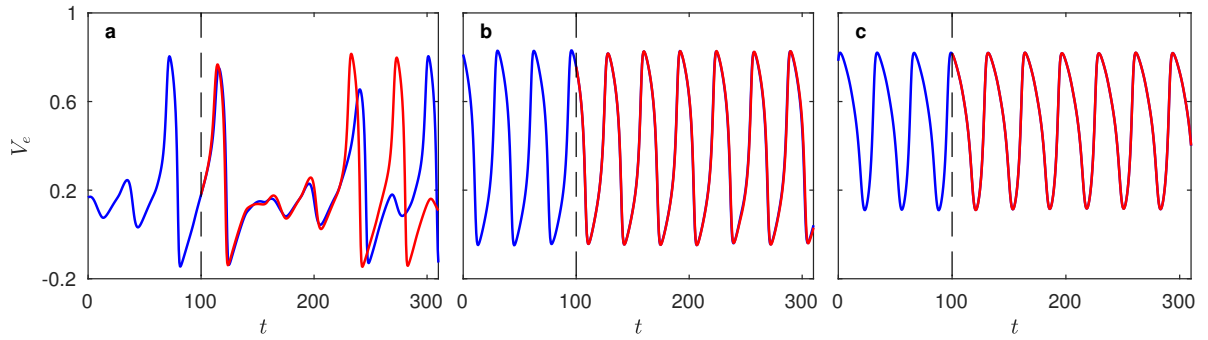
Figure B4: Differential sensitivity to small perturbations in a system of three coupled excitable cells, each attached to a variable number of passive cells, which display coexistence of chaotic and non-chaotic activity for $C_r = 0.19$ and $D = 0.02$ as described in Chapter 3 [see Fig. 3.5]. Each cell is subjected to a perturbation of the same magnitude ($= 10^{-3}$) applied at $t = 100$. While the cell exhibiting chaotic activity [panel (a)] displays exponential divergence of the perturbed trajectory (red) from the original one (blue), in the other two cells showing non-chaotic activity [panels (b) and (c)] the perturbed and original trajectories almost coincide.

This is demonstrated in Fig. B4, where the dynamical state of each unit is independently altered in turn by a very small magnitude perturbation and the subsequent time- evolution (shown in red) is compared with the trajectory of the node in the unperturbed system (shown in blue). As can be seen in Fig. B4(a), in the node exhibiting chaotic activity, the perturbed trajectory rapidly deviates from that observed in absence of perturbation, while for the other two nodes which display periodic activity, the perturbation does not result in

any perceptible deviation [panels (b) and (c)]. The chaotic nature of the dynamics can be quantitatively established by noting that the maximal Lyapunov exponent (calculated by the TISEAN software) is positive.

Comparing the collective dynamics observed in the OE and EP models

In this subsection, we show that similar collective dynamical behavior is displayed by both models [see Fig. B5]. As both models use the FHN model to describe the individual excitable nodes, its parameters A, α, ϵ and k_e are kept the same in the two models such that it is a fair comparison. However, values for the distinct parameters in the two models, viz., b in the OE model and C_r, n_p in the EP model, need to be suitably chosen such that a correspondence can be maintained between them. We note that for a given value of C_r, the resting state or the oscillation frequency of a node in the EP model depends on the value of n_p. On the other hand, in the OE model, it is the value of b which determines these. Thus, we can relate values of $\{C_r, n_p\}$ with those of b that give rise to the same resting state or oscillation frequencies in the two models, respectively.

Fig. B5 (a) shows the time-series of the activation variable V_e for a pair of coupled excitable units in the EP model, one connected to $n_p = 1$ passive cell (shown in blue) and the other to $n_p = 2$ passive cells (shown in red). We observe that while the two are phase synchronized, their amplitudes are different. In the OE model shown in Fig. B5 (b), if we couple two FHN cells having distinct b values such that the coupled system has the same frequency as the EP model, we observe exact synchronization, as is evident from the complete overlap of the two time-series. Thus, not only are two nodes in the OE model phase synchronized (as is also the case in the EP model), they also have identical

83
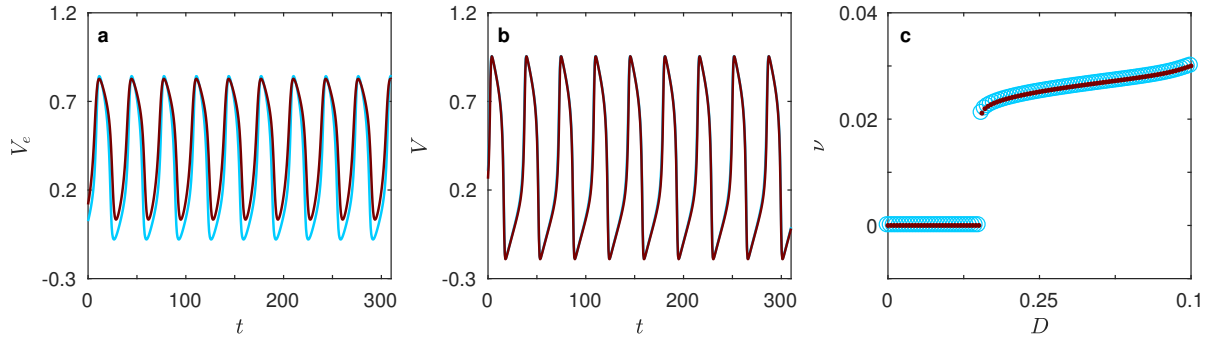
Figure B5: Time-evolution of the activation variables for two nodes coupled to each other in (a) the EP model and (b) the OE model, showing the absence and presence, respectively, of exact synchronization. In (a), the two excitable cells are coupled to $n_p = 1$ (blue curve) and $n_p = 2$ (red curve) passive cells, respectively, with strength $C_r = 0.4$ and interacting with each other with strength $D = 0.2$. In (b) the two cells differ in the numerical value of the FHN model parameter b, which are 0.2 and 0.181 respectively. (c) Oscillation frequencies for a system of two coupled excitable cells, each described by the FHN model but with distinct values for the parameter b ($= 0$ and 0.394, respectively) such that they have very different steady states in isolation. The system is quiescent in the absence of any external stimulation until the coupling strength exceeds a critical value, when spontaneous periodic activity is observed.

amplitudes (unlike in the EP model). Fig. B5 (c) shows the variation of the oscillation frequency ν as a function of the coupling strength D between two FHN nodes having $b = 0$ and 0.394, respectively, in the OE model. The uncoupled cells ($D = 0$) do not show spontaneous oscillations - however, when they are coupled with a sufficient strength D they exhibit synchronized oscillations. The emergence of spontaneous oscillatory activity in the coupled system is similar to that reported for the EP model motifs in Chapter 3 [e.g., see Fig. 3.4 (a)].

Appendix C

The following comprise the supporting information for the interaction of spiral waves in coupled biological oscillators, as described in Chapter 4.

Simulation details

As mentioned in Chapter 4, the Barkley model [134] was used for the simulations corresponding to the subsection "Interaction between spiral waves and target waves". The Barkley model has a form that is similar to the Fitz-Hugh Nagumo (FHN) model but one of the major advantages of using the Barkley model is that the numerical simulations can be performed quickly thereby reducing the computational cost. The subsequent section of Chapter 4 has simulations that were carried out using the Kuramoto model of oscillators [50] and the EP model which comprises excitable cells coupled to passive cells. For systems without noise, the forward Euler scheme is used to integrate the system numerically. For the EP model which has an additive noise, the Euler–Maruyama method, an extension of the Euler method for ordinary differential equations to stochastic differential equations, was used to solve the system numerically. We have used a time-step of $dt = 0.01$ for all the three models used in Chapter 4 and have verified that the results are qualitatively similar for smaller values of dt. The lattice spacing is taken to be 1 in both the horizontal and vertical directions and we use the standard 5-point stencil for the Laplacian

to describe the spatial coupling between the neighbouring elements of the lattice. No-flux boundary conditions are imposed on all the sides of the domain for the Barkley model simulations while simulations were carried out using both periodic and no-flux boundary conditions for the Kuramoto and the EP models. It is to be noted that the results were independent of the boundary conditions. Starting with random initial conditions, we first evolve the systems for a sufficient time to account for the transients and then subsequently start recording the data.

Dynamics of the phase vectors around the tip of a rotating spiral wave

The tip of a spiral wave, which is a phase singularity, can be identified at a particular time t as the point of intersection of the isoclines of the fast variable u ($u = u_0$) and the slow variable v ($v = v_0$). For the simulations reported here, we chose u_0 and v_0 to be 0.5 and 0.2, respectively. The phase θ of each of the oscillator is defined as :

$$\theta(\mathbf{x}, t) = \arctan2(v(\mathbf{x}, t) - v^*, u(\mathbf{x}, t) - u^*) \tag{C1}$$

where (u^*, v^*) is a point enclosed by the trajectory in the phase space. The function `arctan2` computes the principal value of the argument such that it lies in the range $(-\pi, \pi]$.

When the vector $(cos\theta, sin\theta)$ corresponding to the phase θ of the oscillator at a particular lattice point is drawn, we find that a clockwise rotating spiral is different from an anticlockwise rotating spiral dynamically. The phase vectors arrange themselves as a saddle for an anti-clockwise rotating spiral [Fig. C1(a)] while they form a center (or a stable/unstable node for a different time instant) for a clockwise rotating spiral [Fig. C1(b)]. This is surprising as flipping or changing the frame for viewing a clockwise rotating spiral

86
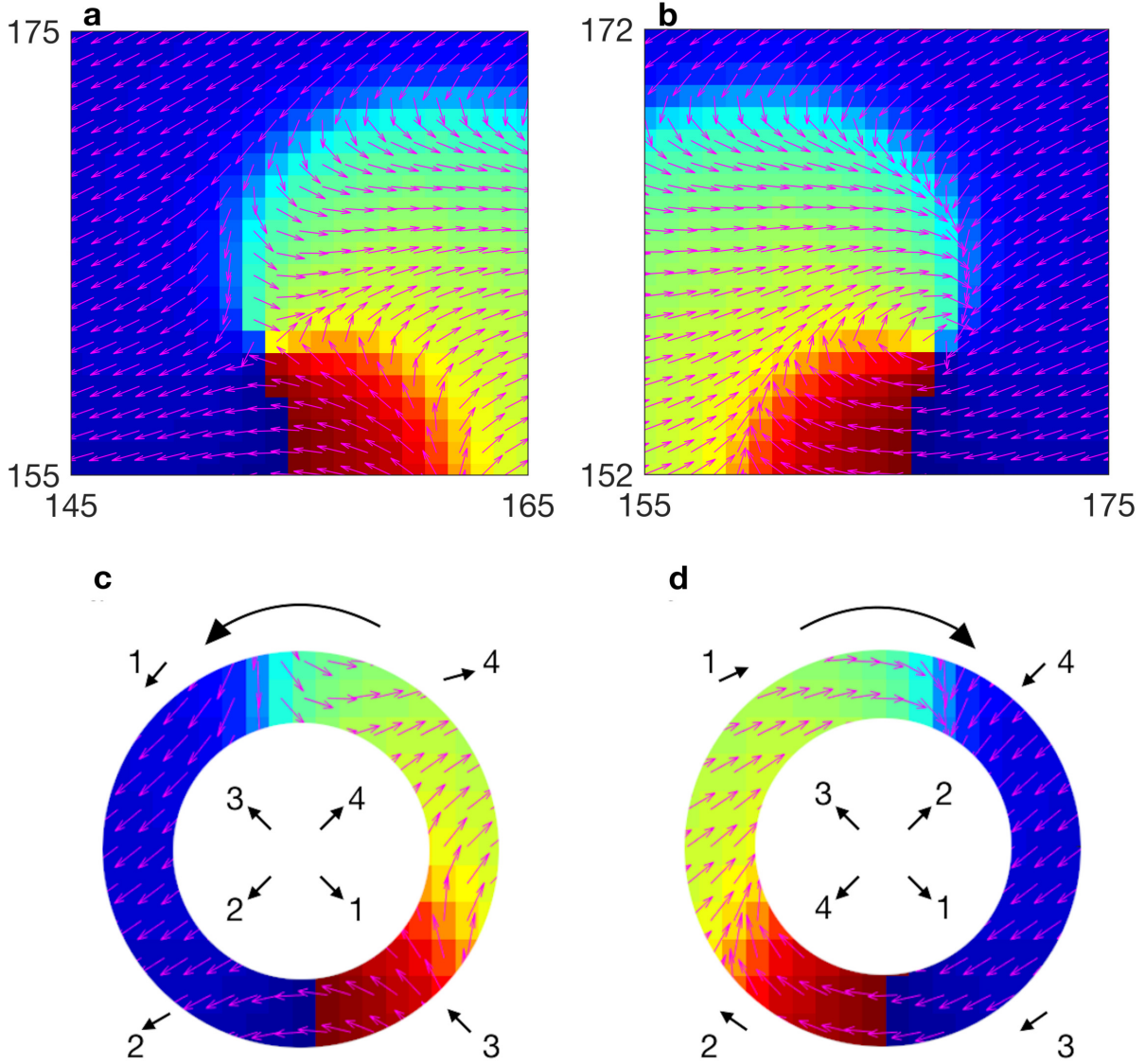
Figure C1: Arrangement of the phase vectors near the tip of a spiral wave. Snapshot of (a) a single anti-clockwise rotating spiral and (b) a single clockwise rotating spiral showing the phase θ alongwith the direction of the phase field with the phase vectors forming a saddle and a center around the respective phase singularities. (c) and (d) show annular cross-sections constructed from (a) and (b) respectively by considering the regions around the spiral tips showing the direction of the rotation of the vectors as one goes around the region in an anti-clockwise manner. This gives the index of the curve which is equal to -1 in (c) and $+1$ in (d).

gives us an anti-clockwise rotating spiral and vice versa, yet they differ dynamically. To understand this better, we consider an annular region around the spiral tip and follow the arrows along the ring. In Fig. C1(c), if we start at **1** and go around the ring in an anti-clockwise manner, the vectors on the ring complete a turn in the clockwise sense. Therefore, the index of the curve is -1 [135]. Similarly, in Fig. C1(d), as we go around the ring anti-clockwise, starting from **1**, the vectors on the ring also move in the anti-clockwise direction. Hence, the index of the curve is $+1$. Thus, the topological charges assigned to a spiral wave is nothing but the index.
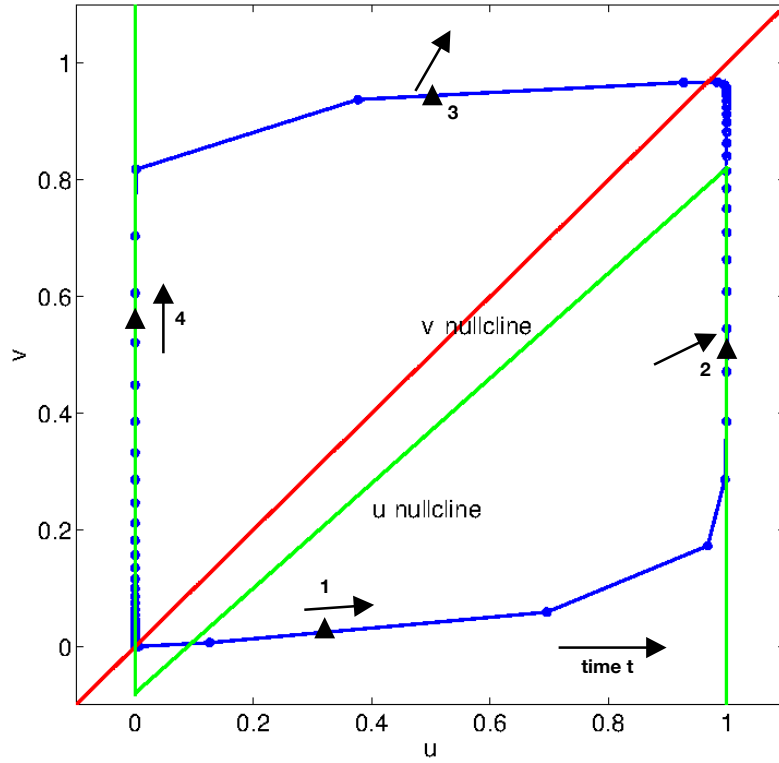
Figure C2: Phase plane trajectory of the Barkley model alongwith the nullclines. The u and the v nullclines are shown in green and red respectively. The phase plane trajectory is shown in blue. The black triangles marked 1, 2, 3 and 4 are the points on the trajectory where the phase angles are computed as time progresses. The corresponding arrows represent the direction of the phase vectors at those points.

Even though flipping a rotating spiral wave makes it rotate with opposite chirality, it does not make the two spirals identical. For this, we look at the (u, v) phase plane of a particular oscillator chosen from a rotating spiral wave. The rotation of vectors over time is shown by the arrows in Fig. C2 for the points marked in black. As time progresses, the trajectory always advances towards its right. The symmetry-breaking arises from the fact that over time, each phase vector moves in an anti-clockwise manner. Thus the direction of rotation of an individual phase vector is different in the two cases thereby making the spiral waves having opposite chirality dynamically different.

Bibliography

[1] D. W. Thompson. *On Growth and Form*, volume 2. Cambridge University Press, Cambridge, 1942.

[2] H. Meinhardt. *Models of biological pattern formation*. Academic Press, California, 1982.

[3] A. T. Winfree. *When time breaks down: the three-dimensional dynamics of electro-chemical waves and cardiac arrhythmias*. Princeton University Press, 1987.

[4] M. C. Cross and P. C. Hohenberg. Pattern formation outside of equilibrium. *Reviews of modern physics*, 65(3):851, 1993. doi:10.1103/RevModPhys.65.851.

[5] I. R. Epstein and J. A. Pojman. *An introduction to nonlinear chemical dynamics: oscillations, waves, patterns, and chaos*. Oxford University Press, 1998.

[6] P. Ball. *The self-made tapestry: pattern formation in nature*. Oxford University Press, 2001.

[7] J. D. Murray. *Mathematical biology II: spatial models and biomedical applications*, volume 3. Springer, New York, 2001.

[8] P. Ball. *Nature's patterns: a tapestry in three parts*. Oxford University Press, 2009.

[9] L. Wolpert, C. Tickle, and A. M. Arias. *Principles of development*. Oxford University Press, 2015.

[10] S. A. Kauffman. Pattern formation in the drosophila embryo. *Philosophical Transactions of the Royal Society of London. B, Biological Sciences*, 295(1078):567–594, 1981. doi:10.1098/rstb.1981.0161.

[11] D. A. Kessler and H. Levine. Pattern formation in *Dictyostelium* via the dynamics of cooperative biological entities. *Physical Review E*, 48(6):4801, 1993. doi:10.1103/PhysRevE.48.4801.

[12] J. D. Gilardi and C. A. Munn. Patterns of activity, flocking, and habitat use in parrots of the peruvian amazon. *The Condor*, 100(4):641–653, 1998. doi:10.2307/1369745.

[13] F. H. Fenton, E. M. Cherry, H. M. Hastings, and S. J. Evans. Multiple mechanisms of spiral wave breakup in a model of cardiac electrical activity. *Chaos: An Interdisciplinary Journal of Nonlinear Science*, 12(3):852–892, 2002. doi:10.1063/1.1504242.

[14] S. Stepanov. Dynamic population gratings in rare-earth-doped optical fibres. *Journal of Physics D: Applied Physics*, 41(22):224002, 2008. doi:10.1088/0022-3727/41/22/224002.

[15] L. F. Chibotaru, A. Ceulemans, V. Bruyndoncx, and V. V. Moshchalkov. Symmetry-induced formation of antivortices in mesoscopic superconductors. *Nature*, 408(6814):833–835, 2000. doi:10.1038/35048521.

[16] M. Kim, M. Bertram, M. Pollmann, A. von Oertzen, A. S. Mikhailov, H. H. Rotermund, and G. Ertl. Controlling chemical turbulence by global delayed feedback: pattern formation in catalytic CO oxidation on Pt (110). *Science*, 292(5520):1357–1360, 2001. doi:10.1126/science.1059478.

[17] J. B. Goodenough. Interpretation of domain patterns recently found in BiMn and SiFe alloys. *Physical Review*, 102(2):356, 1956. doi:10.1103/PhysRev.102.356.

[18] J. P. Keener and J. Sneyd. *Mathematical Physiology.* Springer, New York, 1998.

[19] B. P. Belousov. Periodically acting reaction and its mechanism. *Compilation of Abstracts on Radiation Medicine*, pages 145–147, 1959.

[20] J. E. Truscott and J. Brindley. Ocean plankton populations as excitable media. *Bulletin of Mathematical Biology*, 56(5):981–998, 1994. doi:10.1016/S0092-8240(05)80300-3.

[21] D. P. Zipes and J. Jalife. *Cardiac Electrophysiology: From Cell to Bedside E-book: Expert Consult*. Elsevier Health Sciences, 2009.

[22] J. Xu, S. N. Menon, R. Singh, N. B. Garnier, S. Sinha, and A. Pumir. The role of cellular coupling in the spontaneous generation of electrical activity in uterine tissue. *PLoS ONE*, 10(3): e0118443, 2015. doi:0.1371/journal.pone.0118443.

[23] J. D. Huizinga, L. Thuneberg, M. Klüppel, J. Malysz, H. B. Mikkelsen, and A. Bernstein. *W/kit* gene required for interstitial cells of cajal and for intestinal pacemaker activity. *Nature Neuroscience*, 373:347–349, 1995. doi:10.1038/373347a0.

[24] L. Glass and M. E. Josephson. Resetting and annihilation of reentrant abnormally rapid heartbeat. *Physical review letters*, 75(10):2059, 1995. doi:10.1103/PhysRevLett.75.2059.

[25] S. Sinha and D. J. Christini. Termination of reentry in an inhomogeneous ring of model cardiac cells. *Physical Review E*, 66(6):061903, 2002. doi:10.1103/PhysRevE.66.061903.

[26] S. Sinha, K. M. Stein, and D. J. Christini. Critical role of inhomogeneities in pacing termination of cardiac reentry. *Chaos*, 12(3):893–902, 2002. doi:10.1063/1.1501176.

[27] J. P. Keener. Waves in excitable media. *SIAM Journal on Applied Mathematics*, 39 (3):528–548, 1980. doi:10.1137/0139043.

[28] A. V. Holden, M. Markus, and H. G. Othmer. *Nonlinear wave processes in excitable media*, volume 244. Springer, 2013.

[29] V.S. Zykov. Spiral waves in two-dimensional excitable media. *Annals of the New York Academy of Sciences*, 591(1):75–85, 1990. doi:10.1111/j.1749-6632.1990.tb15082.x.

[30] J. P. Keener. The dynamics of three-dimensional scroll waves in excitable media. *Physica D: Nonlinear Phenomena*, 31(2):269–276, 1988. doi:10.1016/0167-2789(91)90169-A.

[31] E. Meron. Pattern formation in excitable media. *Physics reports*, 218(1):1–66, 1992. doi:10.1016/0370-1573(92)90098-K.

[32] P. Ortoleva. *Geochemical self-organization.* Oxford University Press, Oxford, 1994.

[33] M. C. Cross and H. Greenside. *Pattern formation and dynamics in nonequilibrium systems.* Cambridge University Press, 2009.

[34] A. M. Turing. The Chemical Basis of Morphogenesis. *Philosophical Transactions of the Royal Society of London Series B*, 237(641):37–72, 1952. doi:10.1098/rstb.1952.0012.

[35] N. Kopell and L. N. Howard. Plane wave solutions to reaction-diffusion equations. *Studies in Applied Mathematics*, 52(4):291–328, 1973. doi:10.1002/sapm1973524291.

[36] S. H. Strogatz and I. Stewart. Coupled oscillators and biological synchronization. *Scientific American*, 269(6):102–109, 1993. doi:10.1038/scientificamerican1293-102.

[37] A. Pikovsky, M. Rosenblum, and J. Kurths. *Synchronization: A Universal Concept in Nonlinear Sciences.* Cambridge University Press, Cambridge, 2003.

[38] S. H. Strogatz. *Sync: The emerging science of spontaneous order.* Penguin, UK, 2004.

[39] J. Rayleigh. *The Theory of Sound.* Dover Publishers, New York, 1945.

[40] J. Buck and E. Buck. Mechanism of rhythmic synchronous flashing of fireflies: Fireflies of southeast asia may use anticipatory time-measuring in synchronizing their flashing. *Science*, 159(3821):1319–1327, 1968. doi:10.1126/science.159.3821.1319.

[41] E. V. Appleton. Automatic synchronization of triode oscillators. In *Proceedings of the Cambridge Philosophical Society*, volume 21, page 231, 1922.

[42] B. van der Pol. LXXXVIII. On "relaxation oscillations". *The London, Edinburgh, and Dublin Philosophical Magazine and Journal of Science,*, 2:978–992, 1926. doi:10.1080/14786442608564127.

[43] A. B. Pippard. *The Physics of Vibration.* Cambridge University Press, 1989. doi:10.1017/CBO9780511622908.

[44] A. V. Hill. Wave transmission as the basis of nerve activity. In *Cold Spring Harbor Symposia on Quantitative Biology*, volume 1, pages 146–151. Cold Spring Harbor Laboratory Press, 1933. doi:10.1101/SQB.1933.001.01.019.

[45] J. Ginoux and C. Letellier. Van der Pol and the history of relaxation oscillations: Toward the emergence of a concept. *Chaos*, 22:023120, 2012. doi:10.1063/1.3670008.

[46] R. FitzHugh. Impulses and physiological states in theoretical models of nerve membrane. *Biophysical Journal*, 1(6):445–466, 1961. doi:10.1016/s0006-3495(61)86902-6.

[47] J. Nagumo, S. Arimoto, and S. Yoshizawa. An active pulse transmission line simulating nerve axon. *Proceedings of the IRE*, 50(10):2061–2070, 1962. doi:10.1109/JRPROC.1962.288235.

[48] A. L Hodgkin and A. F. Huxley. A quantitative description of membrane current and its application to conduction and excitation in nerve. *The Journal of Physiology*, 117(4):500–544, 1952. doi:10.1113/jphysiol.1952.sp004764.

[49] G.B Ermentrout and N. Kopell. Frequency plateaus in a chain of weakly coupled oscillators, I. *SIAM Journal on Mathematical Analysis*, 15(2):215–237, 1984. doi:10.1137/0515019.

[50] Y. Kuramoto. *Chemical Oscillations, Waves, and Turbulence.* Dover Publications, 2003.

[51] D. Cumin and C. P. Unsworth. Generalising the Kuramoto model for the study of neuronal synchronisation in the brain. *Physica D Nonlinear Phenomena*, 226: 181–196, 2007. doi:10.1016/j.physd.2006.12.004.

[52] J. A. Acebrón, L. L. Bonilla, C. J. Pérez Vicente, F. Ritort, and R. Spigler. The kuramoto model: A simple paradigm for synchronization phenomena. *Reviews of Modern Physics*, 77:137–185, 2005. doi:10.1103/RevModPhys.77.137.

[53] V.S. Zykov. *Simulation of Wave Processes in Excitable Media.* Manchester University Press, New York, 1987.

[54] P. C. Fife. *Dynamics of Internal Layers and Diffusive Interfaces.* Society for Industrial and Applied Mathematics, 1988. doi:10.1137/1.9781611970180.

[55] A. T. Winfree. Rotating chemical reactions. *Scientific American*, 230(6):82–95, 1974. doi:10.1038/scientificamerican0674-82.

[56] J. Davidenko, A. Pertsov, R. Salomonsz, W. Baxter, and J. Jalife. Stationary and drifting spiral waves of excitation in isolated cardiac muscle. *Nature*, 355:349–351, 1992. doi:10.1038/355349a0.

[57] M. A. Bray, S. F. Lin, R. R. Aliev, B. J. Roth, and J. P. Wikswo Jr. Experimental and theoretical analysis of phase singularity dynamics in cardiac tissue. *Journal of Cardiovascular Electrophysiology*, 12(6):716–722, 2001. doi:10.1046/j.1540-8167.2001.00716.x.

[58] C. S. Buhimsch. Spatiotemporal electromyography during human labor to monitor propagation of the uterine contraction wave and diagnose dystocia. *American Journal of Obstetrics and Gynecology*, 200:1, 2009. doi:10.1016/j.ajog.2008.09.007.

[59] R. Singh, J. Xu, N. G. Garnier, A. Pumir, and S. Sinha. Self-organized transition to coherent activity in disordered media. *Physical Review Letters*, 108:068102, 2012. doi:10.1103/PhysRevLett.108.068102.

[60] V. Jacquemet. Pacemaker activity resulting from the coupling with nonexcitable cells. *Physical Review E*, 74:011908, 2006. doi:10.1103/PhysRevE.74.011908.

[61] J. C. Smith, H. H. Ellenberger, K. Ballanyi, D. W Richter, and J. L. Feldman. Pre-bötzinger complex: a brainstem region that may generate respiratory rhythm in mammals. *Science*, 254(5032):726–729, 1991. doi:10.1126/science.1683005.

[62] C. A. Czeisler, J. F. Duffy, T. L. Shanahan, E. N. Brown, J. F. Mitchell, D. W. Rimmer, J. M. Ronda, E. J. Silva, J. S. Allan, J. S. Emens, D. J. Dijk, and R. E. Kronauer. Stability, precision, and near-24-hour period of the human circadian pacemaker. *Science*, 284(5423):2177–2181, 1999. doi:10.1126/science.284.5423.2177.

[63] N. Koshiya and J. C. Smith. Neuronal pacemaker for breathing visualized in vitro. *Nature*, 400(6742):360–363, 1999. doi:10.1038/22540.

[64] M. W. Young and S. A. Kay. Time zones: a comparative genetics of circadian clocks. *Nature Reviews Genetics*, 2:702–715, 2001. doi:10.1038/35088576.

[65] S. M. Reppert and D. R. Weaver. Coordination of circadian timing in mammals. *Nature*, 418:935–941, 2002. doi:10.1038/nature00965.

[66] G. A. Lincoln, I. J. Clarke, R. A. Hut, and D. G. Hazlerigg. Characterizing a mammalian circannual pacemaker. *Science*, 314(5807):1941–1944, 2006. doi:10.1126/science.1132009.

[67] M. I. Rabinovich, P. Varona, A. I. Selverton, and H. D. I. Abarbanel. Dynamical principles in neuroscience. *Reviews of Modern Physics*, 78:1213–1265, 2006. doi:10.1103/RevModPhys.78.1213.

[68] P. Morquette, D. Verdier, A. Kadala, J. Féthière, A. G. Philippe, R. Robitaille, and A. Kolta. An astrocyte-dependent mechanism for neuronal rhythmogenesis. *Nature Neuroscience*, 18:844–854, 2015. doi:10.1038/nn.4013.

[69] D. DiFrancesco. Characterization of single pacemaker channels in cardiac sino-atrial node cells. *Nature Neuroscience*, 324:470–473, 1986. doi:10.1038/324470a0.

[70] D. DiFrancesco. Pacemaker mechanisms in cardiac tissue. *Annual Review of Physiology*, 55(1):455–472, 1993. doi:10.1146/annurev.ph.55.030193.002323.

[71] L. Thomson, T. L. Robinson, J. C. F. Lee, L. A. Farraway, M. J. G. Hughes, D. W. Andrews, and J. D. Huizinga. Interstitial cells of cajal generate a rhythmic pacemaker current. *Nature Medicine*, 4:848–851, 1998. doi:10.1038/nm0798-848.

[72] J. D. Huizinga, J. H. Chen, Y. F. Zhu, A. Pawelka, R. J. Mcginn, B. L. Bardakjian, S. P. Parsons, W. A. Kunze, R. Y. Wu, P. Bercik, A. Khoshdel, S. Chen, S. Yin, Q. Zhang, Y. Yu, Q. Gao, K. Li, X. Hu, N. Zarate, P. Collins, M. Pistilli, J. Ma, R. Zhang, and D. Chen. The origin of segmentation motor activity in the intestine. *Nature Communications*, 5(3326), 2014. doi:10.1038/ncomms4326.

[73] R. Smith, M. Imtiaz, D. Banney, J. W. Paul, and R. C. Young. Why the heart is like an orchestra and the uterus is like a soccer crowd. *American Journal of Obstetrics and Gynecology*, 213(2):181–185, 2015. ISSN 0002-9378. doi:https://doi.org/10.1016/j.ajog.2015.06.040.

[74] J. H. E. Cartwright. Emergent global oscillations in heterogeneous excitable media: The example of pancreatic beta cells. *Physical Review E*, 62:1149–1154, 2000. doi:10.1103/PhysRevE.62.1149.

[75] C. D. E. Boschi, E. Louis, and G. Ortega. Triggering synchronized oscillations through arbitrarily weak diversity in close-to-threshold excitable media. *Physical Review E*, 65:012901, 2001. doi:10.1103/PhysRevE.65.012901.

[76] K. J. Lee, E. C. Cox, and R. E. Goldstein. Competing patterns of signaling activity in *Dictyostelium Discoideum*. *Physical Review Letters*, 76:1174–1177, 1996. doi:10.1103/PhysRevLett.76.1174.

[77] R. Caldeyro-Barcia, H. Alvarez, and S. R. M. Reynolds. A better understanding of uterine contractility through simultaneous recording with an internal and a seven channel external method. *Obstetrical & Gynecological Survey*, 91:641, 1950. doi:10.1097/00006254-195106000-00005.

[78] S. R. M. Reynolds. Uterine contractility and cervical dilatation. *Proceedings of the Royal Society of Medicine*, 44:695, 1951. doi:10.1097/00006254-195106000-00005.

[79] G. Wolfs and H. Rottinghuis. Electrical and mechanical activity of the human uterus during labour. *Archiv für Gynäkologie*, 208:373, 1970. doi:10.1007/BF00668252.

[80] J. G. Planes, J. P. Morucci, H. Grandjean, and R. Favretto. External recording and processing of fast electrical activity of the uterus in human parturition. *Medical & Biological Engineering & Computing*, 22:585, 1984. doi:10.1007/bf02443874.

[81] T. Y. Euliano, D. Marossero, M. T. Nguyen, N. R. Euliano, J. Principe, and R. K. Edwards. Spatiotemporal electrohysterography patterns in normal and arrested labor. *American Journal of Obstetrics and Gynecology*, 200:54, 2009. doi:10.1016/j.ajog.2008.09.008.

[82] R. Caldeyro-Barcia and H. Alvarez. The normal and abnormal contractile waves of the uterus during labour. *Gynecologic and Obstetric Investigation*, 138:190, 1954. doi:10.1159/000308198.

[83] J. P. Neilson, T Lavender, S Quenby, and S Wray. Obstructed labour: Reducing maternal death and disability during pregnancy. *British Medical Bulletin*, 67(1): 191–204, 2003. doi:10.1093/bmb/ldg018.

[84] E. L. Barber, L. S. Lundsberg, K. Belanger, C. M. Pettker, E. F. Funai, and J. L. Illuzzi. Indications contributing to the increasing cesarean delivery rate. *Obstetrics and Gynecology*, 118(1):29–38, 2011. doi:10.1097/AOG.0b013e31821e5f65.

[85] E. A. Clark and R. M. Silver. Long-term maternal morbidity associated with repeat cesarean delivery. *American Journal of Obstetrics and Gynecology*, 205:S2, 2011. doi:10.1016/j.ajog.2011.09.028.

[86] American College of Obstetricians and Gynecologists (College), Society for Maternal-Fetal Medicine, A. B. Caughey, A. G. Cahill, J. M. Guise, and D. J. Rouse. Safe prevention of the primary cesarean delivery. *American Journal of Obstetrics and Gynecology*, 210(3):179–193, 2014. doi:10.1016/j.ajog.2014.01.026.

[87] W. C. Alvarez. Functional variations in contractions of different parts of the small intestine. *American Journal of Physiology*, 35:177, 1914. doi:10.1152/ajplegacy.1914.35.2.177.

[88] A Bortoff. Myogenic control of intestinal motility. *Physiological Reviews*, 56(2): 418–434, 1976. doi:10.1152/physrev.1976.56.2.418.

[89] H. Miyoshi, M. B. Boyle, L. B. MacKay, and R. E. Garfield. Voltage-clamp studies of gap junctions between uterine muscle cells during term and preterm labor. *Biophysical Journal*, 71:1324, 1996. doi:10.1016/S0006-3495(96)79332-3.

[90] R.E. Garfield and R.H. Hayashi. Appearance of gap junctions in the myometrium of women during labor. *American Journal of Obstetrics and Gynecology*, 140(3): 254–260, 1981. doi:10.1016/0002-9378(81)90270-2.

[91] C. Ramon, H. Preissl, P. Murphy, J. D. Wilson, C. Lowery, and H. Eswaran. Synchronization analysis of the uterine magnetic activity during contractions. *BioMedical Engineering OnLine*, 4:55, 2005. doi:10.1186/1475-925X-4-55.

[92] R. E. Garfield and W. L. Maner. Physiology and electrical activity of uterine contractions. *Seminars in Cell & Developmental Biology*, 18(3):289–295, 2007. doi:/10.1016/j.semcdb.2007.05.004.

[93] C. Rabotti and M. Mischi. Propagation of electrical activity in uterine muscle during pregnancy: a review. *Acta physiologica*, 213:406, 2015. doi:10.1111/apha.12424.

[94] S. Wray, S. Kupittayanant, A. Shmygol, R. D. Smith, and T. Burdyga. The physiological basis of uterine contractility: a short review. *Experimental Physiology*, 86: 239, 2001. doi:10.1113/eph8602114.

[95] A. Shmygol, A. M. Blanks, G. Bru-Mercier, J. E. Gullam, and S. Thornton. Control of uterine Ca2+ by membrane voltage. *Annals of the New York Academy of Sciences*, 1101(1):97–109, 2007. doi:10.1196/annals.1389.031.

[96] M. Yoshino, S.Y. Wang, and C.Y. Kao. Sodium and calcium inward currents in freshly dissociated smooth myocytes of rat uterus. *Journal of General Physiology*, 110(5):565–577, 1997. doi:10.1085/jgp.110.5.565.

[97] R.A. Duquette, A. Shmygol, C. Vaillant, A. Mobasheri, M. Pope, T. Burdyga, and S. Wray. Vimentin-positive, c-KIT-negative interstitial cells in human and rat uterus: A role in pacemaking? *Biology of Reproduction*, 72(2):276–283, 2005. doi:10.1095/biolreprod.104.033506.

[98] S. Sinha and S. Sridhar. *Patterns in Excitable Media: Genesis, Dynamics, and Control.* CRC Press, Boca Raton, FL, 2015.

[99] P. Kohl, A. G. Kamkin, I. S. Kiseleva, and D. Noble. Mechanosensitive fibroblasts in the sino-atrial node region of rat heart: interaction with car-

diomyocytes and possible role. *Experimental Physiology*, 79(6):943–956, 1994. doi:10.1113/expphysiol.1994.sp003819.

[100] J. Xu, R. Singh, N. G. Garnier, S. Sinha, and A. Pumir. The effect of quenched disorder on dynamical transitions in systems of coupled cells. *New Journal of Physics*, 15:093046, 2013. doi:10.1088/1367-2630/15/9/093046.

[101] W. J. E. P. Lammers, B. Stephen, M. A. Al-Sultan, S. B. Subramanya, and A. M. Blanks. The location of pacemakers in the uteri of pregnant guinea pigs and rats. *American Journal of Physiology-Regulatory, Integrative and Comparative Physiology*, 309(11):R1439–R1446, 2015. doi:10.1152/ajpregu.00187.2015.

[102] W. J. E. P. Lammers. The electrical activities of the uterus during pregnancy. *Reproductive Sciences*, 20(2):182–189, 2013. doi:10.1177/1933719112446082.

[103] L. Glass. Synchronization and rhythmic processes in physiology. *Nature*, 410:277–284, 2001. doi:10.1038/35065745.

[104] M. R. Boyett, H. Honjo, and I. Kodama. The sinoatrial node, a heterogeneous pacemaker structure. *Cardiovascular Research*, 47:658, 2000. doi:10.1016/S0008-6363(00)00135-8.

[105] R. Ghosh, P. Seenivasan, S. N. Menon, S. Sridhar, N. B. Garnier, A. Pumir, and S. Sinha. Frequency gradients in heterogeneous oscillatory media can spatially localize self-organized wave sources that coordinate system-wide activity. *arXiv:1912.07271*, 2019.

[106] T. A. Quinn, P. Camelliti, E. A. Rog-Zielinska, U. Siedlecka, T. Poggioli, E. T. O'Toole, T. Knöpfel, and P. Kohl. Electrotonic coupling of excitable and nonexcitable cells in the heart revealed by optogenetics. *Proceedings of the Natural Academy of Sciences*, 113:14852, 2016. doi:10.1073/pnas.1611184114.

[107] R. C. Young. The uterine pacemaker of labor. *Best Practice & Research: Clinical Obstetrics & Gynaecology*, 52:68, 2018. doi:10.1016/j.bpobgyn.2018.04.002.

101

[108] D. Stauffer and A. Aharony. *Introduction to Percolation Theory*. CRC Press, Boca Raton, FL, 1994.

[109] E. Jahn, I. Classen-Linke, M. Kusche, H. M. Beier, O. Traub, R. Grummer, and E. Winterhager. Expression of gap junction connexins in the human endometrium throughout the menstrual cycle. *Human Reproduction*, 10:2666, 1995. doi:10.1093/oxfordjournals.humrep.a135764.

[110] W. C. Tong, C. Y. Choi, S. Karche, A. V. Holden, H. Zhang, and M. J. Taggart. A computational model of the ionic currents, Ca2+ dynamics and action potentials underlying contraction of isolated uterine smooth muscle. *PLoS ONE*, 6:e18685, 2011. doi:10.1371/journal.pone.0018685.

[111] B. V. Safronov, M. Wolff, and W. Vogel. Excitability of the soma in central nervous system neurons. *Biophysical Journal*, 78:2998, 2000. doi:10.1016/S0006-3495(00)76838-X.

[112] J. M. Bekkers and M. Häusser. Targeted dendrotomy reveals active and passive contributions of the dendritic tree to synaptic integration and neuronal output. *Proceedings of the Natural Academy of Sciences*, 104:11447, 2007. doi:10.1073/pnas.0701586104.

[113] G. J. Gutierrez, T. O'Leary, and E. Marder. Multiple mechanisms switch an electrically coupled, synaptically inhibited neuron between competing rhythmic oscillators. *Neuron*, 77:845, 2013. doi:10.1016/j.neuron.2013.01.016.

[114] A. T. Winfree. Varieties of spiral wave behavior: An experimentalist's approach to the theory of excitable media. *Chaos: An Interdisciplinary Journal of Nonlinear Science*, 1(3):303–334, 1991. doi:10.1063/1.165844.

[115] J. Lechleiter, S. Girard, E. Peralta, and D. Clapham. Spiral calcium wave propagation and annihilation in *Xenopus laevis* oocytes. *Science*, 252(5002):123–126, 1991. doi:10.1126/science.2011747.

[116] G. Gerisch. Chapter 6 Cell aggregation and differentiation in *Dictyostelium*. In *Current Topics in Developmental Biology*, volume 3, pages 157–197. Academic Press, 1968. doi:10.1016/S0070-2153(08)60354-3.

[117] N. A. Gorelova and J. Bureš. Spiral waves of spreading depression in the isolated chicken retina. *Journal of Neurobiology*, 14(5):353–363, 1983. doi:10.1002/neu.480140503.

[118] M. T. Keating and M. C. Sanguinetti. Molecular and cellular mechanisms of cardiac arrhythmias. *Cell*, 104(4):569–580, 2001. doi:10.1016/s0092-8674(01)00243-4.

[119] X. Huang, W. Xu, J. Liang, K. Takagaki, X. Gao, and J. Y. Wu. Spiral wave dynamics in neocortex. *Neuron*, 68(5):978–990, 2010. doi:10.1016/j.neuron.2010.11.007.

[120] E. Pervolaraki and A. V. Holden. Spatiotemporal patterning of uterine excitation patterns in human labour. *Biosystems*, 112(2):63–72, 2013. doi:10.1016/j.biosystems.2013.03.012.

[121] V. I. Krinsky (ed.). *Self-organization: Autowaves and Structures Far from Equilibrium.* Springer, Berlin, 1984.

[122] J. P. Keener. A geometrical theory for spiral waves in excitable media. *SIAM Journal on Applied Mathematics*, 46(6):1039–1056, 1986. doi:10.1137/0146062.

[123] A.T. Winfree. Electrical instability in cardiac muscle: Phase singularities and rotors. *Journal of Theoretical Biology*, 138(3):353–405, 1989. doi:10.1016/S0022-5193(89)80200-0.

[124] V. I. Krinsky and K. I. Agladze. Interaction of rotating waves in an active chemical medium. *Physica D*, 8(1-2):50–56, 1983. doi:10.1016/0167-2789(83)90310-X.

[125] A. Pumir, S. Sinha, S. Sridhar, M. Argentina, Ma. Hörning, S. Filippi, C. Cherubini, S. Luther, and V. Krinsky. Wave-train-induced termination of weakly

anchored vortices in excitable media. *Physical Review E*, 81(1):010901, 2010. doi:10.1103/PhysRevE.81.010901.

[126] D. T. Kim, Y. Kwan, J. J. Lee, T. Ikeda, T. Uchida, K. Kamjoo, Y. H. Kim, J. J. C. Ong, C. A. Athill, T. J. Wu, L. Czer, H. S. Karagueuzian, and P. S. Chen. Patterns of spiral tip motion in cardiac tissues. *Chaos: An Interdisciplinary Journal of Nonlinear Science*, 8(1):137–148, 1998. doi:10.1063/1.166294.

[127] C. Zemlin, K. Mukund, M. Wellner, R. Zaritsky, and A. Pertsov. Asymmetric bound states of spiral pairs in excitable media. *Physical Review Letters*, 95:098302, 2005. doi:10.1103/PhysRevLett.95.098302.

[128] R. Ghosh and S. N. Menon. Spontaneous generation of persistent activity in diffusively coupled cellular assemblies. *Physical Review E*, 105(1):014311, 2022. doi:10.1103/PhysRevE.105.014311.

[129] H Lecar and R Nossal. Theory of threshold fluctuations in nerves. II. analysis of various sources of membrane noise. *Biophysical journal*, 11(12):1068–1084, 1971. doi:10.1016/s0006-3495(71)86278-1.

[130] J. H. Goldwyn and E. Shea-Brown. The what and where of adding channel noise to the hodgkin-huxley equations. *PLOS Computational Biology*, 7:1–9, 2011. doi:10.1371/journal.pcbi.1002247.

[131] R. Kenna. The XY model and the Berezinskii-Kosterlitz-Thouless phase transition. *arXiv preprint cond-mat/0512356*, 2005.

[132] E. J. H. Mulder and G. H. A Visser. Braxton hicks' contractions and motor behavior in the near-term human fetus. *American journal of Obstetrics and Gynecology*, 156 (3):543–549, 1987. doi:10.5555/uri:pii:0002937887900470.

[133] M. La Verde, G. Riemma, M. Torella, C. Torre, S. Cianci, A. Conte, C. Capristo, M. Morlando, N. Colacurci, and P. De Franciscis. Impact of braxton-hicks

contractions on fetal wellbeing; a prospective analysis through computerised cardiotocography. *Journal of Obstetrics and Gynaecology*, pages 1–5, 2021. doi:10.1080/01443615.2021.1929115.

[134] D. Barkley. A model for fast computer simulation of waves in excitable media. *Physica D: Nonlinear Phenomena*, 49(1):61–70, 1991. doi:10.1016/0167-2789(91)90194-E.

[135] S. H. Strogatz. *Nonlinear Dynamics and Chaos: With Applications to Physics, Biology, Chemistry and Engineering.* Westview Press, 2000.

[136] E. A. Ermakova, A. M. Pertsov, and E. E. Shnol. On the interaction of vortices in two-dimensional active media. *Physica D: Nonlinear Phenomena*, 40(2):185–195, 1989. doi:10.1016/0167-2789(89)90062-6.

[137] P. M. Chaikin and T. C. Lubensky. *Principles of Condensed Matter Physics.* Cambridge University Press, 2000.

[138] T. E. Lee, H. Tam, G. Refael, J. L. Rogers, and M. C. Cross. Vortices and the entrainment transition in the two-dimensional kuramoto model. *Physical Review E*, 82:036202, 2010. doi:10.1103/PhysRevE.82.036202.

[139] V. Flovik, F. Maciá, and E. Wahlström. Describing synchronization and topological excitations in arrays of magnetic spin torque oscillators through the kuramoto model. *Scientific Reports*, 6:32528, 2016. doi:10.1038/srep32528.

[140] J. M. Kosterlitz and D. J. Thouless. Ordering, metastability and phase transitions in two-dimensional systems. *Journal of Physics C: Solid State Physics*, 6(7):1181, 1973. doi:10.1088/0022-3719/6/7/010.

[141] J. H. E. Cartwright, V. M. Eguíluz, E. Hernández-García, and O. Piro. Dynamics of elastic excitable media. *International Journal of Bifurcation and Chaos*, 9(11): 2197–2202, 1999. doi:10.1142/S0218127499001620.

[142] A. Î U. Kolesov and Y. S. Kolesov. Relaxation oscillations in mathematical models of ecology. In *Proceedings of the Steklov Institute of Mathematics*, volume 199, 1995.

[143] E. E. Goldwyn and A. Hastings. When can dispersal synchronize populations? *Theoretical population biology*, 73(3):395–402, 2008. doi:10.1016/j.tpb.2007.11.012.

[144] U. Alon. *An introduction to systems biology: design principles of biological circuits.* Chapman and Hall/CRC, 2006.

[145] S. Wray. Uterine contraction and physiological mechanisms of modulation. *American journal of physiology-cell physiology*, 264(1):C1–C18, 1993. doi:10.1152/ajpcell.1993.264.1.C1.

[146] P. O'Leary, P. Boyne, P. Flett, J. Beilby, and I. James. Longitudinal assessment of changes in reproductive hormones during normal pregnancy. *Clinical chemistry*, 37 (5):667–672, 1991. doi:10.1093/clinchem/37.5.667.

[147] P. Kumar and N. Magon. Hormones in pregnancy. *Nigerian medical journal: journal of the Nigeria Medical Association*, 53(4):179, 2012. doi:10.4103/0300-1652.107549.

[148] F. M. Fairlie, G. F. Phillips, B. J. Andrews, and A. A. Calder. An analysis of uterine activity in spontaneous labour using a microcomputer. *BJOG: An International Journal of Obstetrics & Gynaecology*, 95(1):57–64, 1988. doi:10.1111/j.1471-0528.1988.tb06480.x.

[149] C. S. Henriquez. *Simulating the Electrical Behavior of Cardiac Tissue Using the Bidomain Model*, volume 21 of *Critical Reviews in Biomedical Engineering*. CRC Press, 1993.

[150] R. C. Young. Myocytes, myometrium, and uterine contractions. *Annals of the New York Academy of Sciences*, 1101(1):72–84, 2007. doi:10.1196/annals.1389.038.